

Aus dem Center for Regenerative Therapies TU Dresden

Direktor: Prof. Dr. Ezio Bonifacio

Identifying Casc15 as a novel regulator of progenitors' proliferation and neuronal migration in the developing neocortex

DISSERTATIONSSCHRIFT

zur Erlangung des akademischen Grades

Doctor of Philosophy (Ph.D.)

vorgelegt

der Medizinischen Fakultät Carl Gustav Carus

der Technischen Universität Dresden

von

Sara S. Tayel

Pharmacist

aus Alexandria, Ägypten

geboren am 05.05.1987 Kafr Elshikh, Ägypten

Dresden 2018

1. Gutachter: Prof. Dr. Marius Ader

2. Gutachter: Prof. Dr. Frank Buchholz

Tag der mündlichen Prüfung: 10.03.2019

gez.:

Vorsitzender der Promotionskommission

Summary

A highly organized multilayer tissue in the mammalian brain called the neocortex performs the higher cognitive functions, including language learning, thinking and spatial reasoning. During evolution, the neocortex has expanded in size to cope with the complex cognitive demands of the higher animals. This cortical expansion is primarily thought to be due to the balance between proliferation and differentiation of the neural stem cells and their progenitors. These processes are highly programmed in space and time, posing many questions over the molecular networks involved. In the last two decades, long non-coding RNAs (lncRNAs) have presented themselves as attractive targets in developmental biology. These molecules revolutionized our perception of the functional unit of a cell as they are known to mediate their functions through their RNA structure. Unlike microRNAs that mediate their functions by regulating protein-coding genes at a post-transcriptional level, lncRNAs act more diversely. Particularly in the brain, the organ that expresses the highest number of lncRNAs and the biggest proportion of tissue and cell specific lncRNAs, they were proven to be involved in almost every process during development and in adulthood.

With the aim to have a better understanding of the molecular mechanisms of brain development, I sought to identify new roles for lncRNAs in neurogenesis. To this end, I made use of a powerful genetic tool that was previously generated in our lab; a transcriptome generated from a mouse line that allows sorting the proliferating, differentiating as well as terminally differentiated cells. Analysis of the differential expression of lncRNAs in the three cell types revealed interesting candidates that potentially have a role in neurogenesis. The manipulation of these candidates was tested *in vivo* by *in utero* electroporation.

In this study, I identify *Casc15* as a regulator of neural stem cell proliferation and neuronal migration. Overexpression of *Casc15* in the developing cortex caused deregulation of genes involved in nervous system development and cell part morphogenesis. Particularly, downregulated genes upon *Casc15* overexpression are physiologically enriched in neurons. These include genes that are responsible for neuronal migration and maturation. *Casc15* was shown to decrease *Tbr2*, a neurogenic transcription factor, at the protein but not the mRNA level. Moreover, using a series of bioinformatic tools, *Casc15* was shown to cause differential gene isoform usage in

the developing cortex, which is suggestive of Casc15 interaction with splicing factors. The effects of Casc15 on gene or transcript expression cannot fully explain Casc15's role in neurogenesis. Particularly, its effect on protein translation and stability needs to be addressed.

Altogether, though mechanistically not very clear, my data shows that Casc15 is an important regulator in cortex development. Further experiments are needed to discuss the molecular aspects of Casc15 functions.

Zusammenfassung

Ein sehr organisiertes vielschichtiges Gewebe im Gehirn von Säugetieren ist der Neokortex, der höhere kognitive Funktionen ausübt wie Erlernen einer Sprache, Denken und räumliches Vorstellungsvermögen. Während der Evolution hat sich der Neokortex vergrößert, um den komplexen kognitiven Bedarf von höher entwickelten Tieren zu bewältigen. Es wird angenommen, dass diese kortikale Expansion primär in der Balance zwischen Proliferation und Differenzierung von neuronalen Stammzellen und deren Vorläuferzellen begründet ist. Diese Prozesse sind sehr stark programmiert in Ort und Zeit, was viele Fragen über die involvierten molekularen Netzwerke aufwirft. In den letzten zwei Jahrzehnten haben sich lange nicht-kodierende RNAs (lncRNAs) als attraktive Ziele in der Entwicklungsbiologie dargestellt. Diese Moleküle haben unsere Wahrnehmung von der funktionalen Einheit einer Zelle revolutioniert, da sie bekannt dafür sind, deren Funktion mittels ihrer RNA Struktur auszuüben. Im Gegensatz zu microRNAs, die ihre Funktion über die Regulation von protein-kodierenden Genen auf post-transkriptionaler Ebene ausführen, agieren lncRNAs unterschiedlicher. Vor allem im Gehirn, dem Organ, was die größte Anzahl von lncRNAs exprimiert und das höchste Verhältnis von Gewebe- und Zell-spezifischen lncRNAs besitzt, wurde nachgewiesen, dass sie in fast jedem Prozess während der Entwicklung und bei Erwachsenen involviert sind.

Mit dem Ziel eines besseren Verständnisses der molekularen Mechanismen der Gehirnentwicklung, habe ich angestrebt neue Rollen für lncRNAs in der Neurogenese zu identifizieren. Dafür habe ich Gebrauch von einem wirksamen genetischen Instrument gemacht, das zuvor in unserem Labor erzeugt wurde: ein Transkriptom von einer Mauslinie, die es ermöglicht, proliferierende, differenzierende und ausdifferenzierte Zellen zu sortieren. Die Analyse der differentiellen Expression von lncRNAs in den drei Zelltypen enthüllte interessante Kandidaten, die möglicherweise eine Rolle in der Neurogenese spielen. Die Manipulation dieser Kandidaten wurde *in vivo* getestet durch *in utero* Elektroporation.

In dieser Studie habe ich *Casc15* als Regulator von neuraler Stammzellproliferation und neuronaler Migration identifiziert. Überexpression von *Casc15* im entwickelnden Kortex verursachte eine Deregulierung von Genen, die in der Entwicklung des Nervensystems und Zellteil-Morphogenese involviert sind. Insbesondere

herunterregulierte Gene nach Casc15 Überexpression sind physiologisch angereichert in Neuronen. Diese schließen Gene ein, die verantwortlich für neuronale Migration und Reifung verantwortlich sind. Es wurde gezeigt, dass Casc15 Tbr2, einen neurogenen Transkriptionsfaktor, auf Protein- aber nicht mRNA-Level verringert. Außerdem wurde mittels einer Serie von bioinformatischen Programmen herausgefunden, dass Casc15 eine differentielle Gen-Isoform Benutzung im entwickelnden Gehirn verursacht, was eine Interaktion von Casc15 mit Spleißfaktoren suggeriert. Die Effekte von Casc15 auf Gen- oder Transkript-Expression kann nicht völlig erklärt werden durch Casc15's Rolle in Neurogenese. Besonders sein Effekt auf Proteintranslation und –stabilität muss adressiert werden.

Alles in allem zeigen meine Daten, wenn auch mechanistisch nicht sehr eindeutig, dass Casc15 ein wichtiger Regulator in der Gehirnentwicklung ist. Weiterführende Experimente sind nötig, um die molekularen Aspekte der Casc15 Funktionen zu erörtern.

Übersetzt von Simon Hertlein

Table of Contents

1	Introduction	1
1.1	Development of the mammalian neocortex	2
1.2	Neurogenesis in the neocortex	4
1.2.1	Neural stem cells	4
1.2.2	Transient amplifying cells	7
1.2.3	Neurogenesis	9
1.3	Molecular control of neurogenesis in neocortex	11
1.3.1	Signaling pathways influencing the onset and progression of neurogenesis 12	
1.3.2	Transcriptional control of neurogenesis	13
1.3.3	Epigenetics, Post-translational modifications and more	15
1.4	Long non-coding RNAs	16
1.4.1	General characteristics of lncRNAs	17
1.4.2	Versatile mechanisms of lncRNAs	20
1.4.3	Expression patterns of lncRNAs	21
1.4.4	lncRNAs in neurogenesis	23
1.5	Btg2^{RFP}/Tubb3^{GFP} mouse line to study cortical development.....	25
1.6	Aim of the study	28
2	Materials and Methods	29
2.1	Materials.....	30
2.1.1	Chemicals, buffers and culture media	30
2.1.2	Antibodies	31
2.1.3	Primers	32
2.1.4	Mouse strains.....	34
2.1.5	Bacterial Strains.....	34
2.1.6	Vectors.....	34
2.1.7	Kits and enzymes	35
2.2	Methods	35
2.2.1	Generation of plasmid.....	35
2.2.2	<i>In utero</i> electroporation	35
2.2.3	Mouse sample collection and treatment.....	36
2.2.4	Immunohistochemistry.....	36
2.2.5	Image acquisition and processing	37

2.2.6	Reverse transcription.....	37
2.2.7	Library preparation and supplemental bioinformatic analyses.....	37
2.2.8	Quantitative-Reverse Transcriptase-PCRs	39
2.2.9	Bioinformatic analysis	39
2.2.10	Statistical analysis.....	40
3	Results	41
3.1	Selection of potential regulators of neurogenesis	42
3.1.1	Differential expression analysis for RNA seq data	42
3.1.2	LincRNAs for <i>in vivo</i> manipulation	44
3.2	In vivo manipulation of K13, K10 and Casc15	48
3.2.1	K13 overexpression does not alter progenitors/neurons distribution in the cortex. 49	
3.2.2	K10 might affect migration of neurons in the developing cortex.....	50
3.2.3	Casc15 disrupted the distribution of cells across the four cortical layers..	50
3.3	Characterization of the cellular phenotype of Casc15	52
3.3.1	Casc15 delays neuronal migration	52
3.3.2	Casc15 does not alter progenitors migration	54
3.3.3	Casc15 does not induce direct neurogenesis.....	54
3.3.4	Casc15 causes subtle changes on cell distribution after 24 hours	56
3.3.5	Effect of Casc16 on progenitors fate	58
3.4	Molecular effects of Casc15	61
3.4.1	Casc15 minimally changes gene expression in the developing cortex	61
3.4.2	Casc15 changes gene exon usage	64
4	Discussion	68
4.1	Casc15 is a potential regulator of neurogenesis.....	69
4.1.1	Casc15 induces proliferation of progenitors in the developing cortex	70
4.1.2	Casc15 delays neuronal migration in the developing cortex.....	71
4.2	Molecular aspects of Casc15 in neurogenesis.....	72
4.2.1	Casc15 roles in neurogenesis cannot be explained in light of changes in gene expression.....	73
4.2.2	Casc15 changes the transcriptome at an isoform level	76
4.3	Concluding remarks	78
5	Appendix.....	79
6	Bibliography.....	87

List of Figures

Figure 1.1 Schematic representation for formation of the neural tube.	3
Figure 1.2: Brain Vesicles.....	4
Figure 1.3: Schamatic diagram of neural stem cells and progenitors in the developing cortex.....	5
Figure 1.4: modes of division of neural progenitors.....	8
Figure 1.5: Projection neurons are produced in an inside-out fashion.	10
Figure 1.6: Dynein and Myosin II act interdependently to mediate nuclear migration.	11
Figure 1.7: subclasses of lncRNAs.	18
Figure 1.8: Different roles of lncRNAs in neurogenesis.	24
Figure 1.9: Generation of the double transgenic mouse line.	26
Figure 1.10: Validation of cell population isolation.	27
Figure 2.1: Schematic representation for the pDSV-mRFPnls.....	34
Figure 3.1:Selecting candidate genes for <i>in vivo</i> studies.	44
Figure 3.2: the genomic context for 2610307P16Rik.....	45
Figure 3.3: Selection of 2010204K13Rik for <i>in vivo</i> manipulation.....	46
Figure 3.4: Selection of E530001K10Rik for <i>in vivo</i> manipulation.	47
Figure 3.5: Selection of 2610307P16Rik for <i>in vivo</i> manipulation.	47
Figure 3.6: IUE a powerful tool for genes' screen.....	49
Figure 3.7: lincRNA induced phenotypes in the lateral cortex.....	51
Figure 3.8: Effect of Casc15 on neuronal migration.....	53
Figure 3.9: Casc15 does not change progenitors migration.....	55
Figure 3.10: Casc15 does not induce direct neurogenesis in APs.	57
Figure 3.11: Effects of Casc15 after 24 hours.	58
Figure 3.12: Casc15 induces proliferation in progenitors.....	60
Figure 3.13: Transcriptome generation after Casc15 overexpression	62
Figure 3.14: Differential expression analysis of RNA-seq.....	63
Figure 3.15: Effects of Casc15 on alternative splicing.....	65
Figure 3.16: Alternative splicing changing the coding sequence of protein-coding genes.	67

List of Tables

Table 1: Protein-coding genes selected for validation by RT-qPCR.....	74
Table 2: List of DownDown lncRNAs ordered by their expression level in PP.	80
Table 3: List of Onswitch lncRNAs ordered by their expression level in DP.....	81
Table 4: List of genes that are up or down regulated upon Casc15 overexpression....	84
Table 5: List of Deregulated genes that show a dose response correlation to Casc15 overexpression.	86

Abbreviations

AP	Apical Progenitor
BP	Basal Progenitor
bHLH	basic helix-loop-helix
BrdU	Bromdesoxyuridin
CNS	Central Nervous System
CP	Cortical Plate
Ct	Cycle threshold
DAPI	4', 6-Diamidin-2-phenylindol
DNA	Deoxyribonucleic acid
DP	Differentiating Progenitors
E	Embryonic day
FACS	Fluorescent Activated Cell Sorting
FDR	false discovery rate
FPKM	fragments per kilobase million
GFP	Green Fluorescent Protein
GO term	gene ontology term
INM	Interkinetic Nuclear Migration
IUE	<i>In Utero</i> Electroporation
IZ	Intermediate Zone
lncRNA	long non-coding RNA
miRNA	micro RNA
ncRNA	non coding RNA
NE	Neuro Epithelial cell
PP	Proliferating Progenitors
RFP	Red Fluorescent Protein
RG	Radial Glial Cell
RNA	Ribonucleic acid
SVZ	Sub-ventricular Zone
VZ	Ventricular Zone

Chapter 1

1 Introduction

As famously quoted by Gregor Eichele “What is perhaps the most intriguing question of all is whether the brain is powerful enough to solve the problem of its own creation”.

The composition of the organ responsible for all cognitive functions received much attention in the studies of developmental biology. The brain coordinates our conscious and unconscious bodily processes and is the organ that perceives, thinks, remembers and even fools itself. These higher cognitive functions are all performed by part of the mammalian brain called the neocortex which is a multi layer tissue labeled from the outermost inwards, I to VI. Owing to its complex organization, the neocortex proposes many questions regarding the cell fate choice between proliferation and differentiation of stem cells. Not only do neural stem cells give rise to neurons, but also they have the ability to specify into different neuronal subtypes according to their differentiation time point. Even more, a fundamental feature of neural development is the differentiation of the neural precursors into neurons followed by astrocytes then oligodendrocytes in overlapping but temporally distinct waves. This timely manner implies that these processes are precisely programmed in the genetic information. In addition to specific signaling and transcriptional regulation, in the last decade, new technologies have provided evidence to more complex interactions that are controlled at different levels. The epigenetic control of gene programmes, the post transcriptional and translational regulations, and the growing field of non-coding RNAs, have all provided new areas of research to better solve the developmental enigmas.

Most research on mammalian development has focused on the mouse embryo, since mice are easy to breed and have relatively large litters. Aiming at adding one more segment to the puzzle, I will use *Mus musculus* to study the molecular regulators of the mammalian neocortex development.

1.1 Development of the mammalian neocortex

Soon after fertilization, the mammalian zygote undergoes rapid proliferative cell divisions to form a two-layer embryo composed of the upper epiblast and lower hypoblast. In mouse this takes place at embryonic day 4.5 (E4.5) (Rossant and Tam, 2009). The hypoblast gives rise to the extraembryonic endoderm which forms the yolk sac. The epiblast cell layer is then split by small clefts that coalesce to separate the embryonic epiblast from the other epiblast cells that form the amniotic cavity, which is filled with amniotic fluid (Gilbert, 2014). The embryonic epiblast gives rise to the three germ layers from which the whole organism is formed. This is likely instructed by exposure to fibroblast growth factors (FGFs). The three germ layers are composed of the inner most **endoderm** that later gives rise to the gut tube, liver, pancreas and lungs, middle **mesoderm** that gives rise to the vascular system, muscles and connective tissue and the outer **ectoderm** which is instructed to form the nervous system and the epidermis (Kandel, 2012). Under the gradient instruction of bone morphogenetic proteins (BMPs), distal ectodermal cells that receive high levels of BMPs form the epidermis, while the cells of the node by secreting BMP antagonists induce the formation of the neural plate in the ectoderm overlying it. Intermediate levels of BMPs in between the neural plate and the epidermis instruct the formation of the neural crest. The neural plate cells are distinguished by their columnar appearance and express the transcription factors Sox1, Sox2 and Sox3 that inhibit epidermal fate, consequently activating genes that specify neural fate (Gilbert, 2014). Soon after its formation, the neural plate folds to form the neural tube by the process of neurulation. The neural tube is created by the bending of the neural plate at its midline forming the neural groove with its edges thickening and moving upward to form the neural folds (Figure 1.1). As the bending proceeds, the neural folds are brought into proximity at the dorsal midline, they adhere to each other and the cells that form the two folds merge. Thus, during neurulation the original ectoderm is divided into three sets of cells: first, the internally positioned neural tube that will form the brain and the spinal cord, second, the externally positioned epidermis of the skin and third, the neural crest cells, originating from the neural folds, that connects the epidermis and the neural tube. Neural crest cells then migrate away as they generate cells of the peripheral nervous system among other things.

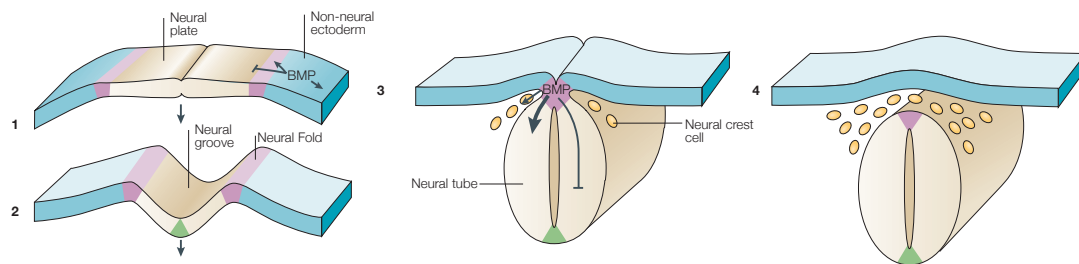


Figure 1.1 Schematic representation for formation of the neural tube.

(1) This process relies on the inhibition of (BMP) signaling. (2) The neural plate folds to produce the neural groove and the neural folds. (3) At the end of neurulation, the lateral edges of the neural plate fuse and the neural crest cells migrate. (4) The neural tube segregate from the non-neural epithelium, the roof plate and floor plate form at the dorsal and ventral midline of the neural tube (Adapted from Liu and Niswander, 2005).

In mouse the neural tube closure starts at E8.5, however it does not occur at the same time along the rostral-caudal axis. Even before the most caudal part is formed, the rostral neural tube undergoes rapid proliferation and gives rise to the three brain vesicles that will form the brain (Figure 1.2). These three brain vesicles: the prosencephalic or the forebrain vesicle, the mesencephalic or the mid brain vesicle and the rhombencephalic or hindbrain vesicle (Figure 1.2; left). These three vesicles further develop into secondary vesicles by the time the caudal neural tube, which will form the spinal cord, is closed (Figure 1.2; middle). The hindbrain vesicle divides to form the metencephalon, that forms the cerebellum, and myelencephalon, that gives rise to the medulla oblongata. The midbrain vesicle does not form secondary vesicles but matures to form the cerebral aqueduct. The forebrain vesicle divides into the anterior telencephalon, that will form the cerebral hemispheres, and the posterior diencephalon, from which thalamic and hypothalamic brain regions are formed. Furthermore, the telencephalon is further subdivided into dorsal region, which develops into the cerebral cortex, and ventral region, that will generate the basal ganglia. The patterning across the rostral-caudal and dorso-ventral axes is dictated by morphogens, that instruct downstream transcription factors according to the distance from the signaling centers (Gilbert, 2014; Kandel, 2012).

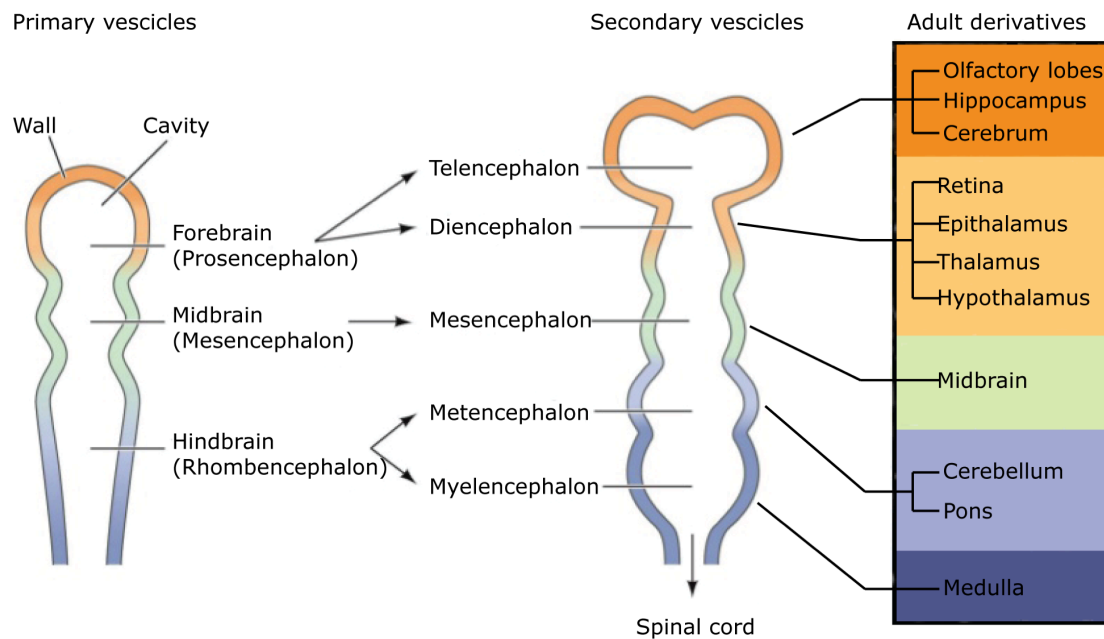


Figure 1.2: Brain Vesicles.

The rostral neural tube differentiates into the forebrain, midbrain and hindbrain vesicles (left). These 3 vesicles further subdivide into the five main brain vesicles (middle) that mature into the different structures of the adult brain (right)(adapted from Gilbert et al., 2013).

1.2 Neurogenesis in the neocortex

1.2.1 Neural stem cells

The neural plate and the neural tube are composed of a single layer of neural stem cells called neuroepithelial cells (Götz and Huttner, 2005). Neuroepithelial cells are, like other epithelial cells, polarized along their apical-basal axis (Huttner and Brand, 1997). These cells are highly elongated cells with thin processes extending to the neural tube and the basal lamina forming the apical and basal plasma membranes, respectively (Figure 1.3; left). The two membranes exhibit different features, for example, the apical plasma membrane contains tight junctions and adherens junctions, while receptors for basal lamina constituents such as integrin $\alpha 6$ are feature of the basal plasma membrane (Wodarz and Huttner, 2003). The neuroepithelium is pseudostratified; the nuclei of the neuroepithelial cells are found at various positions along the apical-basal axis during the different phases of the cell cycle, in a process known as interkinetic nuclear migration (INM), resulting in a multilayer appearance (Sauer, 1935; Takahashi et al., 1993). INM refers to the migration of neuroepithelial nuclei during G1 phase towards the basal membrane where S phase takes place. Conversely, they migrate during G2 towards the apical membrane as mitosis takes

place at, or very close to, the apical surface. At the onset of neurogenesis, neuroepithelial cells give rise to a more fate-restricted cell type called the radial glial cells (Götz and Huttner, 2005). Radial glial cells exhibit residual neuroepithelial properties and acquire, in addition, astroglial properties (Kriegstein and Götz, 2003). As neurogenesis proceeds, radial glial cells substitute the neuroepithelial cells in the brain and a multi-cell layer tissue is formed. The most apical cell layer that lines the ventricle and has most of the progenitors cell bodies is referred to as the ventricular zone (VZ). Radial glial cells are also polarized with a longer basal process, which grew in length concomitant with the formation of neuronal layers, to maintain contact with the basal lamina (Figure 1.3; middle). Both neuroepithelial and radial glial cells undergo mitosis at the apical membrane of the VZ and, hence, collectively called apical progenitors (APs) (Götz and Huttner, 2005).

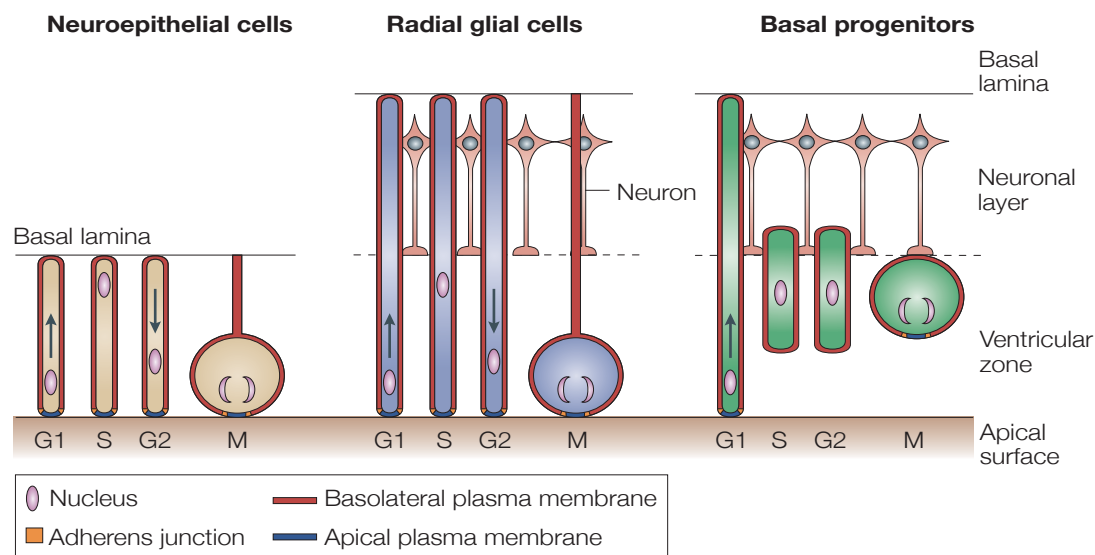


Figure 1.3: Schematic diagram of neural stem cells and progenitors in the developing cortex.

(Left) At the onset of neurogenesis, the neural tube is composed of a layer of NE stem cells that are elongated cells spanning the apical-basal axis. The nuclei undergo INM during different stages of the cell cycle and mitosis takes place at the apical membrane lining the ventricles. (Middle) NE cells develop into radial glial cells that retain the cell polarity, undergo INM. However because neurons are produced causing thickening of the cortex, INM of radial glial cells is now confined between the apical membrane and the basal side of the germinal layer, rather than the whole cortex thickness. (Right) The production of BPs occurs after the onset of neurogenesis. BPs are more committed progenitors that form the SVZ and retract their apical process (Adapted from Gotz and Huttner 2005).

INM and its effect on cortical expansion

As mentioned above, nuclei of APs (neuroepithelial cells and radial glial cells) undergo INM during different phases of the cell cycle (Figure 1.3left and middle). A key difference between neuroepithelial cells and radial glial cells is that in the latter INM is confined to the limits of the VZ. An important consideration for AP nuclei

migration towards the apical surface is the localization of the centrosome, which sets up the mitotic spindle, at the apical membrane throughout the cell cycle except for mitosis (Dubreuil et al., 2007). This is so because the primary cilium, which forms one centriole of the centrosome via its basal body, protrudes from the apical plasma membrane (Taverna and Huttner, 2010). Numerous reports, however, showed that INM is dispensable for cell cycle progression of APs with mitosis not confined to the apical surface but throughout the VZ (abventricularly) in case basal-to-apical INM was perturbed, or S-phase occurring more apically in case apical-to-basal INM was inhibited (Schenk et al., 2009; Taverna and Huttner, 2010).

Another important consideration in INM of APs is the involvement of different machinery in basal-to-apical versus apical-to-basal nuclear translocations in the developing cortex of rodents. Basal-to-apical INM is primarily thought to be mediated through the dynein motor system; a minus-end-directed microtubule-based motor protein (Taverna and Huttner, 2010). The microtubules in APs are oriented parallel to the apical-basal axis with the plus end directed away from the centrosome. The interaction of the integral membrane protein of the nuclear envelope, Syne2a, with dynactin anchors the nucleus to the dynein motor complex causing the AP nucleus to move as a cargo along microtubule tracks (Del Bene et al., 2008; Taverna and Huttner, 2010; Zhang et al., 2009). This process involves Lis1 protein which interacts with and regulates dynein (Gambello et al., 2003; McKenney et al., 2010; Tsai and Gleeson, 2005). On the other hand, the study of apical-to-basal INM in APs has faced extra challenges because apical-to-basal nuclear migration is a feature that APs share with other neural progenitors and newborn neurons. This makes it difficult to dissect APs-specific apical-to-basal INM (Taverna and Huttner, 2010). Currently, two machineries are known to be involved in apical-to-basal INM in AP. The first is the involvement of the plus-end-directed microtubule-based motors of the kinesin type (Baye and Link, 2008; Taverna and Huttner, 2010; Zhang et al., 2009). The second is primarily mediated through actomyosin contractility, where the nucleus is not moved as a cargo but, rather via directional myosin-II-dependent constriction (Schenk et al., 2009). Intriguingly, the current evidences does not support the involvement of actomyosin contractility in basal-to apical INM of APs in the developing cortex of rodents (Schenk et al., 2009; Taverna and Huttner, 2010).

INM of APs allows reserving the limited apical space for mitosis by moving the interphase nuclei away from the apical surface, thereby promoting the expansion of

APs (Taverna and Huttner, 2010). Moreover, in the developing mouse cortex, perturbation of apical-to-basal INM caused an increase in the neurogenic basal progenitors (BPs, see below) at the expense of the proliferative APs (Schenk et al., 2009). Therefore, INM is not only responsible for the pseudostratification of the neuroepithelium but is also necessary for cortex expansion and for the neural stem cell and progenitor fate.

1.2.2 Transient amplifying cells

The vast majority of APs, at the onset of neurogenesis around E9, divide by symmetric proliferative divisions to expand the stem pool (Götz and Huttner, 2005). But a minor fraction divides asymmetrically to produce an AP daughter cell and a neuron by neurogenic division, known as direct neurogenesis (Figure 1.4). Alternatively, APs divide into an AP and a more differentiated daughter cell by differentiative division. These neurogenic progenitors are known as BPs, because their nuclei undergo mitosis at the basal side of the VZ (Figure 1.3; right). BPs originate from the apical mitosis of APs and migrate towards the basal side of the VZ for S-phase (Haubensak et al., 2004; Miyata et al., 2004). These cells may still have apical contact and their apical-to-basal nuclear migration is similar to that of the APs. BPs, then, retract their apical processes by delamination of these cells from the apical adherens junctions and their centrosomes move to a perinuclear area. Actomyosin contractility is mainly involved in the apical-to-basal nuclear migration of BPs, while the basal-to-apical nuclear migration is not significantly seen in rodent BPs (Taverna and Huttner, 2010). At E13.5, BPs form another germinal layer, the subventricular zone (SVZ), basal to the VZ in the telencephalon of the mammalian brain (Haubensak et al., 2004). BPs differ from APs in gene expression, where they specifically express the non-coding RNA *Svet1* and the genes that encode the transcription factors *Cux1*, *Cux2* and *stab2* (Nieto et al., 2004; Tarabykin et al., 2001). BPs also express *Eomes*, also known as *Tbr2*, a transcription factor that is transiently expressed in these progenitors and used as a main marker to identify them (Englund et al., 2005). A minor fraction of BPs can undergo proliferative divisions producing BPs. However, BPs mainly divide symmetrically to produce two neuronal daughter cells (Figure 1.4B) thus they are also known as “intermediate progenitors” or “transit amplifying progenitors” that allow a further round of cell division increasing the final output of neurons (Götz and Huttner, 2005).

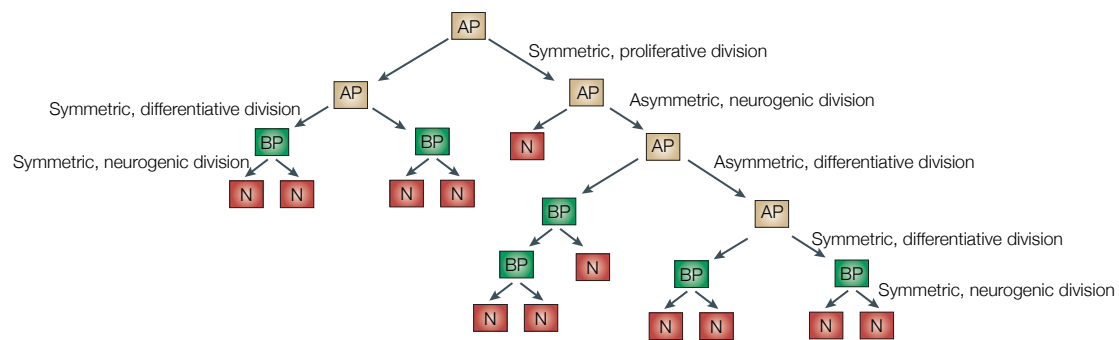


Figure 1.4: modes of division of neural progenitors.

AP: apical progenitors. BP: basal progenitors. N: neurons. Modes of divisions are indicated. (adapted from (Götz and Huttner, 2005).

Btg2 as a marker of differentiative divisions

During mid neurogenesis (E14.5) two main progenitor populations coexist in the germinal layers, APs in the VZ and BPs in the basal side of the VZ and the SVZ. BPs are produced from the differentiative divisions of APs and are marked with the expression of Tbr2. Notably both APs and BPs can undergo either proliferative divisions (to expand their pool) or differentiative divisions (to produce a more committed progenitor for APs or a neuron for BPs), which adds another level of complexity on the pool of progenitors (Figure 1.4). Trying to resolve the mechanisms switching neurogenesis on, it is important to study the differences between both modes of division and, hence, it is important to distinguish the subpopulations of progenitors undergoing either proliferation or differentiation while they coexist in the germinal layers. The identification of Btg2, also called Tis21 an anti-proliferative gene, allowed the discrimination between proliferative and differentiative progenitors (Haubensak et al., 2004; Iacopetti et al., 1999). Btg2 is expressed during the G1 phase of the cell cycle in progenitors that will generate either a neuronal-committed progenitors or a neuron in the next mitosis, thereby, marking only a sub-fraction of APs and BPs. Using Btg2 as a marker for differentiating cells, it is currently known that, during mid neurogenesis at E14.5, almost 60% of APs, which are Tbr2⁻, undergo proliferative divisions to expand the stem cell pool and therefore are Tbr2⁻,Btg2⁻ (Arai et al., 2011). The remaining 40% of APs undergo asymmetric differentiative divisions, to produce an AP and a more committed BP, this fraction expresses Btg2 and therefore is identified as (Tbr2⁻,Btg2⁺). On the other hand, almost 90% of BPs, which are Tbr2⁺, also express Btg2 and undergo symmetric differentiative divisions to

produce two post-mitotic neurons ($Tbr2^+, Btg2^+$), while a minor fraction undergoes proliferative divisions ($Tbr2^+, Btg2^-$) (Arai et al., 2011). Thus, proliferative progenitors, hereafter called PPs ($Btg2^-$), represent the pool of symmetrically expanding cells generating daughters that are cell biologically identical to their mother regardless of whether they are apical or basal progenitors. While differentiating progenitors, hereafter called DPs ($Btg2^+$), generate at least one daughter with a more restricted potential and depleting the progenitor pool. As neurogenesis progresses, more progenitors undergo symmetric terminal divisions in which both daughters differentiate, consequently, the expansion of the progenitor pool gradually slows and then stops. Premature transition from proliferative to neurogenic divisions besides decreasing neuronal output causing microcephaly, it also alters the balance between different neuronal populations causing developmental abnormalities (Manzini and Walsh, 2011; Rubenstein, 2011). Conversely, protraction of progenitors expansion phase in human is thought to output an increased number of late born cortical neurons connecting different cortical areas (Rakic, 1995).

1.2.3 Neurogenesis

Neocortical progenitors begin to produce excitatory projection neurons around E10.5 in mice (Greig et al., 2013). The earliest neurons migrate basally away from the apical surface through the intermediate zone (IZ) and form the preplate. Cajal-retzius neurons, generated in sites external to the cortex, form the more superficial marginal zone of the preplate (O'Leary et al., 2007). The preplate is then split into the subplate and the marginal zone (which forms layer I in the adult neocortex), establishing the cortical plate (CP) in between (Greig et al., 2013; Kandel, 2012). Throughout corticogenesis, newborn neurons migrate into the CP in an inside-out fashion, where early born neurons occupy deeper layers, while late-born neurons migrate past them and progressively populate more superficial layers of the CP, with the last few neurons generated by E17.5 (Angevine and Sidman, 1961) after which astrogenesis takes place. Neurons located in deep layers mostly project to subcortical targets such as thalamus and spinal cord while neurons in superficial layers project to other parts of the cortex (Martynoga et al., 2012).

Neuronal migration

The generated neurons initially take a multipolar morphology in the SVZ, but, then, convert to a bipolar migratory shape with a migratory process ahead and a trailing axon. The migrating neurons ascend along the AP processes to their final destination in the developing neuronal layers of the developing cortex (Vallee et al., 2009).

In migrating neurons both dynein and myosin II act interdependently to coordinate nuclear movement. Migrating cells contain a single centrosome situated ahead of the nucleus (Schaar and McConnell, 2005). Particularly, in embryonic rodent brain neocortical slices, the distance between the centrosome and the nucleus is 20 μm and microtubules were observed to emanate from the centrosomal region and extend outward in both the migratory and the axonal processes (Rakic et al., 1996; Schaar and McConnell, 2005; Tsai et al., 2007). An observed feature of the migrating neural cells is the formation of transient swellings within the migratory processes that are enriched for dynein (Vallee et al., 2009).

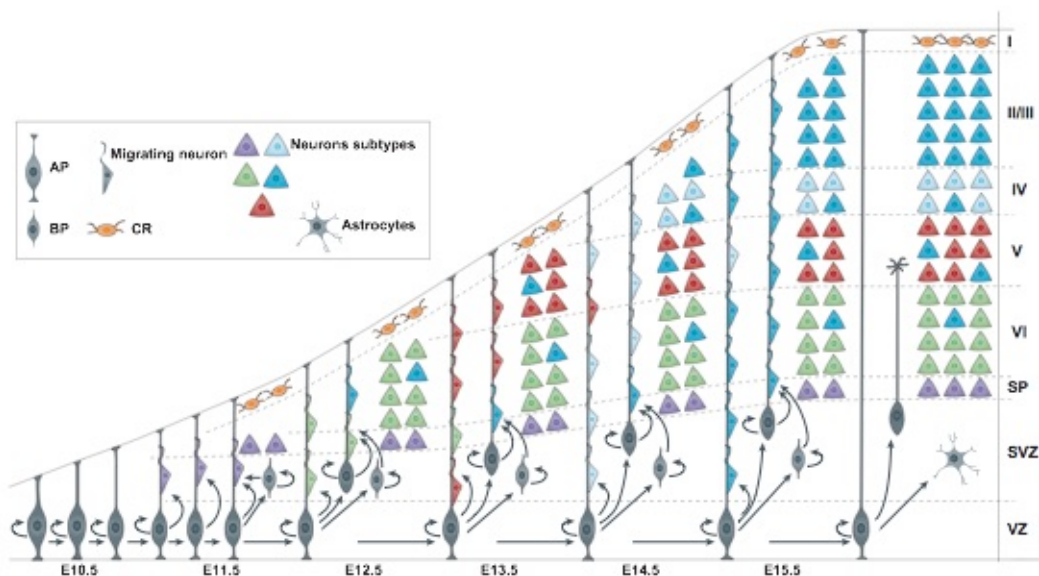


Figure 1.5: Projection neurons are produced in an inside-out fashion.

APs in the VZ undergo rounds of proliferative divisions and produce BPs that migrate into the SVZ. Neurons are generated in the VZ and SVZ and migrate along the AP processes to the cortical layers that form sequentially (Adapted from (Greig et al., 2013)).

During radial migration, the centrosome together with the microtubule cytoskeleton advance towards the swellings suggestively pulled by dynein (Tsai et al., 2007). The nucleus follows the centrosome and microtubules but often with a substantial delay

and physical separation, this could be due to the weaker molecular links between the centrosome and nucleus compared to other cell types i.e. fibroblasts (Solecki et al., 2004; Tsai et al., 2007). The process of nucleus translocation of the nucleus into the proximal leading process during radial migration is known as nucleokinesis. An adaptation to the extreme resistance to nuclear movement is the involvement of Myosin II in nuclear movement. Inhibition of myosin II perturbed nuclear behavior in neocortical embryonic rat slices although it did not affect centrosome movement in migrating neurons (Tsai et al., 2007). In tangentially migrating neural precursors Myosin II was concentrated at the rear of the nucleus, suggesting that myosin II-mediated actin contractility might serve to push the nucleus forward from behind (Bellion et al., 2005; Tsai et al., 2007).

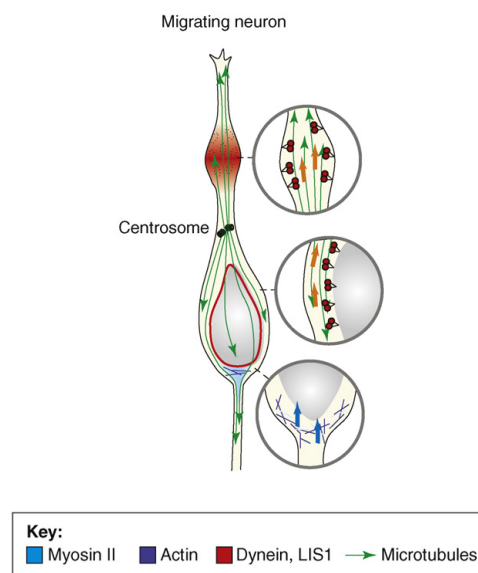


Figure 1.6: Dynein and Myosin II act interdependently to mediate nuclear migration.

Microtubules emanate from the centrosomal region and extend outward in both the migratory and the axonal processes. Myosin II-mediated actin contractility pushes the nucleus forward from behind. For explanation see the main text (adapted from (Vallee et al., 2009)).

1.3 Molecular control of neurogenesis in neocortex

In the developing cortex, the acquisition of radial glial features, proliferation versus differentiation of progenitors, the promotion of neurogenesis and subsequent termination of neurogenesis are tightly regulated process in space and time. These involve a complex network of extrinsic signaling that mediate intrinsic transcriptional changes, both ultimately direct cell fate through regulation of gene expression.

Frequently, the same signaling pathway may operate differently in neighboring cells or even in the same cell at different stages causing completely different effects. This is thought to be due to the variation in the effector molecules availability in different cells and the epigenetic states of the target genes (reviewed in (Martynoga et al., 2012)).

1.3.1 Signaling pathways influencing the onset and progression of neurogenesis

The Notch pathway has a well-established role in maintaining the undifferentiated state in progenitors in CNS (Artavanis-Tsakonas et al., 1999). However, it is now evident that Notch signaling has a more complex role in neural development. In the dorsal telencephalon, the transition from NE to RG has been shown to be induced by Notch signaling (Hatakeyama et al., 2004). Notch signaling is activated through its major ligand Delta-like 1 (Dll1), leading to expression of the downstream main effector transcription repressors, Hes1 and Hes5. Another direct target of Notch pathway is the Neuregulin receptor ErbB2, which through its ligand Neuregulin 1(Nrg1), promote RG identity (Schmid et al., 2003). Notch pathway is not only essential for RG development but also their maintenance in undifferentiated state as the activation of Notch was reported to inhibit the development of RG into BPs (Hatakeyama et al., 2004).

In a similar fashion to Notch, the *fibroblast growth factor receptor 2* (Fgfr2) acts through its ligand Fgf10 to promote acquisition of RG cell identity (Yoon et al., 2004). FGF ligands also promote proliferation of cortical progenitors and inhibit neurogenesis by regulating the duration of the cell cycle (Raballo et al., 2000). It has been shown that FGF2 upregulates the expression of cyclin D1 and down regulates the expression of the cyclin dependent kinase (cdk) inhibitor p27 (Kip1) (Lukaszewicz et al., 2002). Indeed, a shorter duration of the cell cycle, particularly the G1 phase, is a feature of proliferative divisions in progenitors (Calegari et al., 2005; Lange et al., 2009; Lukaszewicz et al., 2005). Thus, FGF signaling is also important to slow down the progression of RG to BPs.

Another important determinant for progenitors proliferation is *Wnt signaling*. Wnt activity in the CNS is complex and time-dependent (Martynoga et al., 2012). In early stages, canonical Wnt signaling, involving β -catenin, promotes progenitors proliferation in developing cortex. On the other hand, at a later stage (after E13.5 in mouse), Wnt activity shifts to promote neurogenesis presumably by inducing the

expression of the proneural genes neurogenin1 and neurogenin2 (Ngn1 and Ngn2, see below). FGF2 signaling has been proposed to influence the choice between the proliferative and the differentiative activity of Wnt/ β -catenin signaling, however refuting data for this also exist (Martynoga et al., 2012; Tiberi et al., 2012).

Similar to Wnt, the *bone morphogenetic proteins (BMPs)* have been shown to have complex inputs depending on the developmental stage. In early cortical progenitors (mouse E12-E13) BMP induces neurogenesis (Li et al., 1998), however after E14, BMPs block neurogenesis and promote astrocyte differentiation (Gross et al., 1996), that in standard conditions, starts after termination of neurogenesis.

1.3.2 Transcriptional control of neurogenesis

The basic-helix-loop-helix (bHLH) family are a large family of transcription factors, several of them have been implicated in the formation of cortex with pro-neural or anti-neural effects (Ross et al., 2003). Two classes of inhibitory bHLH proteins are involved in maintaining a proliferative undifferentiated state of the progenitors, Hes and Id factors. The Id factors promote cell cycle progression through interacting with components of the cell cycle machinery. They also inhibit the activity of some proneural bHLH factors through sequestering E proteins that are needed for their activity (Norton, 2000; Ross et al., 2003). In addition, Hes1 and Hes5, acting downstream of Notch signaling, antagonize the effect of the proneural genes through two distinct mechanisms. First, Hes proteins form homo and heterodimers with close family members and bind DNA elements (CACNAG) to repress the expression of target genes, such as Mash1, that is required for neural differentiation (Davis and Turner, 2001). Alternatively, Hes factors interact physically with the proneural bHLH proteins, therefore recruited to the bHLH downstream target sites. Through recruitment of repressors, Hes proteins inhibit proneural bHLH activity on downstream targets (Sasai et al., 1992).

On the other hand, for a cell that is specified to a neuronal fate, the transition from proliferation to neurogenesis involves a coordinate increase in the proneural bHLH activity and decrease in Hes and Id activity. Neurogenesis is mediated through two broad classes of bHLH factors; proneural factors involved in initiating neurogenesis (e.g., Ngn1, Ngn2 and Mash1) and neuronal differentiating factors involved in mediating terminal differentiation (e.g., NeuroD) (Ross et al., 2003). Both classes are transcriptional activators that bind DNA after formation of heterodimers with the

corresponding E protein (Bertrand et al., 2002). The transactivation is mediated through interaction with chromatin remodeling factors such as the histone acetylases p300/CBP and PCAF and leads to activating the effectors of neuronal differentiation (Roth et al., 2001). Proneural genes, Ngn1 and Ngn2 and to a less extent Mash1 start to be expressed in the radial glial cells of the developing cortex and their expression allows the asymmetric division into non equal descendants, one of them is a neurogenic progenitor or a neuron. Newly formed neurons upregulate Dll1, the Notch ligand, that acts on the adjacent progenitors blocking their differentiation in a process known as lateral inhibition. Thus, lateral inhibition only allows some progenitors to differentiate into neurons. As these neurons migrate away from the germinal layers into the CP, the effect of inhibition is diluted allowing another cascade of neurogenesis to take place (Ross et al., 2003).

Upstream of the bHLH proneural genes, *paired homeobox factor 6* (Pax6), is a transcription factor that plays an important role in neurogenesis. Pax6 is expressed both in NE and RG cells and was found to regulate the balance between proliferation and differentiation in the developing cortex (Guillemot, 2007). Pax6 has two different protein subdomains that have opposite effects in regulating pro- or anti-proliferative factors in progenitors (Walcher et al., 2013). Defects in progenitors division and brain growth was observed in mutant mice for, besides Pax6, the homeobox proteins Lhx2 and Arx, in addition to the winged-helix protein Foxg1 and the nuclear receptor Tlx (reviewed in (Martynoga et al., 2012)). The proliferative mechanism of Pax6 involves induction of multiple gene targets including transcription factors, signaling molecules and cell cycle regulators i.e. cdk4. Moreover, Pax6 can instructively promote neurogenesis in progenitors through induction of Ngn2 expression (Scardigli et al., 2003). However, Pax6 was also shown to reprogram astrocytes into neurons through an Ngn2-independent mechanism (Heins et al., 2002).

Another group of transcription factors named the SoxB genes, were shown to inhibit neurogenesis (Bylund et al., 2003). SoxB proteins, Sox1, Sox2 and Sox3 play an important role in maintaining the undifferentiated state of neural stem cells. Sox1-3 block the proneural bHLH protein activity through an unidentified mechanism. For neural stem cells to differentiate, SoxB genes are, then, suppressed. This is achieved by proneural genes that either directly repress Sox1-3 genes expression or through the upregulation of the Sox21 gene expression (Bylund et al., 2003; Sandberg et al.,

2005). Sox21 protein blocks the activity of Sox1-3, presumably by blocking their targets therefore promoting neurogenesis.

At the transition from RG to BPs another set of transcription factors were found to be crucially involved. Ngn2, Insm1 and AP2 γ can induce the expression of the T-box protein Tbr2, a transcription factor that is required for production of BPs and is specifically expressed in the SVZ of the cortex (reviewed in (Martynoga et al., 2012)). Tbr2, also called Eomes, promote differentiative divisions in the APs, increasing the proportion of basally dividing progenitors when expressed (Sessa et al., 2008). Foxg1, subsequently, acts to promote the division of BPs in the cortex (Siegenthaler et al., 2008).

For neuronal differentiation, neurogenins induces the sequential expression of the NeuroD family belonging to the bHLH proteins (Guillemot, 2007). In addition, Tbr1 that is required for the differentiation of cortical neurons is also induced (Hevner et al., 2006).

1.3.3 Epigenetics, Post-translational modifications and more

Additional levels of complexity are elucidated in the involvement of posttranslational modifications, epigenetics, alternative splicing and non-coding RNAs. For example, TRIM32 is expressed in RG cells and is asymmetrically divided in the daughter cells. The TRIM32-inheriting daughter cell is prone to differentiate into a neuron (Schwamborn et al., 2009). Two mechanisms were shown for TRIM32 activity; first, it enhances the degradation of the pro-proliferative protein c-Myc owing to its ubiquitin ligase activity. Second, through binding to the Argonaute complex, it promotes the activity of Let-7, a microRNA that promotes neuronal differentiation. Similarly, Huwe1 is an E3 ubiquitin ligase that degrades n-Myc, which can no longer activate the Notch ligand Dll3, promoting neurogenesis in the cortex (Zhao et al., 2009). On the other hand, the E3 ubiquitin ligase TRIM11, promotes the degradation of Pax6 and therefore suppresses neurogenesis (Tuoc and Stoykova, 2008).

Epigenetic modifications provide another level of control of gene expression. The polycomb complex members Ring1b or EZH2 catalyze the tri-methylation of lysine 27 on the tail of histone 3 (H3K27me3) thereby repressing the transcription of Ngn1 and inhibiting neurogenesis (Hirabayashi et al., 2004). On the other hand, induction of Jmid3, an H3K27me3 demethylase, by retinoic acid pathway was proven to activate genes associated with neurogenesis in cortical progenitors (Jepsen et al., 2007). Apart

from chromatin histone modifications, direct methylation of DNA by Dnmt1 causes a premature termination of neurogenesis by adding the methyl group, repressive mark, to the target genes (Fan et al., 2005). And recently, our group showed that the sites of decreased DNA methylation increase the DNA hydroxymethylation and this is correlated to the upregulation of neurogenic genes (Noack et al, in progress).

In the above review, I aimed to give a brief, yet incomprehensive, overview of the main regulators of neurogenesis in the developing cortex. To date, the understanding of the interactions between the signaling pathways and the transcription factors is far from being complete, which prompts further studies at genetic, epigenetic, transcriptional and translational levels to approach a better understanding of this complex process.

In the recent years, a class of non-coding RNAs, the so-called long non-coding RNAs (lncRNAs), has received a lot of attention in the context of neurogenesis. Owing to their different modes of action, lncRNAs were shown to modulate neurogenesis at epigenetic, transcriptional, posttranscriptional and posttranslational levels (reviewed in (Aprea and Calegari, 2015). What are lncRNAs, what are their different subtypes, what functions do they have and what are their mechanisms of action are all questions whose answers are, to date, expanding.

1.4 Long non-coding RNAs

lncRNAs are a class of regulatory non-coding RNAs that are more than 200 base pair long (Rinn and Chang, 2012). Unlike the small non-coding RNAs that are 18 to 32 nucleotides long including miRNAs, siRNAs and piRNAs and have a role in post-transcriptional regulation of gene expression (Pauli et al., 2011), the functions of lncRNAs are much more diverse. lncRNAs lack a coding potential of messenger RNAs (mRNAs), this is identified by the lack of a conserved open reading frame (ORF) or the lack of an ORF that is more than 100 amino acids in length (Dinger et al., 2008; Ulitsky and Bartel, 2013). Due to the absence of a protein product, lncRNAs are thought to mediate their functions through their RNA secondary structures (Kapusta and Feschotte, 2014).

1.4.1 General characteristics of lncRNAs

lncRNA molecules are generally similar to mRNAs. They are transcribed by RNA polymerase II are mostly polyadenylated, and have a 5' cap (Ulitsky and Bartel, 2013). An exception to the polyadenylation is the emerging group of circular RNAs (Salzman et al., 2012), lncRNAs flanked by snoRNAs (Yin et al., 2012) or those with a triple helical structure at their 3' end (Wilusz et al., 2012). lncRNAs have shorter sequences than protein coding genes and have lower number of exons (2-3 exons on average). lncRNAs also undergo alternative splicing, though splicing is thought to be less efficient (Ulitsky and Bartel, 2013). On the other hand, lncRNAs have lower sequence conservation compared to mRNAs and their expression was found to be almost ten times lower than mRNAs (Guttman et al., 2009; Ulitsky and Bartel, 2013). Because of these differences, lncRNAs have long been thought to be byproducts of transcription from cryptic promoters or intergenic sequences that happen to have high affinity for the transcription machinery (Khaitovich et al., 2006; Ulitsky and Bartel, 2013). This transcription will result in lowly expressed and unstable transcripts that lack signs of sequence conservation. This argument is, however, debated owing to the clear signs of evolutionary conservation in certain lncRNAs (discussed below). Moreover, as a group, they present a wide range of transcript half-lives similar to that of mRNAs, thus they are not regarded as unstable transcripts (Clark et al., 2012). Furthermore, lncRNAs have shown a tissue-specific or, even, cell specific expression pattern that is suggestive of their functional roles (Djebali et al., 2012). In addition, even lowly expressed lncRNAs may have a regulatory function that does not require a high concentration of the effector molecule. Finally, many lncRNAs are currently phenotypically or mechanistically validated (Aprea and Calegari, 2015; Geisler and Collier, 2013).

Subclasses of lncRNAs

Based on their genomic context, lncRNAs are further classified into subclasses (Hrdlickova et al., 2014). lncRNAs can be transcribed overlapping with a protein coding genes, these include: antisense, sense intronic, and sense overlapping transcripts. Antisense transcripts are lncRNAs that are expressed from the opposite strand of protein coding genes, these are further subdivided into natural antisense transcripts and intronic lncRNAs. Sense intronic lncRNAs are those expressed from the introns on the same strand of a protein coding gene. Conversely, sense

overlapping transcripts, are also expressed from the same strand of a protein coding gene, however they contain the sequence of the protein coding gene in their introns (Figure 1.7). Another subclass comprises long intergenic non-coding RNAs (lincRNAs) that do not overlap with any protein coding genes and sometimes expressed from “gene deserts”. lincRNAs might also be transcribed from active enhancers to produce long, polyadenylated and spliced transcripts (Koch et al., 2011). These are different from the enhancer RNAs (eRNAs) which are bidirectionally transcribed from active enhancers producing shorter, unspliced, unpolyadenylated and unstable transcripts.

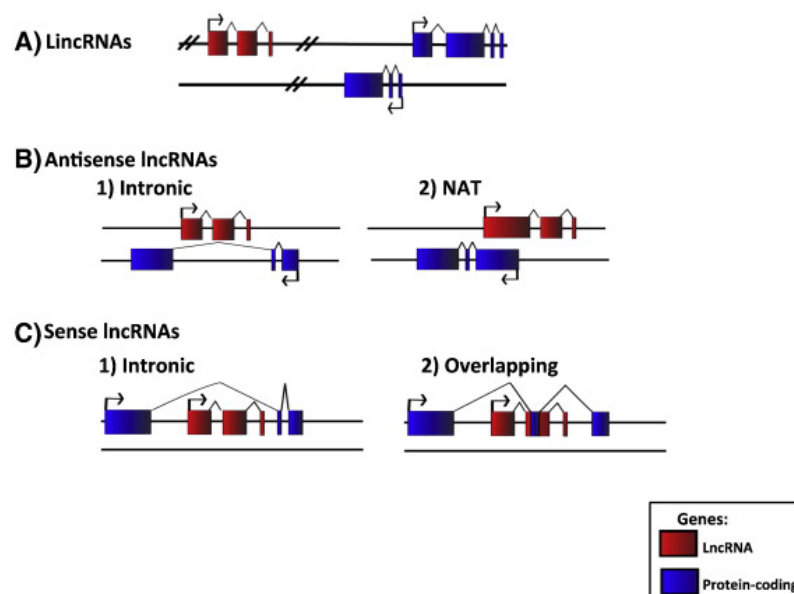


Figure 1.7: subclasses of lincRNAs.

A: lincRNAs do not overlap with protein coding genes on the sense or antisense strands. B: Antisense lincRNAs are transcribed from the opposite strand of protein coding genes and further subdivides into NATs and Intronic. C: Sense lincRNAs are either Intronic that are generated from the introns of a protein coding genes, or Overlapping which contains the exons of protein coding genes in their introns (Adapted from (Hrdlickova et al., 2014).

Evolutionary conservation of lincRNAs

lincRNAs present a lower signal of sequence conservation compared to mRNAs, however, there are concerns on the sequences used as controls in these conservation analysis. Sequences of lincRNAs are distinctly more conserved than ancient repeats and they present higher signals of sequence conservation at splice site, exons and in small domains surrounded by less constrained sequences (Guttman et al., 2009; Ponjavic et al., 2007). In addition, many lincRNAs have a recent evolutionary origin; while the majority are primate-specific and some are rodent-specific, only 3 % of the lincRNA families have originated more than 300 million years ago (Derrien et al.,

2012; Necsulea et al., 2014). Interestingly, sequence conservation in the primate-specific lncRNAs is even lower than random intergenic regions whereas ancestral lncRNAs present sequence constraints similar or even higher than coding sequences (Necsulea et al., 2014). Because the functional unit in lncRNAs is the RNA structure, which can tolerate mutations as long as the intramolecular folding or intermolecular interactions are maintained, sequence conservation probably lacks sensitivity to detect lncRNAs' evolutionary constraints. Therefore the study of evolutionary conservation of RNA secondary structure might be more relevant (Kapusta and Feschotte, 2014). Some efforts were successful in this aspect; some human lncRNAs have been shown to be enriched in evolutionarily conserved RNA structures that do not overlap with any sequence-constrained element (Aprea and Calegari, 2015). A good example of that is Xist, a lncRNA with a poor sequence conservation. Xist contains tandem repeats in its 5' region that are proposed to be important for its function (Wutz et al., 2002; Zhao et al., 2008). Conversely, stretches with higher sequence conservation in Xist do not seem to be functional (Brockdorff, 2002). It's worth mentioning that, still, methods for detection of RNA secondary structures are still noisy and prone to false positives.

Another useful method to study evolutionary conservation is by investigating the presence of ortholog loci that present similar transcriptional regulation and display similar expression patterns across species. In this context, the proportion of human lncRNAs with orthologous transcripts increases from one third among placental mammals to 63-72% in primates and 80-92% in hominids, this is higher than expected by chance (Necsulea et al., 2014). At the level of transcriptional regulation, promoters of lncRNAs show conservation levels identical to those of protein coding genes (Guttman et al., 2009; Ponjavic et al., 2007). Moreover, sequence conservation of transcription factor-binding sites is even stronger than in protein coding genes (Necsulea et al., 2014). Consistently, their tissue-specific expression patterns (described below) seem to be remarkably conserved among primates and across mammals.

1.4.2 Versatile mechanisms of lncRNAs

With thousands of documented lncRNAs, we are still far from ascribing biological functions to the vast array of non-coding transcripts.

One of the most well studied roles of lncRNAs is their ability to control protein-coding gene expression in *cis* and in *trans*. A common mechanism was illustrated in which lncRNAs regulate transcription through chromatin modulation (reviewed in (Geisler and Collier, 2013)). This function is suggestively conserved across a broad range of eukaryotes. Numerous lncRNAs physically associate with histone modifying complexes and target them to specific loci. One such example is the human lncRNA HOTAIR (Hox transcript antisense RNA) which physically associates with Polycomb repressive complex 2 (PRC2) as well as lys-specific demethylase 1 (LSD1) (Tsai et al., 2010). PRC2 and LSD1 are responsible for the deposition of the repressive histone mark H3K27me3 and removal of active H3K4me2 marks, respectively. ANRIL (also known as CDKN2B antisense RNA) binds PRC1 and PRC2 (Kotake et al., 2011; Yap et al., 2010). These lncRNAs and many others have been proposed to function as scaffolds that coordinate the targeting of distinct repressive histone modifying complexes to target loci. However, it remains unclear how those lncRNAs target specific DNA regions. In other cases, the act of transcription itself at the gene locus rather than the lncRNA product is required for silencing, where the movement of the polymerase along the DNA locus can result in deposition of histone modifications which in turn repress expression from nearby promoters. Transcription of lncRNAs can also result in chromatin remodeling that can either favor or inhibit the binding of regulatory factors leading to, depending on the regulatory factor, gene activation or repression (Geisler and Collier, 2013).

Aside from modulating chromatin, lncRNAs can influence the transcription machinery directly. One such example are lncRNAs that are generated from Alu SINE elements. These interact with polymerase II inhibiting the transcription of target mRNAs during heat shock (Mariner et al., 2008). Furthermore, many lncRNAs can regulate the binding and/or activity of transcription factors on their downstream target genes. One such example is paupar, a lincRNA that is transcribed from an enhancer region 8.5 kb away from pax6 (Vance et al., 2014). The expression of Paupar in the CNS correlates with Pax6 and Paupar was shown to directly control the transcription of pax6. Moreover, Paupar apparently interacts with Pax6 and other neural

transcription factors to target specific genomic regions thereby affecting neural stem cell fate.

In addition to their modes of regulating transcription, NAT antisense lncRNAs have been shown to influence how an mRNA arising from the sense strand is processed. In some instances, the NAT and pre-mRNA form RNA-RNA duplexes thereby inhibiting splicing (Krystal et al., 1990; Munroe and Lazar, 1991). On the other hand, MALAT1 lncRNA affects splicing through interacting with and influencing the nuclear distribution of active Ser/Arg splicing factors (Tripathi et al., 2010). Similarly, snoRNAs, a new class of lncRNAs flanked with small nucleolar RNA sequences, influence splicing via physical interactions with an alternative splicing regulator i.e. FOX2 (Yin et al., 2012).

lncRNAs can, as well, regulate mRNA translation and miRNA mediated repression. Those functions are performed through base pairing between the mRNA and the effector domains in the ncRNA sequence. lncRNAs inhibit miRNA mediated repression by acting as decoys or sponges that sequester the miRNA inhibiting it from binding its target mRNAs. Moreover, lncRNAs can also alter mRNA stability by competitively binding DICER thus preventing the processing of small RNAs. Alternatively, lncRNAs may bind TDP43 that is implicated in pre-mRNA splicing, mRNA transport, translation and stability. This binding can result in either stabilization or destabilization of mRNA targets (reviewed in (Geisler and Coller, 2013)).

Although various functional roles are now attributed to lncRNAs, it is likely that as we dig deeper into the molecular biology of lncRNAs more functions will emerge.

1.4.3 Expression patterns of lncRNAs

lncRNAs present cell, tissue and/or developmental specific expression patterns to a degree higher than that of protein coding genes (Derrien et al., 2012; Djebali et al., 2012; Guttman et al., 2009). These expression patterns are characteristic of genes with regulatory functions. Expression specificity of lncRNAs is an evidence of their functional roles in cell identity and in development as it is unexpected for non-functional transcripts to be expressed more specifically than protein-coding genes and to have tissue-specific splicing patterns (Aprea and Calegari, 2015). Another important feature of lncRNAs is their preferential genomic localization in proximity to or overlapping developmental regulators or transcription factors (Guttman et al.,

2009; Pauli et al., 2011; Ponjavic et al., 2007). This feature supports their role in development and is perhaps related to their specific expression patterns. Many studies have shown that the expression of lncRNAs positively correlate with those of neighbouring protein coding gene, suggestive of their role in regulating nearby gene expression in *cis* (Derrien et al., 2012; Guttman et al., 2009; Ponjavic et al., 2007). This was, indeed, proven for at least some lncRNAs including HOTTIP that was shown to activate HOXA genes across 40 kb (Wang et al., 2011). However, the tight correlation between lncRNAs and neighbouring genes expression does not exclusively reflect a *cis*-regulatory function. In fact, the tight correlation might reflect the involvement of lncRNAs in biological pathways similar to those of the neighboring protein-coding genes. That was shown for HOTAIR that is expressed antisense to the HOXC genes. HOTAIR represses the HOXD locus on another chromosome by recruiting the polycomb repressive complex 2 (PRC2) through direct interaction with the SUZ21 subunit (Rinn et al., 2007). Thus, HOTAIR is not involved in regulating HOXC genes in *cis* but rather involved in the same biological process as HOXC by controlling embryonic body plan through HOXD expression.

Brain-specific lncRNAs

The organ where lncRNA function appears to be particularly relevant is the brain, where lncRNAs seem to act as novel regulators in the temporal and spatial control of its developmental programme, cell fate and function (Aprea and Calegari, 2015). lncRNAs expressed in the brain present a higher degree of evolutionary conservation. Furthermore, brain-expressed lncRNAs have been found to be enriched in predicted conserved RNA structures which is more likely to present conserved functions (Ponjavic et al., 2009). Interestingly, the brain is the organ expressing the largest number of lncRNAs and the highest proportion of tissue-specific lncRNAs in species ranging from fly to humans (Derrien et al., 2012; Necsulea et al., 2014). This tissue specificity shows a remarkable conservation across species. Furthermore, within the brain, lncRNAs show high temporal and spatial specificity where lncRNAs in cortex, cerebellum and hippocampus are differentially expressed over time and/or brain areas in development and adulthood (Mercer et al., 2008). These expression patterns showed specificity even greater than those of protein-coding genes (Ramos et al., 2013). Moreover, transcriptome analysis of specific cell types coexisting in the developing cortex has identified lncRNAs selectively expressed in neural stem cells as opposed to neurogenic progenitors or newborn neurons (Aprea et al., 2015, 2013).

These cell-type specific expression patterns point to lncRNA contribution to cell fate, lineage specification and maintenance of cell identity during the development of the mammalian cortex.

1.4.4 lncRNAs in neurogenesis

Several lncRNAs have been characterized to play a role in the complex process of neurogenesis, most of which acting through regulating the neighbouring transcription factors. Among the validated lncRNAs, many overlap active enhancers or localize within 50 kb of transcription factors centrally involved in neurogenesis. Besides Paupar's regulation of Pax6 (Vance et al., 2014), Emx2OS, whose transcription start site overlaps Emx2 first exon, has been shown to regulate the expression of EMX2, a homeodomain transcription factor regulating proliferation and differentiation in the CNS (Spigoni et al., 2010) (Figure 1.8A and B). Similarly, utNgn1 regulates Ngn1, the bHLH transcription factor promoting neuronal differentiation in the neural tube (Onoguchi et al., 2012). Likewise, Evf2, also called Dlx6os, a lncRNA conserved in vertebrates and transcribed antisense to Dlx6, acts as a transcriptional regulator of its own locus both in *cis* and in *trans* and its absence leads to defects in interneuron generation (Bond et al., 2009; Kohtz, 2014)(Figure 1.8C). Moreover, Nkx2.2 and Six3 are homeodomain transcription factors expressed in the ventral neural tube and regulated by the lncRNAs, Nkx2.2AS and Six3OS, respectively (Aprea and Calegari, 2015)(Figure 1.8D and E). These lncRNAs are transcribed from the opposite strand of the neighbouring protein-coding gene and share their expression patterns.

An example of a lncRNA modulating a neighbouring gene at a post-transcriptional level is Fgf2-AS. Fgf2-AS is expressed from the opposite strand of Fgf2, a morphogen involved in the maintenance of neural progenitors proliferation at the onset of corticogenesis. Overexpression of Fgf2-AS was shown to inhibit proliferation by reducing Fgf2 mRNA stability and translation efficiency. It is thought the Fgf2-AS exerts its effects on Fgf2 through base pairing between Fgf2-AS and Fgf2 3'UTR in an Ago2-dependent mechanism (Li and Murphy, 2000; MacFarlane et al., 2010).

lncRNAs can also act exclusively in *trans* to regulate neurogenesis. A good example of which are Rmst and Tuna, two long non-coding RNAs (lncRNAs) that have been shown to modulate Sox2 actions in neurogenesis. Rmst is a transcriptional coregulator of Sox2, where its upregulation during neuronal differentiation is required for Sox2 binding at loci of genes involved in neuronal function (Ng et al., 2013). On the other

hand, Tuna was shown to form an RNA-multiprotein complex that acts at the Sox2 gene promoter (Lin et al., 2014)(Figure 1.8F). The knockdown of Tuna in mESC and developing zebrafish downregulated genes involved in neurogenesis and cell proliferation resulting in reduced differentiation (Lin et al., 2014; Ulitsky et al., 2011). Last but not least, Miat is a lncRNA with orthologs in *Xenopus*, chicken, mouse and human (Rapicavoli et al., 2010). In the developing cortex, Miat was shown to induce the generation of committed progenitors and altering their fate from differentiation to proliferation (Aprea et al., 2013). Miat has been found to interact with the splicing factors SF1, QK1 and SRSF1 and is thought to cause alternative exon usage of cell fate determinants (Barry et al., 2014; Rapicavoli et al., 2010; Tsuiji et al., 2011)(Figure 1.8G).

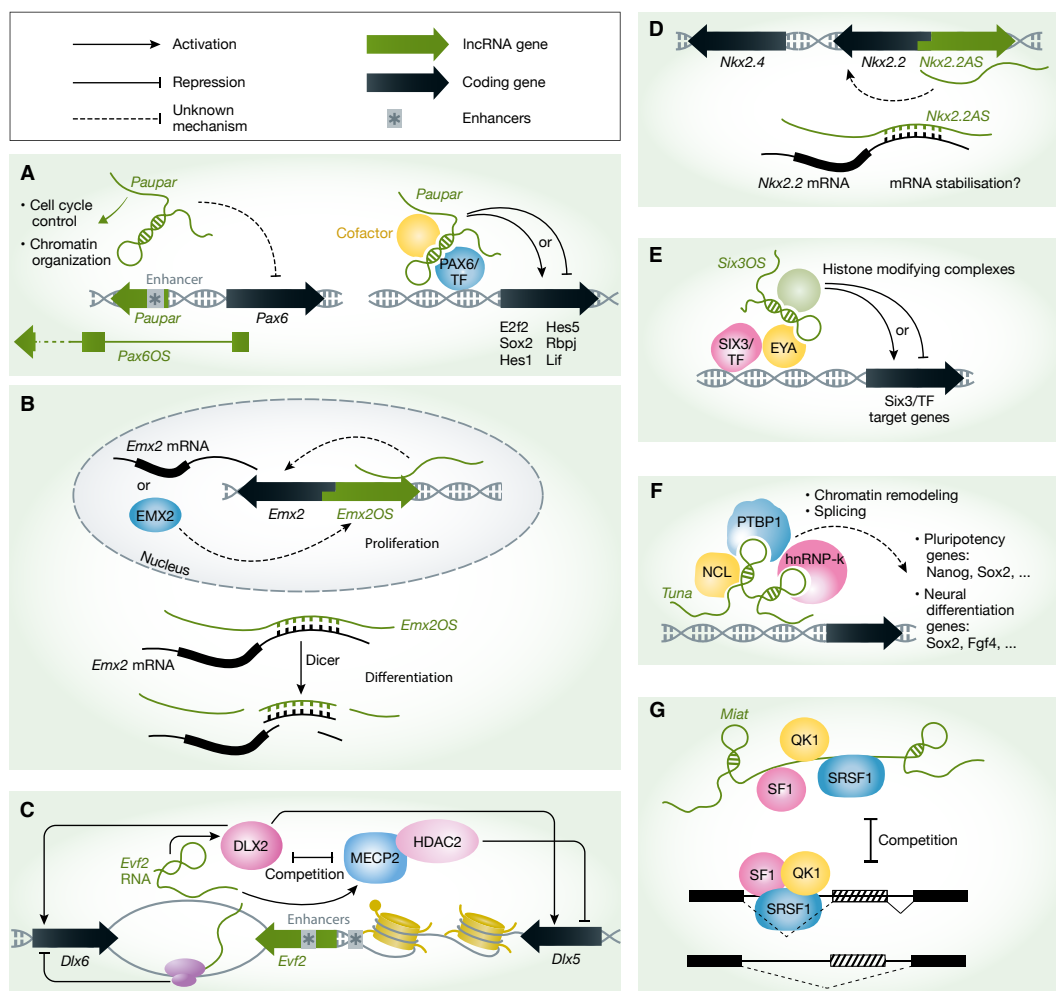


Figure 1.8: Different roles of lncRNAs in neurogenesis.

For explanation, see the main text. (Adapted from (Aprea and Calegari, 2015)).

The number of characterized lncRNAs in neurogenesis at a phenotypic or mechanistic level does not well represent the hundreds of lncRNAs that are expressed in the CNS. Unraveling new roles of lncRNA in neurogenesis necessitates identifying their cell specific expression in the cell-intermingled developing brain. This implies studying the expression of lncRNAs in systems that allows the discrimination between the proliferating stem cells, the committed progenitors and the terminally differentiated neurons during development.

1.5 Btg2^{RFP}/Tubb3^{GFP} mouse line to study cortical development

Several efforts have been made to discriminate cell types in the developing cortex. In these studies, single reporter mouse lines were generated to identify BPs (Tbr2⁺), DPs (Btg2⁺) or neurons (Tubb3⁺) (Attardo et al., 2008; Haubensak et al., 2004; Kwon and Hadjantonakis, 2007). However, due to the transient nature of progenitors and the inheritance of the reporter protein from the developing mother, these strategies were not perfectly achieving homogenous cell population. Complementing the past efforts, our lab previously generated a double transgenic mouse line that allows the discrimination between proliferating progenitors (PPs), differentiating progenitors (DPs) and neurons (Aprea et al., 2013). In our double reporter mouse line, DPs were identified by RFP that was expressed under the promoter of Btg2, while neurons were identified by the expression of GFP under the control of Tubb3. Double transgenic embryos at mid neurogenesis (E14.5), as identified by their colours using whole-mount stereomicroscopy, were used to isolate PPs (RFP⁻/GFP⁻), DPs (RFP⁺/GFP⁻) and neurons (RFP⁺/GFP⁺) by fluorescent activated cell sorting (FACS). After extraction of total RNA, the poly(A) fraction was enriched and libraries for massive parallelized sequencing were prepared from each population in three biological replicates. Sequencing was performed on the Illumina HiSeq2000 platform, resulting in 30–40 million reads per sample, a depth sufficient to achieve high transcriptome coverage for robust differential analyses of gene expression.

The success of isolating the different cell populations was evident from the validation of the differential expression of specific cell markers. For APs/PPs, these included nestin, Glast (Slc1a3), vimentin, Fabp7, Pax6 as well as markers of proliferating neural (and other somatic) stem cells such as Notch1, noggin, Nanog, Sox2 and

musashi that were all >2-fold down-regulated in RFP⁺ relative to RFP⁻ cells and virtually absent in GFP⁺ cells. Conversely, markers of BPs/DPs, including *Tbr2*, *Insm1*, *Neurog2*, *Emx1*, *Dll1* and *Btg2* itself as well as markers of early neurogenic commitment such as *Neurod1*, *Insc*, *Numbl* and *Ascl1* were also >2-fold down-regulated in both RFP⁻ and GFP⁺ relative to RFP⁺ cells.

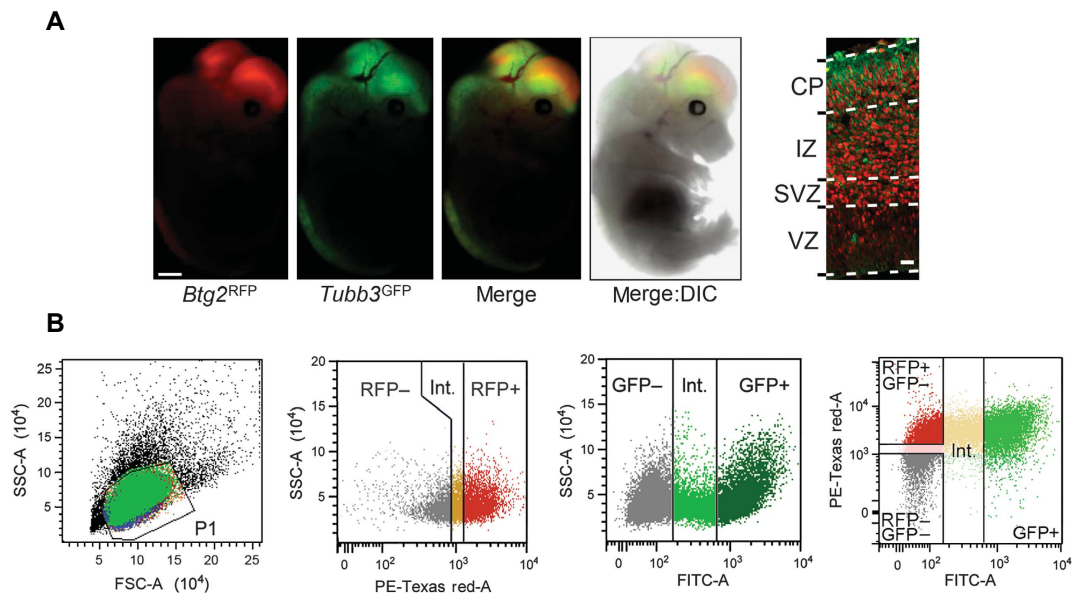


Figure 1.9: Generation of the double transgenic mouse line.

A: RFP is expressed under the promoter of *Btg2* in differentiating progenitors, while GFP is expressed in under the promoter of *Tubb3*. B: FAC sorting of the three cell populations, PP (RFP⁻), DP (RFP⁺), neurons (GFP⁺, adapted from (Aprea et al., 2013))

While the neuronal markers *Tubb3*, *Tbr1*, *Dcx* as well as neuronal-specific cytoskeletal and synaptic genes, pumps, channels and receptors (*Nefm*, *Eno2*, *Elavl3*, *Snap25*, *Gabrg2*, *Syp* and *Chgb*) were absent in both RFP⁻ and RFP⁺ as compared to GFP⁺ cells.

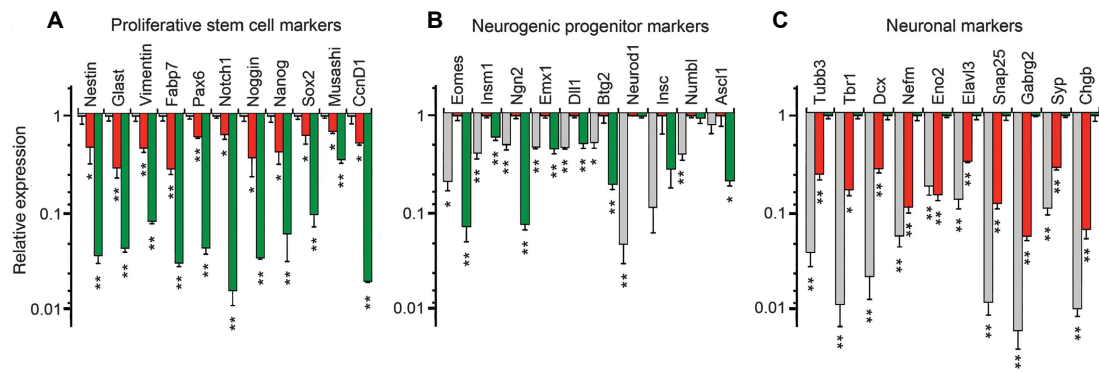


Figure 1.10: Validation of cell population isolation.

The transcriptome generated from the double transgenic mouse line shows enrichment of cell specific marker in the respective population. Normalized counts in cell type (colours) are represented on a logarithmic scale relative to the population of reference within each panel. By this, the expression of markers of PPs, DPs and neurons is defined = 1 in A, B and C panels, respectively. Error bars = standard deviation; *P<0.05; **P<0.005 (Adapted from (Aprea et al., 2013)).

The transcriptome generated from the 3 cell populations comprised a comprehensive list of protein coding genes and a catalogue of 2762 annotated lncRNAs (Aprea et al., 2015, 2013). Although many of the protein-coding genes have a known function, most of the lncRNAs were not studied in the context of neurogenesis or not yet studied at all. Interestingly, our group previously described the involvement of TOX, a protein-coding gene, and Miat, a lincRNA, in corticogenesis (Aprea et al., 2013; Artegiani et al., 2015). In addition, using Cufflinks, novel transcripts were predicted to be expressed in the developing brain. These transcripts are not associated or in close proximity (<2000 bp) with any annotated transcript. The sequencing reads were re-aligned to the genome and were predicted to be novel lncRNAs as they lack the protein-coding conservation signatures (Aprea et al., 2015).

The high abundance of lncRNAs in the developing brain and the availability of the tool that allowed identification of their cell-specific expression, promoted the characterization of new roles of lncRNAs in neurogenesis.

1.6 Aim of the study

As lncRNAs are highly expressed in the brain, and showing an interesting tissue and/or cell specific expression patterns, this study aims at identifying new roles for relevant lncRNAs in neurogenesis.

During the last decades, much attention was given to miRNAs that were shown to play vital roles in neurogenesis through their post-transcriptional gene repression. Recently, growing interest was directed to lncRNAs owing to their versatile functions and mechanisms of action. Increasing evidence has supported the pivotal roles of lncRNAs in development. Particularly in brain development, reports are accumulating for lncRNAs to mediate changes in gene expression, epigenetic changes and post-transcriptional/translational modifications. With the scientific urge to understand the molecular cues that govern the balance between proliferation and differentiation in the developing cortex, the key factors responsible for the switch in the mode of division of progenitors and neuronal organization and maturation, lncRNAs present themselves to be targets for extensive research.

Many of the functional studies of lncRNAs have been performed in *in vitro* systems. In this study, I aim to functionally validate the role of at least one lncRNA in the developing cortex. With the aid of the transcriptome generated from our double reporter mouse line, candidate lncRNAs will be selected for phenotype screens. Using *in utero* electroporation, the effects of manipulating lncRNA expression during development will be traced. lncRNA's effects will be characterized at a cellular and molecular level. Using multiple molecular biology and bioinformatics tools, I aim to unravel new roles of lncRNAs in brain development.

Chapter 2

2 Materials and Methods

2.1 Materials

2.1.1 Chemicals, buffers and culture media

Standard chemicals used were from Sigma-Aldrich, Merck or Roth

Phosphate buffer	110 mM Na ₂ HPO ₄ /NaH ₂ PO ₄ in H ₂ O pH 7.4 @ 25°
Phosphate bufere saline (PBS)	137 mM NaCl 2.7 mM KCl 10 mM Na ₂ HPO ₄ 1.8 mM KH ₂ PO ₄ in H ₂ O pH 7.4 @ 25°
PFA 4%	1.3 M formaldehyde in phosphate buffer
Tris-borate-EDTA (TBE) buffer	89 mM Tris base 89 mM boric acid 2 mM EDTA in H ₂ O pH 8.0 @ 25°
Sucrose solution	30% w/v sucrose in PBS
LB medium	1% w/v Tryptone 0.5% w/v Yeast extract 171 mM NaCl in H ₂ O pH 7.0 @ 25°
LB agar	1.5% agar in LB medium

SOC medium	2% w/v Tryptone 0.5% w/v Yeast extract 8.56 mM NaCl 2.5 mM KCl 10 mM MgCl ₂ 20 mM glucose in H ₂ O pH 7.0 @ 25°
For Immunohistochemistry	
Cryoprotectant solution	25% v/v ethylene glycol 25% v/v glycerol in phosphate buffer
Citrate buffer	10 mM trisodium citrate in H ₂ O to pH 6.0 with citric acid 2 M
Glycine solution	100 mM Glycine in PBS
Blocking/Permeabilization buffer	10% w/v donkey serum 0.3% v/v Triton X-100 in PBS
Incubation buffer	3% w/v donkey serum 0.3% v/v Triton X-100 in PBS
DAPI (1000X)	0.1% w/v DAPI in H ₂ O

2.1.2 Antibodies

Primary antibodies

Antigen	Company	Cat. Nr.	Working Dilution
Caspase-3 (rabbit)	Sigma	C8487	1:300
BrdU (rat)	Abcam	ab6326	1:250
GFP (chicken)	Abcam	ab13970	1:500
GFP (goat)	Rockland	600-101-215	1:400

RFP (rat)	Chromotek	5F8	1:500
RFP (rabbit)	Rockland	600-401-379	1:2000
SOX2 (goat)	Abcam	ab110145	1:200
Tbr2/Eomes (rabbit)	Abcam	ab183991	1:500
Tubb3 (mouse)	Sigma	T8660	1:1000

Secondary Antibodies

All secondary antibodies are from Jackson ImmunoResearch Laboratories, Inc.

Antigen	Fluorophore	Cat.no.	Working Dilution
Donkey anti-rat	Cy3	712-165-150	1:1000
Donkey anti-rat	Alexa 488	712-545-150	1:1000
Donkey anti-rabbit	Cy3	711-165-152	1:1000
Donkey anti-rabbit	Alexa 488	711-545-152	1:1000
Donkey anti-rabbit	Alexa 647	711-605-152	1:1000
Donkey anti-goat	Alexa 488	705-545-003	1:1000
Donkey anti-goat	Alexa 647	705-605-147	1:1000
Donkey anti-chicken	Alexa 488	703-545-155	1:1000
Donkey anti-mouse	Alexa 488	715-545-151	1:1000

2.1.3 Primers

Cloning of K13, K10 and Casc15

Gene-Restriction Enzyme	Sequence 5'---3' orientation
K13-EcoRI-fwd	CAATGAATTCAAGTCAGCCGTGCCG
K13-XbaI-rev	CGGGTCTAGATTTACTTTTGGCTACTTTATTGGG
K10-XhoI-fwd	CAATCTCGAGACTGAAGGAGAACTGTTTT
K10 XhoI-fwd	CCGGTCTAGAAGAATGAAATGCACATTTAATTGGAGG
Casc15-XhoI-fwd	CAATCTCGAGGTCTGCTCTGGGACTT
Casc15-XbaI-rev	CAGTTCTAGATCTTGTAAGGCAGTCAGATCCA

Casc15 isoform validation

Isoform	Sequence 5'---3' orientation
Casc15-204-fwd	GCTGTGCTGTGGATTTGTTTTTCAGGATG
Casc15-204-rev	ACATGTGGTTTCCAGAGGCATACAAGAAGA
Casc15-202-fwd	ACCCAGCACGCTCAGAAAGTACTG
Casc15-202-rev	GGCCATCACTCATTCCCATCATGACATAA
Casc15-205-fwd	AGCACGCTCAGGGTTGATGGCCTA
Casc15-205-rev	CATCACTCATTCCCATCGACATCTGTGC
Casc15-203-fwd	GGGAGAAGGTGTCATACCAGCGAC
Casc15-203-rev	CTCATTCCCATCTGAGCGTGCTGG

Sequencing Primers

Primer name	Sequence 5'---3' orientation
Fwd-seqPrimer	GCTTTTGCAAAAAGCTTGCCACAACCCGCTA
Rev-T3promoter	ATTAACCCTCACTAAAGG

Quantitative-Reverse Transcriptase-PCRs

Primer name	Sequence 5'---3' orientation	Product length
Casc15	GGGATTTTCGACAAGGCTTTCCTT CTCATTCCCATCTGAGCGTGCTGG	131 bp
Sox4	GACATGCACAACGCCGAGAT GTTGCCCGACTTCACCTTCTT	168 bp
Tbr2	TGTGACGGCCTACCAAACA TCTAGGGGAATCCGTGGGAG	132 bp
Kit	GCAATGGCCTCACGAGTTC CCCTCTGACAGACCCACAG	145 bp
Rbfox1	ACTGTCCCTGACCACACATT CATCATCTGTCTGTGTGGCG	112 bp
Pdk1	TTCGGTGAAAAGGAAGTCC AAATCACAAAGCCGCCTAGC	102 bp
Stmn2	TTGAAGCCACCATCTCCCAT CACCTGAGCCTCTTGAGACT	131 bp

Vegfa	CATCTTCAAGCCGTCCTGTG TTTGGTGAGGTTTGATCCGC	128 bp
Eef1a1	ACAAGCGAACCATCGAAAAG GTCTCGAATTTCCACAGGGA	142 b

2.1.4 Mouse strains

C57BL/6JOlaHsd Inbred wild-type mouse line provided by the Biomedical Services Facility (MPI-CBG) used for *in utero* electroporation and breedings with the transgenic mouse lines (colony maintenance and expansion)

Tis21-GFP Knock-in mouse line expressing a nuclear localized GFP from the Tis21 locus (Haubensak et al., 2004)

2.1.5 Bacterial Strains

One Shot® TOP10F' (Invitrogen)	F' lacIq Tn10 (TetR) mcrA Δ(mrr-hsdRMS-mcrBC) Φ80lacZΔM15 ΔlacX74 recA1 araD139 Δ(ara-leu)7697 galU galK rpsL endA1 nupG
--------------------------------	--

2.1.6 Vectors

pDSV-mRFPnls (Lange et al., 2009)

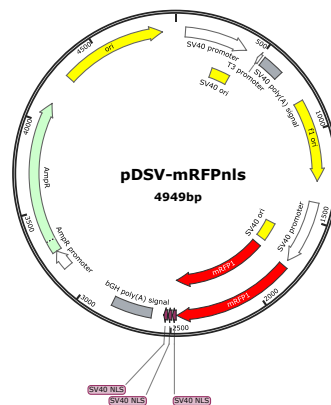


Figure 2.1: Schematic representation for the pDSV-mRFPnls.

pDSV-mRFPnls is a mammalian expression plasmid that expresses mRFP.nls sequence under the control of SV40 promoter with polyadenylation signal (Bovine GHpolyA+). It contains a second SV40 promoter followed by a multiple cloning site and SV40 polyadenylation signal. The plasmid encodes an ampicillin resistance cassette for selection, a ColE1 origin of replication for propagation in *Escherichia coli*.

2.1.7 Kits and enzymes

Endofree Plasmid Maxi Kit	Qiagen
QIAprep Spin Miniprep Kit	Qiagen
Invisorb Fragment CleanUP	STRATEC molecular
Quick-RNA™ MiniPrep	Zymo Research
Quick-RNA™ MicroPrep	Zymo Research
Neural Tissue Dissociation Kit	Miltenyi Biotec
Superscript™ III Reverse Transcriptase	ThermoFischer Scientific
iQ™ SYBR® Green Supermix	Bio-Rad

2.2 Methods

2.2.1 Generation of plasmid

2610307P16Rik plasmid was generated by inserting the full length 2010204K13Rik, E530001K10Rik and 2610307P16Rik cDNA sequence into the pDSV-mRFPnls vector. Initially, the gene was amplified by PCR from E14.5 mouse brain cDNA (see section 2.2.6) using Phusion High-Fidelity DNA polymerase (New England Biolabs) and primers that span the whole sequence and containing 5' recognition sites for restriction enzymes (see section 2.1.3). Then, the PCR product and the vector were digested with the corresponding restriction enzymes following the manufacturer's instructions. The vector's backbone was, then, treated with Antarctic Phosphatase to remove the 5' phosphates. The PCR product and the vector were then purified using Invisorb Fragment CleanUP followed by a ligating the PCR into the vector using T4 DNA ligase. The ligation product was, then, introduced into the One Shot® TOP10F' following the manufacturer's guidelines. Plasmids were purified from selected bacterial colonies using QIAprep Spin Miniprep Kit and sent for sequencing (Eurofins Genomics) with primers for sequencing (see section 2.1.3)

2.2.2 *In utero* electroporation

For *in utero* electroporation, plasmids were purified using the EndoFree Plasmid Maxi Kit according to manufacturer protocol with the following modification: plasmids were resuspended in sterile PBS to a final concentration of 1.5-4µg/µl.

Plasmids were injected in the dorsal telencephalon of E13.5 embryos. For this, pregnant C57BL/6J OlaHsd (supplied by Janvier) or Tis21-GFP mice were anaesthetized with isofluran. An incision was performed through the skin and abdominal muscles to expose the uterus. Plasmid solution was loaded into glass capillary (World Precision Instruments) and injected through the uterus, chorion, amnion and dorsal telencephalon into the lateral ventricle together with Fast Green FCF (Sigma-Aldrich) for visualization of the targeted area using a pneumatic picopump (World Precision Instruments). Subsequently, 6 electric pulses of 30 V and 50 ms with 1 s intervals were applied through 1 mm platinum electrodes (Sonidel) with a square-shape electroporator (BTX(R)-ECM(R)830, Harvard Apparatus). The uterus was then placed back into the abdominal cavity, the abdominal muscles sutured, the skin closed with clips and disinfected with povidone-iodine.

To reduce suffering, 100 μ l of 50 mg/ml Rimadyl (Pfizer) was injected subcutaneously. Gestation was kept for 24 or 48h. After dissection, targeted embryos were identified under a fluorescence dissection microscope.

2.2.3 Mouse sample collection and treatment

Pregnant females were anaesthetised with isofluran and sacrificed through cervical dislocation. Uteri were removed and placed in ice cold PBS and the embryos dissected. For embryos that underwent IUE, brains were collected (either E14.5 or 15.5) without removing the meninges. Samples were fixed in 4% paraformaldehyde at 4°C overnight, cryoprotected with 30% sucrose in PBS at 4°C overnight, embedded in Tissue Freezing Media, snap frozen in dry ice and cryosectioned (Microm HM560, Thermo Scientific). Series of 6 sections (10 μ m) were collected on Superfrost® Plus adhesive microscope slides (Thermo Scientific) and stored at -20°C.

For RNA collection, brains from E14.5 embryos were collected and the lateral cortex was isolated after removal of the meninges and the ganglionic eminences. Tissue was then dissociated using the Neural Tissue Dissociation Kit (Miltenyi Biotech) according to manufacturer protocol. RNA was extracted using Quick-RNA Mini Prep (Zymo Research) or Quick-RNA Micro Prep according to manufacturer's protocol.

2.2.4 Immunohistochemistry

Sections were hydrated with PBS and incubated for 1.5h in blocking-permeabilization buffer at RT followed by primary antibody diluted in incubation at 4°C overnight.

Samples were then washed with PBS and incubated with the appropriate secondary antibody for 2h at RT. Nuclei were counterstained with DAPI for 10 min at RT. Samples were, then, washed with PBS and mounted using Aqua- Poly/Mount (Polysciences, Inc.).

For Tbr2 staining, an antigen retrieval step was performed by incubating in citrate buffer at 70°C C for 60 min and quenched with glycine solution.

For BrdU staining, epitope exposure was achieved by treatment with 2M HCl for 25 min followed by extensive washes with PBS.

2.2.5 Image acquisition and processing

Immunohistochemistry images were acquired using an automated apotome microscope (Zeiss ApoTome-Zeiss). Pictures of the different focal planes were acquired using the Apotome optical sectioning system (Z-stack). Objectives used are: Zeiss Plan-Apochromat 20x 0.8 and Zeiss EC Plan-Neofluar 10x 0.3 Ph1.

Stitching of mosaics and maximum intensity projections of Z-stack were performed using Axiovision (Zeiss). Photoshop CS6 (Adobe) was used for colouring images and for adjusting its tonal range and color balance.

2.2.6 Reverse transcription

E14.5 mouse embryos or FACS sorted cells were collected as in section 2.2.3. Total RNA was isolated using Quick-RNA Mini Prep (Zymo Research) or Quick-RNA Micro Prep (zymo research) according to the manufacturer's instructions. To remove genomic DNA, on-column DNase treatment was performed. After the necessary washes the RNA was eluted in nuclease free water and stored in -80° C. cDNA was synthesized using superscript III reverse transcriptase enzyme and oligo dT primers (both from Invitrogen) following the manufacturer's instructions. The cDNA was stored in -20°C and was used for cloning of 2610307P16Rik-203 and for quantitative PCR.

2.2.7 Library preparation and supplemental bioinformatic analyses

Library preparation and enrichment was performed using 15 µl Sera-Mag Oligo(dT) beads (Thermo Scientific) in 50 µl 10 mM Tris-HCl. Samples were treated with 1U Turbo DNase (Ambion) and purified with Agencourt RNAClean XP beads. Eluted mRNA (18 µl) was chemically fragmented with NEBNext-Mg RNA Fragmentation Module (New England Biolabs), re-purified with RNAClean XP beads and eluted in

13,5 µl nuclease-free water. First strand cDNA synthesis was performed using 0.15 µg/µl Random Primers (New England Biolabs), 1x First Strand Synthesis Reaction Buffer (New England Biolabs), 10 U/uL Superscript II (Invitrogen) with an initial hybridization for 5 min at 65°C with mRNA and primers followed by incubation at 25°C for 10 min, 42°C for 50 min, and 70°C for 15 min. After purification with Agencourt Ampure XP-beads (Beckman Coulter), second strand synthesis was performed using the Second Strand Synthesis module (New England Biolabs) replacing the 2nd strand synthesis buffer with an NTP-free buffer and adding equimolar 2.5 mM of d-nucleotides. Incubation for 2.5 h at 16°C was followed by Ampure XP beads purification as described above. End-Repair was done with the NEBnext End Repair Module (New England Biolabs) followed by XP beads purification and A-Tailing using the NEBnext dA-Tailing Module. Adaptors were ligated (Adaptor-Oligo 1: 5'-ACA-CTC-TTT-CCC-TAC-ACG-ACG-CTC-TTC-CGA-TCT-3', Adaptor-Oligo 2: 5'-P-GAT-CGG-AAG-AGC-ACA-CGT-CTG-AAC-TCC-AGT-CAC-3') using 1x NEBnext Quick Ligation Buffer (New England Biolabs), 0.3 uM DNA Adaptors, 1 uL Quick T4 DNA Ligase (New England Biolabs) in 50 µl. XP beads purification was followed by dUTP cleavage with 1 U USER enzyme mix (New England Biolabs) per sample and direct enrichment using the PCR Enrich Adaptor Ligated cDNA Library module (New England Biolabs) with indexed primers. After sequencing, FastQC (<http://www.bioinformatics.babraham.ac.uk/>) was used to perform a basic quality control on the resulting reads. As an additional control, library diversity was assessed by investigating redundancy within the mapped reads. A splice junction library of 120 nucleotides length was created with RSEQTools (Habegger et al., 2011) and alignment to the mm10 transcriptome performed with pBWA (<http://pbwa.sourceforge.net/>). All reads that mapped at an identical start position were considered to be redundant and therefore only counted once. For all samples, library diversity started at 88% for a random subsample of 1 million reads. Normalization did not include length since we tested for differential expression of the same gene across samples. A table of raw readcounts per gene was created based on the overlap of the uniquely mapped reads with the mm10 Ensembl Genes annotation v. 87 using BEDtools (v. 2.11). The DESeq R package (v.1.8.1) (Anders and Huber, 2010).

2.2.8 Quantitative-Reverse Transcriptase-PCRs

Relative changes in the expression of Sox4, Tbr2, Rbfox1, Stmn2, Pdk1, Vegfa and Kit were measured by quantitative RT-PCRs after Casc15 over expression. In brief, Casc15 or control plasmids were introduced in the lateral cortex of E13.5 embryos by IUE. 24 hours later, brains were dissected and single cell suspension was prepared using Neural Tissue Dissociation Kit after removal of meninges and ganglionic eminences. Targeted (RFP⁺) cells were FACS sorted using Becton Dickinson Aria III (performed by Katja Schneider at the FACS facility, CRTD). Cells were then pelleted at 300 g for 10 minutes and lysed in RNA lysis buffer. RNA was extracted using Quick-RNATM MicroPrep with an on-column DNase treatment. cDNA was synthesized as described above. Primers were designed to span an exon-exon junction (see section 2.1.3). iQTM SYBR[®] Green Supermix was used together with 250 nM primer pair in a 20- μ l reactions. Stratagene MX 3005P system was used with a two-step PCR program: 95°C for 3 minutes followed by 40 cycles of: 95°C for 15 sec, 57°C for 40 sec. Melting curves were generated by heating to 95°C for 60 sec, then cooling at 55°C and 95°C again for 30 sec.

Results were analyzed using the $2^{-\text{ddCt}}$ method (Livak and Schmittgen, 2001) using Eef1a1 as a house keeping gene.

2.2.9 Bioinformatic analysis

R project for statistical computing was used to analyze the transcriptome for differential gene expression using the Dplyr package. Density plots were generated from gene normalized read counts (FPKM) by using ggplot packages. To study alternative splicing Kallisto (Bray et al., 2016) was used to align the raw reads to the reference genome mm10 Ensembl Genes annotation v. 87. Kallisto generates the normalized transcripts' reads in transcript per kilobase million (TPM). TPM values for different transcripts were then used as file inputs in SUPPA (Trincado et al., 2018) to calculate the relative abundance of each gene isoform in different conditions, Casc15 versus control. The relative abundance is calculated as a percentage spliced in (psi), which reflect the proportion of an isoform relative to the total gene expression. Again, SUPPA was used to calculate the differential isoform usage as difference in psi (dpsi) and outputs a p-value for each dpsi. “-gc” was used to perform correction per gene. The p-values from all isoforms of the same gene are corrected for multiple testing, which is a Benjamini & Hochberg correction.

2.2.10 Statistical analysis

All quantifications were performed at least in triplicates, with pups from at least two independent mothers. Sample means were compared with Student's t-test and differences were considered significant when two-tailed p-value < 0.05.

Chapter 3

3 Results

3.1 Selection of potential regulators of neurogenesis

3.1.1 Differential expression analysis for RNA seq data

The transcriptome previously generated from our lab comprises protein coding genes and lncRNAs in proliferating progenitors (PP), differentiating progenitors (DP) and neurons (Aprea et al., 2013). In attempt to identify novel factors involved in neurogenesis, I focused on the lncRNA catalogue comprising 2762 genes. The first encounter was to objectively identify genes that are biologically significant. Transcriptomes are generated as raw reads that are aligned to the reference genome. The read counts per gene are then normalized by DESeq resulting in a range of normalized reads per gene ranging from zero to many thousands. Particularly, in our dataset, the reads for each gene were in triplicates for each of the 3 cell types: PP, DP and neurons. The problem that arises when analyzing these datasets is determining the threshold of reads that represents biological expression. Routinely, researchers arbitrarily choose one cutoff, for example, 10 reads to consider gene expression. I sought to identify a more reliable way that describes gene expression in biological samples. To this end, the reads per gene were normalized for the gene length using cuffdiff (done by Matthias Lesche, deep sequencing facility Biotec). Cuffdiff outputs gene expression in fragment per kilobase million (FPKM) values. Therefore, the expression of each gene is now represented by an FPKM value in triplicates per each cell type. Next, using R, for statistical computing and graphics, the mean FPKM in each cell type was calculated for each gene. Next, I aimed to visualize the expression profile of all genes in the transcriptome. The mean FPKM of each gene was used to generate a density distribution plot for the three cell types (Figure 3.1A). In the three cell types, lncRNAs are expressed in almost an identical pattern showing a two-peak density distribution, with one broader peak ranging from 0-0.47 and a second peak starting at FPKM 0.47. Based on this analysis, an FPKM of 0.47 represented a minimal threshold that discriminates the transcribed genes and noise. Therefore, for further analysis, I included genes that have an expression of ≥ 0.47 in at least one population, thereby neglecting those that have minimal expression in the three populations together. Out of 2762 lncRNAs, 1003 genes (36%) exceeded the cutoff threshold and their expression patterns in PP, DP and N was, then,

examined. lncRNAs that are hoped to play a role in neurogenesis are expected to be differentially expressed particularly between proliferation (PPs) and differentiation (DPs). With at least 50% fold change (FC) between two populations, lncRNAs were sorted as upregulated ($\log_2 \text{FC} \geq 0.58$, p-adjusted value ≤ 0.05) or downregulated ($\log_2 \text{FC} \leq -0.58$, p-adjusted value ≤ 0.05). Out of 1003, 857 lncRNAs (85.4%) have similar expression in PPs and DPs, while 71 and 75 genes were upregulated or downregulated from PPs to DPs, respectively (Figure 3.1B). Out of the 71 lncRNAs upregulated from PPs to DPs, 32 lncRNAs are also upregulated in neurons compared to DPs, while 15 genes were downregulated from DPs to neurons. On the other hand, out of 75 lncRNAs that are downregulated from PPs to DPs, 35 lncRNAs are also downregulated in neurons compared to DPs, while 6 lncRNAs are upregulated from DPs to neurons (Figure 3.1B). The two subsets of lncRNAs (PPs<DPs>N), those I call the “Onswitch” genes, and (PPs>DPs>N), those I call the “DownDown”, were particularly interesting for my study. The Onswitch genes were particularly interesting because their expression behavior might reflect a potential role in the switch from proliferation to differentiation in progenitors. Many characterized neurogenic protein-coding genes were found to have an Onswitch expression pattern (Aprea, 2013). As for the DownDown, their enrichment in PPs is suggestive of a potential involvement in the maintenance of the stem cell pool. The list of 15 Onswitch lncRNAs, and 35 DownDown lncRNAs comprises different subclasses of lncRNAs (See subclasses of lncRNAs, section 1.4.1) Therefore, the genomic context for those lncRNAs was examined and I found that 7 of the “Onswitch” and 9 of the “DownDown” are lincRNAs while the rest are antisense lncRNAs (Figure 3.1C). Of note, we consider lncRNAs to be intergenic only if they are ≥ 5 kb from the nearest protein-coding gene, therefore do not overlap with the promoters of neighbouring genes. For my study, I decided to focus on lincRNAs to avoid the technical limitation of interfering with the overlapping protein-coding transcript while manipulating the antisense lncRNA expression.

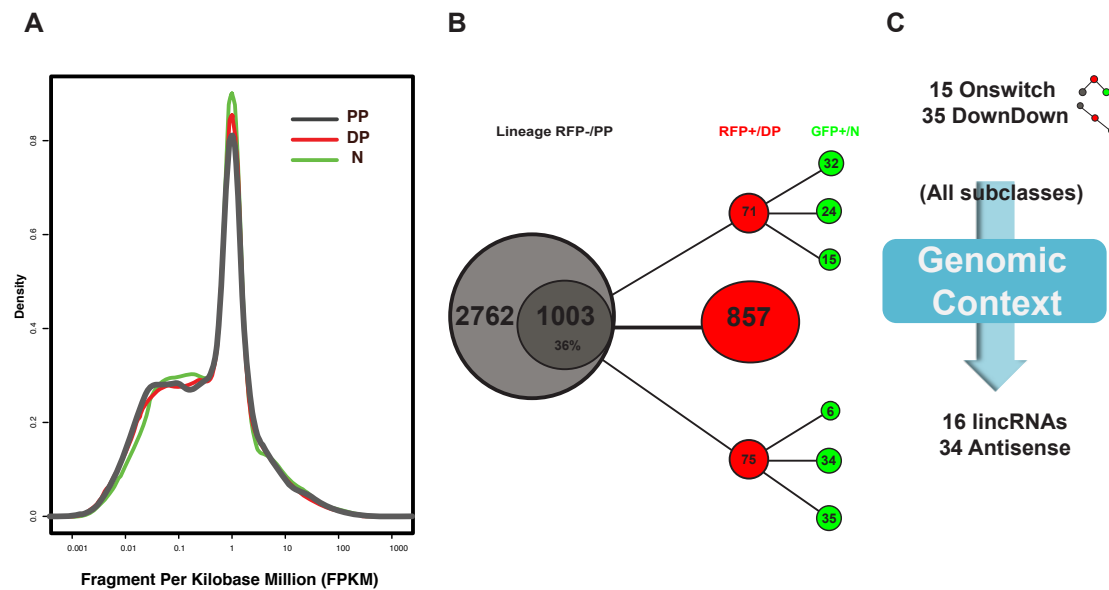


Figure 3.1: Selecting candidate genes for *in vivo* studies.

A: density plot showing the distribution of lncRNA catalogue expression in PP (grey), DP (red) and Neuron (green). B: fishbone chart summarizing the differential expression of lncRNAs in PP (grey), DP (red) and Neuron (green). Differential expression was considered when genes show more than 50% upregulation or downregulation between the three cell populations with a false discovery rate (FDR) less than 5%. C: Categorizing of subclasses of lncRNAs according to their genomic context.

3.1.2 LincRNAs for *in vivo* manipulation

In the shortlisted Catalogue of “DownDown” lincRNAs, 2010204K13Rik and E530001K10Rik showed the highest expression among all (Table 2). Both lincRNAs have no identified human orthologue. 2010204K13Rik is transcribed from the reverse strand of the X chromosome. The nearest protein-coding gene is Usp27x, a ubiquitin specific peptidase, at 36.3 Kb. E530001K10Rik, also called Mir670hg, is transcribed from the reverse strand of chromosome 2. Mir670, which has no described function in neurogenesis, is transcribed from the first intron of E530001K10Rik.

The list of Onswitch lincRNAs included Miat and Rmst, two lincRNAs that have human orthologues and both have been described for their role in neurogenic commitment (Aprea et al., 2013; Ng et al., 2013). The second most expressed lincRNA, after Miat, is 2610307P16Rik which has an uncharacterized role in neurogenesis (Table 3). 2610307P16Rik shows minimal conservation across vertebrates (Figure 3.2A), and stronger conservation signals around at its transcription start site and around exonic regions as per UCSC genome browser alignment (Figure 3.2B). 2610307P16Rik is transcribed from the negative strand of chromosome 13, ~ 63 kb downstream from Sox4, a transcription factor promoting neuronal differentiation. 2610307P16Rik aligns to Cancer susceptibility 15 (Casc15) on

chromosome 6 in the human genome, a lincRNA ~ 66 kb away from human Sox4. The conserved genomic location and transcriptional orientation suggest that Casc15 is the human orthologue of 2610307P16Rik (Figure 3.2C).

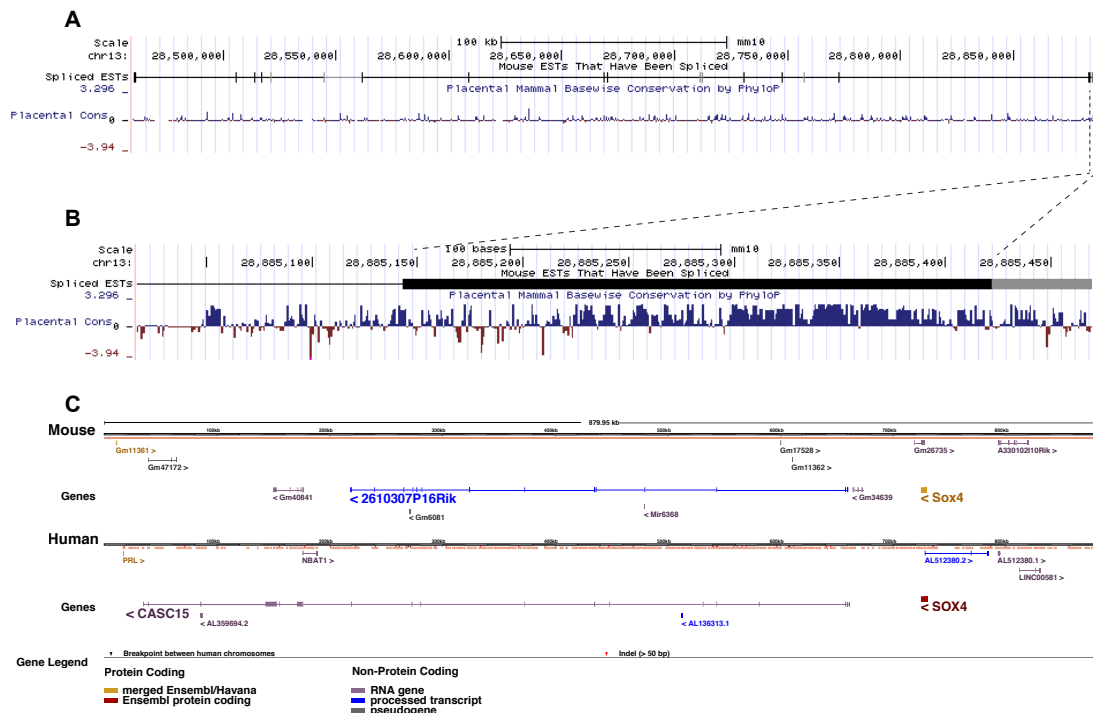


Figure 3.2: the genomic context for 2610307P16Rik.

A: UCSC genome browser 2610307P16Rik alignment on the mouse genome showing its weak conservation across placenta. B: conservation of the transcription start site and the first exon of 2610307P16Rik across vertebrates. The signal of sequence conservation is represented by the dark blue peaks together with the conservation score. Bottom: alignment of 2610307P16Rik on the human genome showing the conserved genomic location and transcriptional orientation for 2610307P16Rik and human Casc15.

Next, for *in vivo* manipulation, full length cDNA of the selected lincRNAs should be cloned on expression vectors. As mentioned in section 1.4.1, lincRNAs undergo alternative splicing similar to mRNA, yet with lower efficiency. Thus for the proper *in vivo* manipulation of candidates, the identification of the lincRNAs' splice isoforms that are transcribed in the developing cortex is mandatory. However, this was challenging because most protein-coding genes and lincRNAs are so badly annotated at the isoform level. Moreover, there are hardly any publicly available data of the isoform expression of lincRNAs in different tissues. To solve this problem and because growing evidence is supporting the role of specific gene isoforms in different tissues, our lab aimed at identifying the transcriptome of the developing cortex at an isoform level (independent project by Leila Alieh, unpublished data). In that work, the raw reads generated from the previously described RNA-seq from the 3 cell types

(Apréa et al., 2013) were mapped to the reference genome mm9 Ensembl Genes annotation v. 67 using TopHat. The mapped reads are then assembled into transcripts using Cufflinks and merged to produce a final transcriptome assembly with Cuffmerge. Cuffdiff is then applied to calculate the differential expression of isoforms in the 3 cell types. I, then, used this database to identify the abundant transcripts and their differential expression for my candidate lincRNAs.

Four different splice variants are transcribed from 2010204K13Rik as per Ensembl mm9 and mm10 annotations (Figure 3.3A). For 2010204K13Rik, 2010204K13Rik-201 is the only expressed isoform in the developing cortex (Figure 3.3B, data not published). 2010204K13Rik-201, hereafter K13, is down regulated by two folds from PPs to DPs and more than ten folds between DPs and N. Thus full-length K13 was cloned on an expression vector for *in vivo* manipulation (Figure 3.3C).

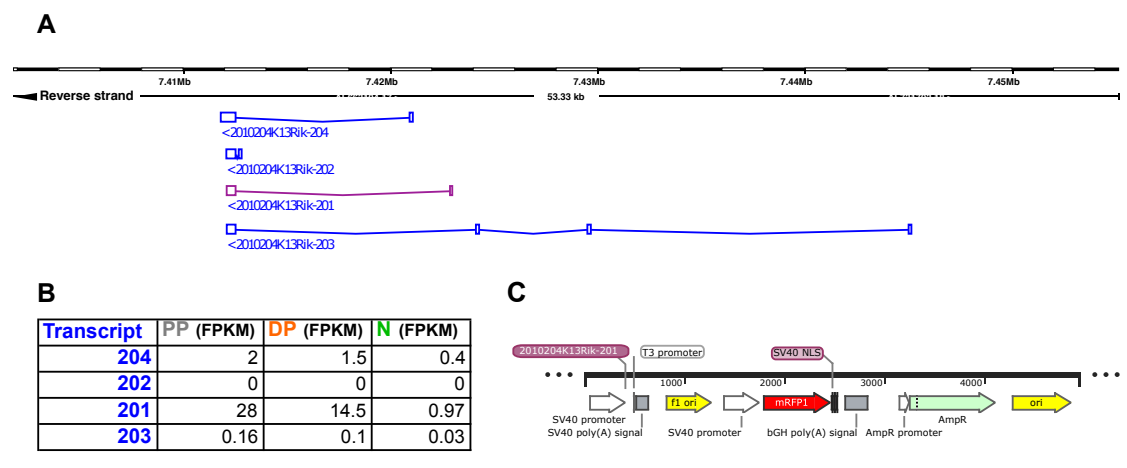


Figure 3.3: Selection of 2010204K13Rik for *in vivo* manipulation.

A: schematic representation for 2010204K13Rik isoforms as per the Ensembl mm9 and mm10. B: table summarizing the abundance of the 4 isoforms in fragment per kilobase million (FPKM) in PP, DP and N. C: 2010204K13Rik-201 full length transcript is cloned on an expression vector, coexpressing RFP.

For E530001K10Rik, two different splice variants are transcribed from the E530001K10Rik gene as per the Ensembl mm9 (Figure 3.4A), however in the latest annotations in mm10, the number of splice variants increased to seven. Because our transcriptome was mapped to the mm9 annotation, the RNA-seq reads were assigned to either of the two isoforms only and thus it was deduced that the abundant isoform in the developing cortex is E530001K10Rik-002, hereafter K10 (Figure 3.4B). K10 is downregulated by three folds between PPs and DPs and almost four folds between DPs and N. So, full-length K10 was cloned for *in vivo* manipulation.

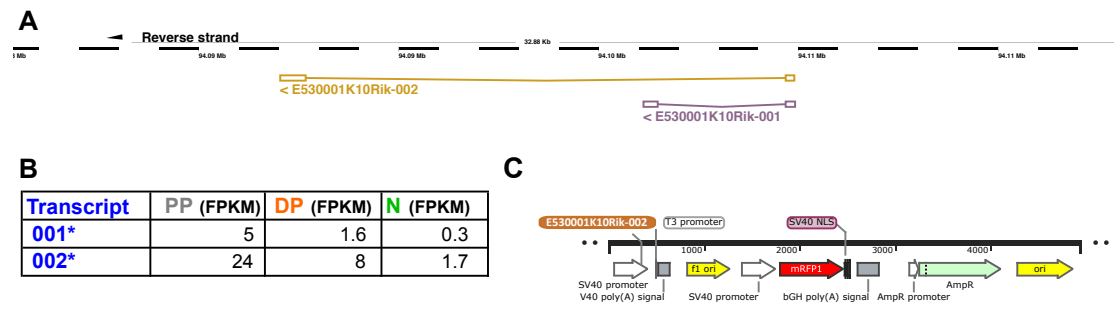


Figure 3.4: Selection of E530001K10Rik for *in vivo* manipulation.

A: schematic representation for E530001K10Rik isoforms as per the ensembl mm9 1. B: table summarizing the abundance of the 2 isoforms in fragment per kilobase million (FPKM) in PP, DP and N. C: E530001K10Rik-002 full length transcript is cloned on an expression vector, coexpressing RFP.

On the other hand, seven different splice variants are transcribed from 2610307P16Rik as per Ensembl mm9 and mm10 annotations (Figure 3.5A), five of which are predicted to be expressed in the developing cortex (Figure 3.5B). The expression of the 4 most abundant isoforms 203, 204, 205, 202 was confirmed by PCR by isoform specific primers (Figure 3.5C). The expression data of the different isoforms highlights isoform 203 to have the highest expression in the mouse cortex and shows that isoform 2610307P16Rik-203 is approximately 2 folds upregulated in DPs as compared to PPs and N (Figure 3.5B). Thus, 2610307P16Rik-203, hereafter Casc15, is selected for *in vivo* studies.

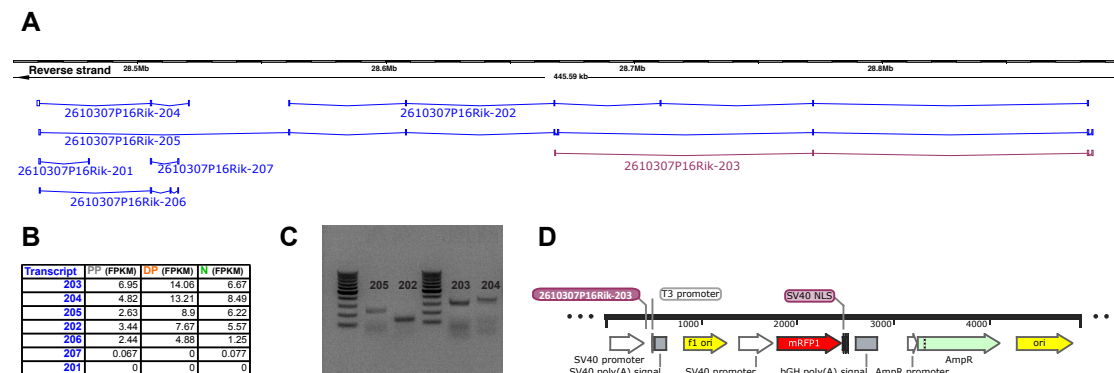


Figure 3.5: Selection of 2610307P16Rik for *in vivo* manipulation.

A: 7 isoforms are expressed from 2610307P16Rik gene locus using the ensemble mm10 database. B: table summarizing the abundance of the 7 isoforms in FPKM in PP, DP and N. C: Amplification of the top abundant isoforms using isoform specific primers visualized on agarose gel. 2610307P16Rik-203 full-length transcript is cloned on an expression vector, coexpressing RFP.

3.2 In vivo manipulation of K13, K10 and Casc15

In order to screen for the potential roles of K13, K10 and Casc15 in neurogenesis, the effects of their over expression in the mouse neocortex was analyzed. To this end, full-length cDNA of K13 (Figure 3.3C), K10 (Figure 3.4C) and Casc15 (Figure 3.5D), was cloned into a dual promoter vector co-expressing RFP. The respective plasmids or control plasmids, only with RFP, were introduced to the developing cortex using *in utero* electroporation (IUE).

IUE as a powerful tool for candidate genes screen

IUE allows targeting the neural stem cells in the developing cortex. In IUE the uterus of a pregnant mouse is exposed and plasmids are injected in the lateral ventricles of the developing embryos. With the application of small voltage, the plasmids are electroporated in the apical progenitors (APs) lining the ventricle. With the aid of a reporter protein, targeted cells together with their progeny become fluorescent easing the detection of any developmental abnormalities at cellular and molecular levels. The experimental paradigm chosen was to perform the IUE at E13.5 and collect the brains at E15.5, mid neurogenesis. Unlike the onset of neurogenesis and the terminal differentiation stages, mid-neurogenesis is a stage where both APs and basal progenitors (BPs) undergo proliferation and differentiation at defined percentages and where new-born neurons are readily generated. Having different progenitors population as well as terminally differentiated neurons allows tracing different changes happening at the progenitors level or at the maturation levels. After 48 hours of IUE, the RFP signal in the dividing APs is passed to BPs in VZ that migrate basally and form the SVZ. BPs also divide inheriting the RFP expressing plasmids to newborn neurons that migrate towards the early IZ and finally to their destination in the CP. As mentioned in section 1.2.1 the balance between proliferation and differentiation in progenitors is detrimental for neuronal output in the CP. Similarly, progenitors death or premature neurogenesis should affect neuronal output. Moreover, defects in migration should result in neurons being retained and stuck in the IZ not reaching the CP. Therefore in IUE, the read out of the experiment is by immunofluorescent detection and determination of the distribution of RFP⁺ cells across the layers of the lateral cortex and comparing it between candidate genes and control brains. Consequently, one can deduce if candidate gene's overexpression causes changes in proliferation of progenitors, cell fate or survival, progenitors or neurons

migration among other cell factors. This is easiest detected in the CP, where the increase or decrease in the number of neurons, usually reflects changes caused by genetic manipulation (Figure 3.6).

A limitation of the IUE is that targeting the plasmids in particular spots of the neocortex is a challenge. Generally the plasmids are introduced in the ventricles and by electroporation they are uptaken by AP lining the ventricles. However, neurogenesis along the rostral-caudal and medial-lateral axis is not identical. Therefore in an ideal setup, one should match the candidate gene and the respective control brain electroporations to be in similar spots along the different axes. This consumes time and animals for optimal results. Because of this, I initially screened only three candidate lncRNAs.

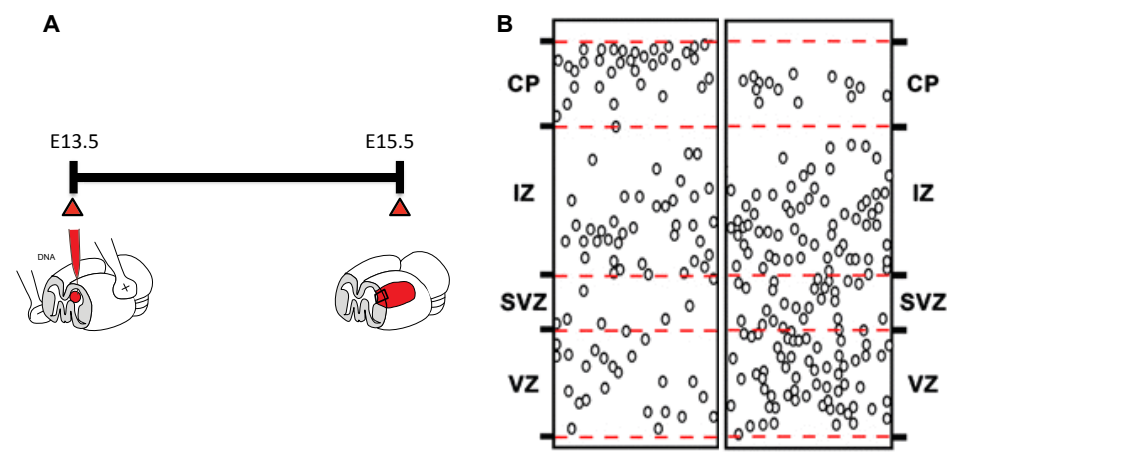


Figure 3.6: IUE a powerful tool for genes' screen.

A: Schematic representation of the experimental paradigm of IUE and B: Distribution of targeted cells across the cortical layers 48 hours post in IUE in control (left) and Miat (right). The increase in progenitors in VZ and decrease in neurons in the CP in Miat reflects an effect of Miat on neurogenesis (Adapted from (Aprea et al., 2013). Cortical layers are indicated.

3.2.1 K13 overexpression does not alter progenitors/neurons distribution in the cortex.

The earliest effects of K13 overexpression were analyzed 48 hours post IUE. The dissected brains were fixed in 4% PFA and embedded in OCT. The brains were cut into 10 μ M-coronal cryosections. The cryosections were examined with fluorescence microscopy. The distribution of the RFP⁺ cells was visually identical in K13-expressing and control brains. For the proper quantification of the percentage of RFP⁺ cells across the cortical layers, delimiting the cortical layers is mandatory. Therefore, brain sections were immunostained for Tbr2 to label BPs in both VZ and

SVZ together with 4', 6-diamidino-2-phenylindole (DAPI) that labels cell nuclei. The SVZ was discriminated from the VZ based on the increase in the density of Tbr2⁺ cells, as virtually the majority of cells in SVZ are BPs. As well, BPs in the SVZ change their orientation to have their nuclei perpendicular to the ventricular surface. The limit between IZ and SVZ is decided based on the weakened signal of Tbr2 in newborn neurons, while CP is identified based on the increased nuclear density towards the basal plane compared to the IZ. With the aid of Tbr2 staining the percentage of RFP⁺ cells was determined in the four cortical layers and the quantitation confirmed the lack of significant change in RFP⁺ cell distribution in K13-expressing brains compared to controls (Figure 3.7A).

3.2.2 K10 might affect migration of neurons in the developing cortex.

Similarly, K10 cloning and overexpression *in vivo* was achieved in a similar fashion. The 48 hours coronal sections showed a decrease in the neurons in the CP. However, for the proper quantification, combination of Tbr2 and DAPI staining was performed and cells were quantified across the four cortical layers. In K10, there was no significant difference in the percentage of cells in the VZ ($28.56 \pm 1.54\%$ n=3, average \pm SD) compared to controls ($24.99 \pm 0.44\%$ n=3, average \pm SD, two-tailed p-value= 0.089). Similarly, in the SVZ, there was no significant difference in the percentage of cells in K10 ($14.72 \pm 0.32\%$ n=3, average \pm SD) compared to controls ($13.5 \pm 0.84\%$ n=3, average \pm SD, two-tailed p-value= 0.24). However, in the IZ, there was a slight insignificant increase in the percentage of cells in K10 ($45.39 \pm 1.45\%$ n=3, average \pm SD) compared to controls ($40.62 \pm 1.36\%$ n=3, average \pm SD, two-tailed p-value= 0.074). While in the CP, the percentage of cells was significantly lower in K10 ($11.32 \pm 2.3\%$ n=3, average \pm SD) compared to controls ($20.89 \pm 1.02\%$ n=3, average \pm SD, two-tailed p-value= 0.019) (Figure 3.7B). The tendency towards increase in the percentage of cells in the IZ with concomitant decrease in the CP suggests the K10 affects neuronal migration in the cortex.

3.2.3 Casc15 disrupted the distribution of cells across the four cortical layers.

As for Casc15, repeating the same electroporation/analysis paradigm, the results were more interesting. The brain cryosections indicated a decrease in the number of cells in

the CP in *Casc15*-expressing cortices as compared to controls. For quantification, Tbr2/DAPI immunostaining was performed and the percentage of cells across VZ, SVZ, IZ and CP were quantified. In *Casc15*-expressing brains there was ~ 25% more cells in the VZ in *Casc15* brains ($31.3 \pm 1.1\%$, average \pm SD, $n=10$) compared to controls ($25.2 \pm 0.5\%$, average \pm SD, $n=9$, p -value = 0.0001) (Figure 3.7C). Similarly, in the SVZ, there was a ~ 25% increase in the percentage of cells in *Casc15* brains ($15.8 \pm 0.7\%$, average \pm SD, $n = 10$) compared to controls ($12.9 \pm 0.6\%$, average \pm SD, $n = 9$, p -value = 0.0051). In the CP, the percentage of cells in *Casc15* brains was almost half ($10.6 \pm 1.1\%$, average \pm SD, $n = 10$) the respective percentage in the control brains ($20.3 \pm 0.9\%$, average \pm SD, $n = 9$, p -value < 0.0001). And although there was no significant difference in the percentage of cells in the IZ between *Casc15*-expressing ($42.3 \pm 0.9\%$, average \pm SD, $n = 10$) and control brains ($41.4 \pm 0.8\%$, average \pm SD, $n = 9$, p -value = 0.5), it was observed that early born neurons in the IZ reside closer to the SVZ suggesting an effect of *Casc15* on cell migration (Figure 3.7B). Because *Casc15* showed the most robust phenotype and RFP⁺ cell distribution indicate an effect on progenitors in the germinal layers, it was chosen for further analysis.

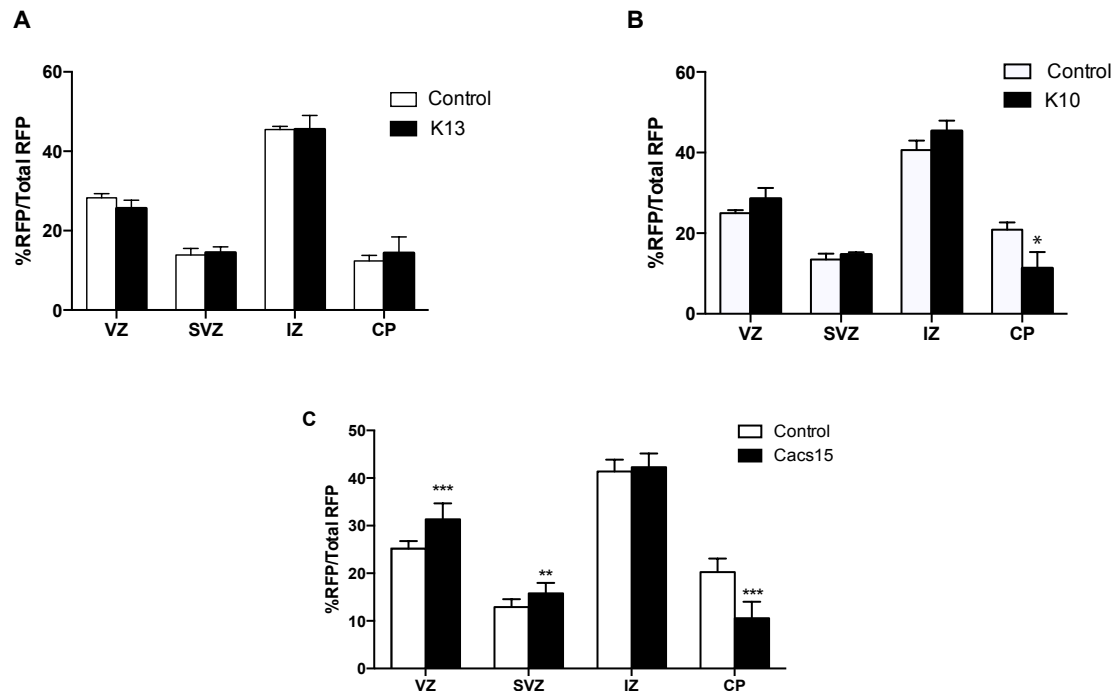


Figure 3.7: lincRNA induced phenotypes in the lateral cortex.

A, B and C: Column graph representing the quantification of the percentage of RFP⁺ in the 4 cortical layers. Cortical layers are indicated. Significance is indicated by *, *** p -val < 0.0001, ** p -val < 0.005, * p -val < 0.05. Error bars represent SD.

3.3 Characterization of the cellular phenotype of *Casc15*

3.3.1 *Casc15* delays neuronal migration

The residence of neurons closer to the SVZ/IZ limit in *Casc15* brains suggests an effect of it on neuronal migration. To address whether *Casc15* has an effect on neuronal migration, E13.5 embryos were IUE with *Casc15* or control plasmids and sacrificed at E15.5, the mothers were injected with one intraperitoneal injection of 5-bromo-2'-deoxyuridine (BrdU) at E14.5, 24 hours before sacrifice (Figure 3.8A). BrdU crosses the placenta wall, diffuses through cell membranes and is incorporated in the DNA of proliferating cells in the embryo, thereby labeling dividing APs and their progeny in a 24-hours frame. In 24 hours APs and BPs have completed one cell cycle and BrdU label is passed to their daughter cells from progenitors and newborn neurons migrating through the IZ to the CP. Doing this, all targeted neurons that were born in 24 hours are traced as they migrate across the IZ. To delimit the VZ and SVZ Sox2 and BrdU antibodies were used, respectively (Figure 3.8B). The IZ was divided into 3 equal bins; early IZ, middle IZ and late IZ and the CP was counted as the 4th bin. A fraction of the total of the double positive migrating neurons (RFP⁺/BrdU⁺) cells in each segment was counted and normalized to the total double positive in the four bins. Interestingly, there was a significant increase in the percentage of double positive cells retained in the early IZ in *Casc15*-expressing brains (62.45 ± 3.96 , average \pm SE of diff, n=4) compared to controls (45.14 ± 3.96 , average \pm SE of diff, mean diff = -17.32, n=5, Sidak's multiple comparisons test pval-adj = 0.0006) with a concomitant decrease in percentage of cells in the middle IZ in *Casc15* (31.81 ± 3.96 , average \pm SE of diff, n=4) compared to controls (44.57 ± 3.96 , average \pm SE of diff, mean diff = 12.76, n=5, Sidak's multiple comparisons test pval-adj = 0.013). There was no significant change in the percentage of cells localized in the 3rd segment in *Casc15* (3.79 ± 3.96 , average \pm SE of diff, n=4) and controls (9 ± 3.96 , average \pm SE of diff, mean diff = 5.21, n=5, Sidak's multiple comparisons test pval-adj = 0.59) and there was almost an absence for double positive cells in the CP (Figure 3.8B and C). This confirms an effect of *Casc15* on neuronal migration. However, because the total percentage of neurons in IZ is similar in *Casc15*-expressing and control brains (Figure 3.7B, third column), delayed neuronal migration alone cannot explain the decreased

neuronal output in CP nor can it explain the increased percentage of cells in the VZ (Figure 3.7B, forth and first column, respectively).

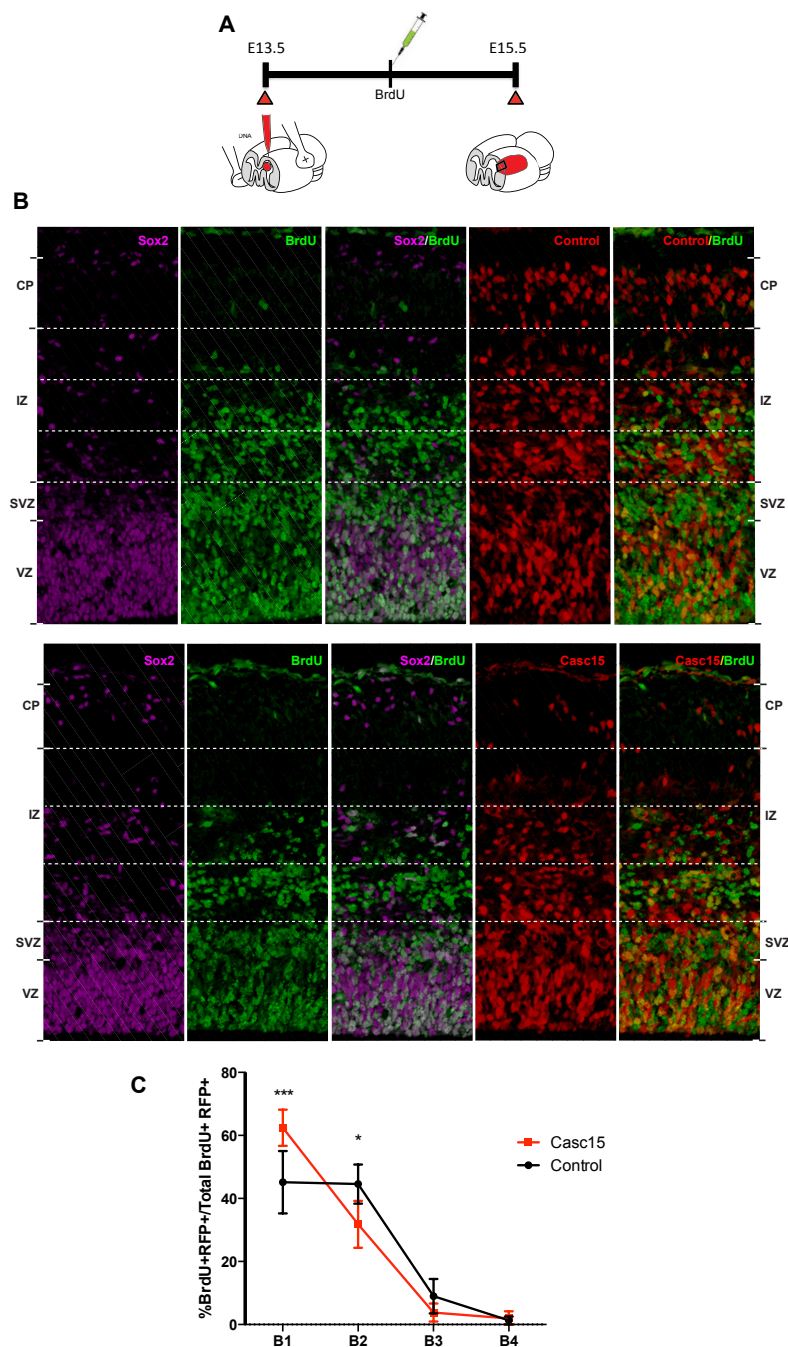


Figure 3.8: Effect of Casc15 on neuronal migration.

A: Experimental protocol, IUE was performed at E13.5 and brains were collected at E15.5. At E14.5, 24 hours before sacrifice, the mothers were injected with BrdU intraperitoneal to label all birth-dated cells in 24 hours. B: Immunofluorescent images of coronal sections of control (up) and Casc15 (bottom) brains 48 hours post IUE. Antibodies are indicated in colours. Cortical layers VZ, SVZ, IZ and CP are indicated. The IZ was divided into 3 equal bins and the CP was counted as the 4th bin indicated in dashed lines. C: XY line graph representation of the neuronal distribution in the IZ and CP. Percentage of BrdU labeled neurons in each bin was quantified over the total labeled neurons in the 4 segments. Error bars represent SD, significance of the line was calculated using two-way Anova for multiple comparisons. *** p-val < 0.001, * p-val < 0.05. n= 5 and 4 for controls and Casc15, respectively.

3.3.2 **Casc15 does not alter progenitors migration**

Progenitors in the developing cortex undergo INM during different phases of the cell cycle. Both the microtubule-based and actin-myosin-based machinery that are involved in the oscillation of progenitors between the apical membrane and the basal side of the germinal layers are also involved during neuronal migration. So, next, it was important to investigate whether Casc15 also affects progenitors migration. The cell cycle progresses in progenitors even when INM is perturbed. However mitosis, then, can take place abventricularly in the VZ and not necessarily at the apical plane (See section 1.2.1 **INM and its effect on cortical expansion**). To determine the effects of Casc15 on progenitors migration, phosphohistone (PH3) staining, a marker of cell mitosis, was performed in 48-hours Casc15 overexpressing brains and controls. Initially, the percentage of mitotic cells (PH3⁺/RFP⁺) was assessed in both Casc15 and control. The data show that Casc15 has no impact on cell mitosis, where the percentage of mitotic cells from all progenitors in the germinal layers in Casc15 (4.72 ± 0.77 , average \pm SD, n=5) was similar to controls (4.33 ± 0.7 , average \pm SD, n=4, two-tailed t-test p-value = 0.72). Next, the percentage of mitotic cells on the apical surface lining the ventricles was compared between Casc15 and controls. There was no significant difference in apical mitosis between Casc15 (29.82 ± 3.5 , average \pm SD, n=5) and controls (37.34 ± 3.7 , average \pm SD, n=4, two-tailed t-test p-value = 0.19). It stands to reason that also the percentage of basal mitotic cells in the VZ and SVZ together was also not affected between Casc15 (70.18 ± 3.52 , average \pm SD, n=5) and controls (62.66 ± 3.7 , average \pm SD, n=4, two-tailed t-test p-value = 0.19).

3.3.3 **Casc15 does not induce direct neurogenesis**

APs differentiate asymmetrically producing an AP and a BP or to a much less extent an AP and a neuron. If APs prematurely increase their neurogenic divisions (producing an AP and a neuron), this will lead to the appearance of neurons in the VZ. If those neurons suffer a migration delay as presented earlier for Casc15, they will be retained in the germinal layers explaining the increase in the percentage of cells in the VZ and SVZ and decreasing the percentage of cells in the CP (Figure 3.7C). To answer whether Casc15 overexpression led to increased neurogenic divisions in APs, it was necessary to identify the type of cells in the VZ in both Casc15 and controls.

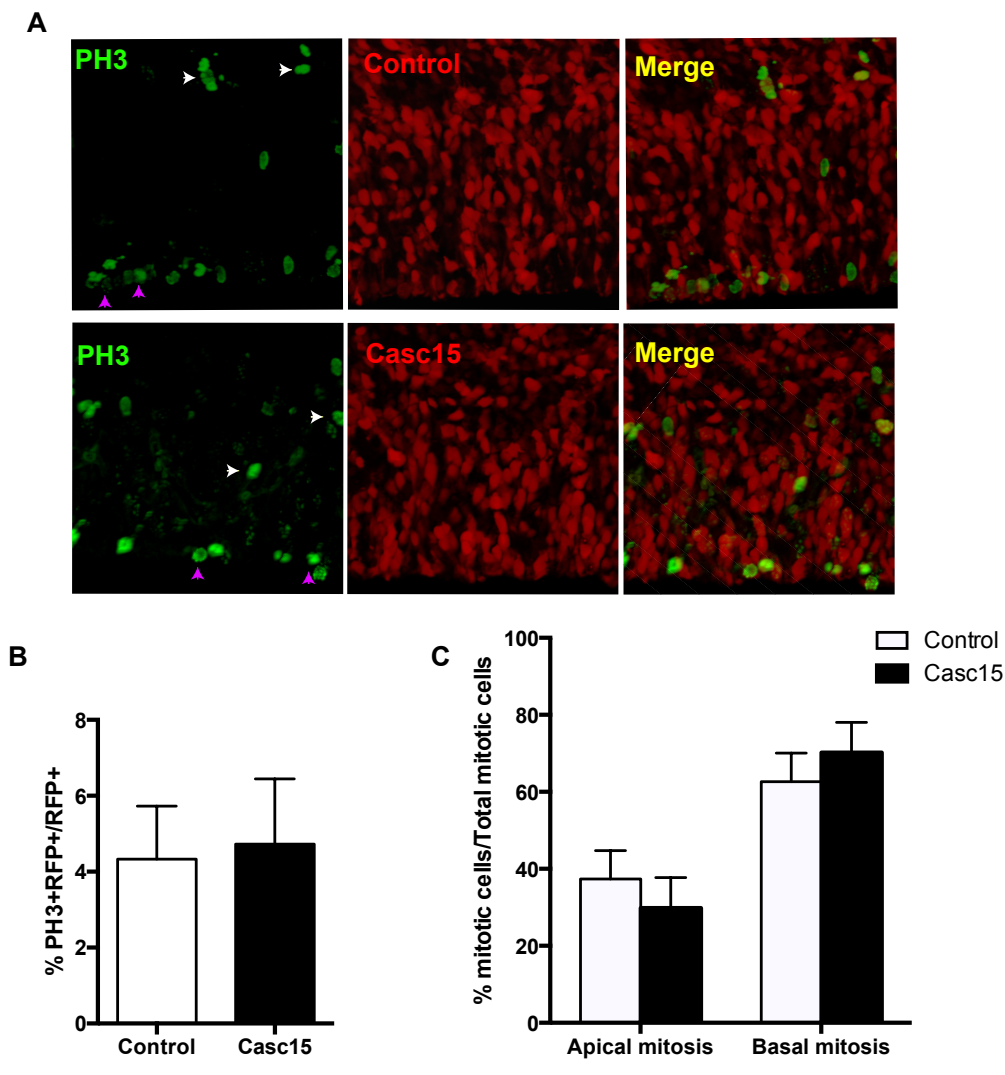


Figure 3.9: Casc15 does not change progenitors migration.

A: Immunofluorescent images for coronal sections of control (up) and Casc15 (bottom) brains 48 hours post IUE. PH3, marker of mitotic cells in green. Magenta arrows represent apical mitosis and white arrows are for basal mitosis. B: Column graph representing the percentage of mitotic cells over all RFP+ cells in the germinal layers (VZ and SVZ). C: Column graph representing the percentage of apical mitosis and basal mitosis over total mitotic cells error bars represent SD, n = 4 and 5 for controls and Casc15, respectively.

Sox2 is virtually expressed in all AP and BP in the VZ, very weakly expressed in the SVZ and absent in post-mitotic neurons. Therefore, 48 hours Casc15 overexpressing and control brains were stained with Sox2 and quantification of double positive Sox2⁺RFP⁺ was compared between the two conditions. In controls, almost all of RFP⁺ cells in the VZ were Sox2⁺ (88.63 ± 2.4 , average \pm SD, n=4), thus belonging to the progenitors populations. Similarly, in the VZ of Casc15 overexpressing brains, there was no observed or quantitative difference in the percentage of RFP⁺Sox2⁺ cells (88.67 ± 2.6 , average \pm SD, n=3) (Figure 3.10A and B).

Another helpful assay to assess direct neurogenesis in APs is using the newborn neurons marker Tubb3. In standard conditions, Tubb3 is almost absent in the progenitors in the VZ, while it is readily detected in the SVZ and through the neuronal layers IZ and CP. To this end, the 48 hours Casc15 overexpressing brains were analyzed for the neuronal marker Tubb3 and compared to controls. For immunohistochemistry, I used Tubb3 together with Tbr2 antibodies to label newborn neurons and delimit the VZ/SVZ, respectively. Consistent with the above data, Tubb3 signal was almost absent in the VZ of control brains and only detected in the SVZ (Figure 3.10C). Similarly, Casc15 overexpressing VZs did not present any marked increase in Tubb3 signal after 24 hours or 48 hours. Together with the above data, this observation rules out that Casc15 potentiates direct neurogenesis.

3.3.4 Casc15 causes subtle changes on cell distribution after 24 hours

Another explanation for the increased percentage of progenitors and decreased neuronal output after 48 hours of Casc15 overexpression is a disturbed balance of proliferation/differentiation in progenitors. To resolve the changes on the progenitors population, the effects encountered upon Casc15 overexpression at the 24 hours time point was examined. This time point should reveal the earliest changes in the developing brain. Therefore, IUE was performed at E13.5 and animals were sacrificed at E14.5. The cryosections were examined with fluorescence microscopy. The distribution of the RFP⁺ cells was visually identical in Casc15-expressing and control brains. With the aid of Tbr2 staining the percentage of RFP⁺ cells was determined in the VZ, SVZ and early intermediate zone (the 3 layers that contain RFP⁺ cells at this time point) and the quantitation confirmed the lack of significant change in RFP⁺ cell distribution in Casc15-expressing brains compared to controls (Figure 3.11B). Two important highlights were observed in the 24 hours overexpressing Casc15 brains. First, there was a large variability among the replicates. Second, an observed tendency towards a decrease in the number of cells in the SVZ in Casc15 ($18.74 \pm 1.7\%$ n=6, average \pm SD) compared to controls ($23.03 \pm 1.3\%$ n=7, average \pm SD, p-val=0.0685). This decrease, yet not significant, suggests a depletion of 20% of the progenitors localizing to the SVZ after only 24 hours of Casc15 overexpression.

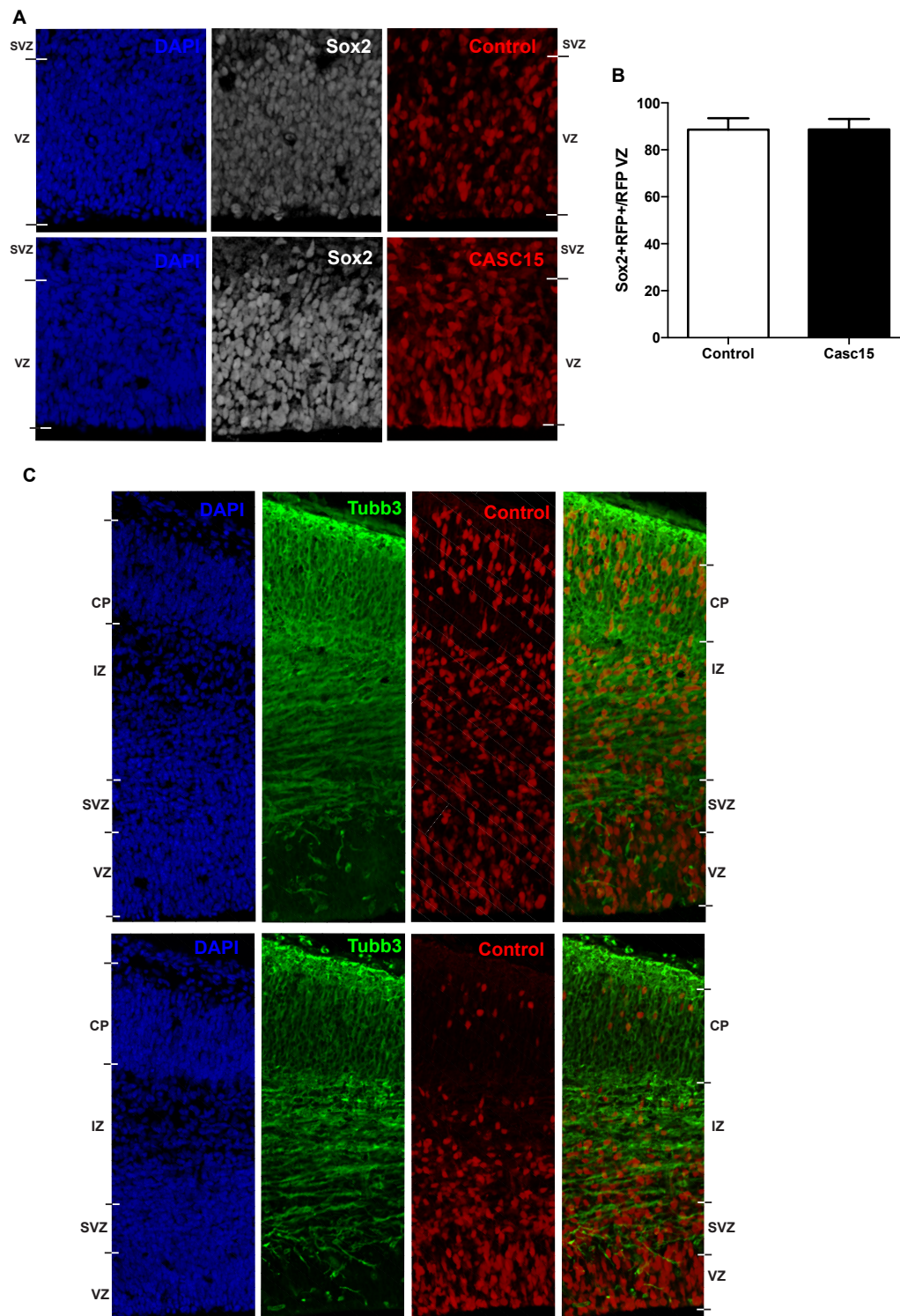


Figure 3.10: Casc15 does not induce direct neurogenesis in APs.

A: Immunofluorescent images for coronal sections in control (up) and Casc15 (bottom) 48 hours post IUE. B: Column graph representing the quantification of the RFP⁺Sox2⁺ cells in control and Casc15 brains. Error bars indicate SD, n= 4 and 3 for controls and Casc15, respectively. C: Immunofluorescent images for coronal sections of 48 hours overexpressing control brains (up) and Casc15 (bottom). Cortical layers VZ, SVZ, IZ and CP are indicated. SVZ was delimited by Tbr2 immunostaining (not shown). B-tubulin 3 (green) is used as marker for early born neurons.

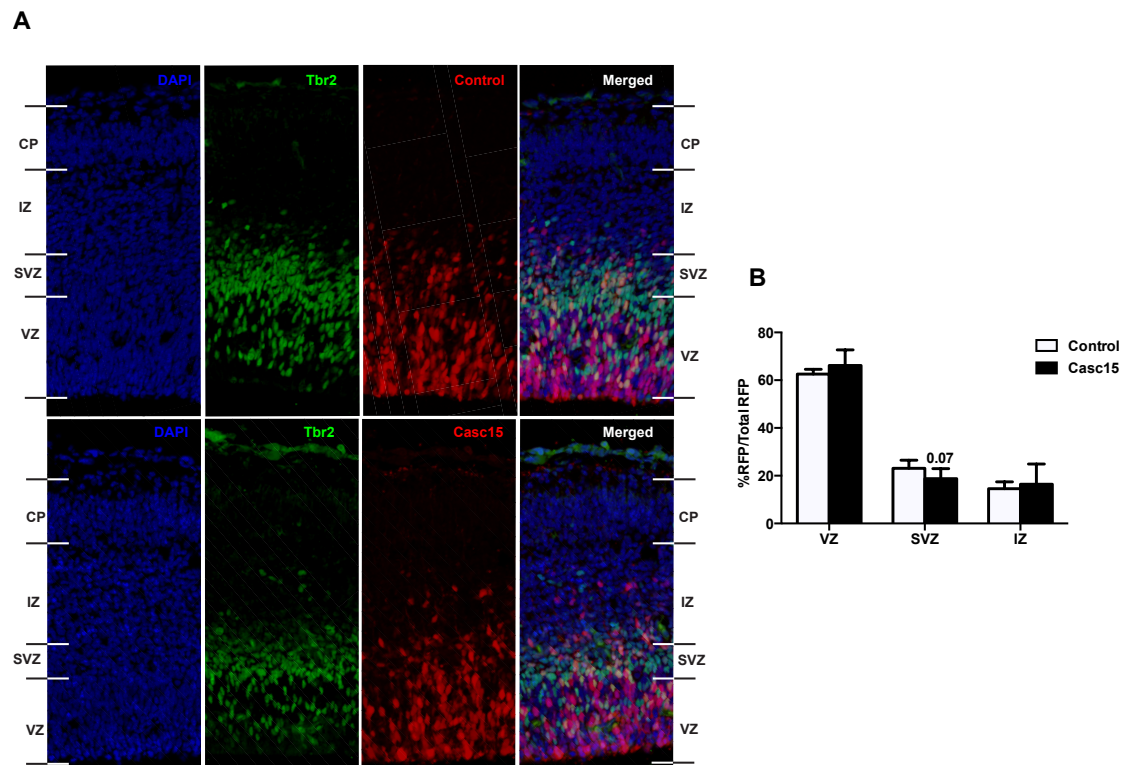


Figure 3.11: Effects of Casc15 after 24 hours.

A: Immunofluorescent images of coronal sections of control (up) and casc15 (bottom) brains 24 hours post IUE, immunostaining with Tbr2 to delimit the SVZ. Cortical layers VZ, SVZ, IZ and CP are indicated. B: Column graph representing the quantification of the percentages of RFP⁺ cells in VZ, SVZ and IZ. Error bars indicate SD, n = 7 and 6 for controls and Casc15, respectively.

3.3.5 Effect of Casc16 on progenitors fate

As discussed earlier (see section 1.2.1) the balance between proliferation and differentiation of the AP (Tbr2⁻) and BP (Tbr2⁺) is detrimental for neurogenesis where any bias towards either modes of division in early progenitors leads to decreased neuronal output. To question whether Casc15 has an effect on cell fate, two markers are of particular help; Btg2, which labels differentiating progenitors, and Tbr2, which labels BPs. If Casc15 changes the progenitors' mode of division we expect to see a change in BPs production (labeled with Tbr2). So, initially I sought to determine the percentage of AP and BPs in the 24 and 48 hours Casc15 overexpressing brains.

After 24 hours of Casc15 overexpression, it was observed that there was a decrease in the Tbr2⁺ cells around the site of electroporation (Figure 3.12A). Upon quantification of the Tbr2⁺ cells in Casc15 overexpressing brains, there seemed to be a tendency towards a decrease in the percentage of RFP⁺Tbr2⁺ cells, though not significant, in the

VZ (19.02 ± 2.3 , average \pm SD, $n=6$) and the SVZ (54.9 ± 7.6 , average \pm SD, $n=6$) compared to control VZ (24.8 ± 1.67 , average \pm SD, $n=7$, two-tailed t-test p -value = 0.0598) and SVZ (72.8 ± 4.96 , average \pm SD, $n=7$, two-tailed t-test p -value = 0.0674), respectively (Figure 3.12B). However, when the BP population (all RFP⁺Tbr2⁺ in VZ and SVZ together) was quantified as a fraction of the total number of RFP⁺ cells, a significant drop in the percentage of BPs (33%) was observed in Casc15 (22.52 ± 2.27 , average \pm SD, $n=6$) compared to controls (32.38 ± 2.16 , average \pm SD, $n=7$, two-tailed t-test p -value = 0.0093) (Figure 3.12C). The decrease in BPs in Casc15 overexpressing brains reflects, after excluding premature neurogenesis in APs, increased proliferative divisions in APs.

Next, the percentage of Tbr2⁺ cells was quantified in 48 hours Casc15 overexpressing brains and compared to controls. After 48 hours, in the VZ, there was no significant change in the percentage of Tbr2⁺ cells in Casc15 (30.4 ± 1.23 , average \pm SD, $n=10$) compared to controls (31.89 ± 1.6 , average \pm SD, $n=8$, two-tailed t-test p -value = 0.4632) (Figure 3.12D and E). Similarly, in the SVZ there was no significant difference in the percentage of the Tbr2⁺ cells in Casc15 overexpressing brains (75.13 ± 2.05 , average \pm SD, $n=10$) compared to controls (75.53 ± 2.93 , average \pm SD, $n=7$, two-tailed t-test p -value = 0.6489) (Figure 3.12E). However, the percentage of the AP (Tbr2⁻ in the VZ), BP (Tbr2⁺ in VZ and SVZ) and neurons (Tbr2⁻ in SVZ, IZ and CP) were significantly different between Casc15 and controls (Figure 3.12F). In casc15, the percentage of APs was significantly higher (21.85 ± 0.95 , average \pm SD, $n=10$) compared to controls (16.84 ± 0.32 , average \pm SD, $n=7$, two-tailed t-test p -value = 0.0007). Similarly, BPs were significantly higher in Casc15 (21.35 ± 0.59 , average \pm SD, $n=10$) compared to controls (18.12 ± 0.72 , average \pm SD, $n=7$, two-tailed t-test p -value = 0.0032), representing a \approx 30% increase in APS and \approx 17% increase in BPs. The percentage of neurons, however, was less in Casc15 (56.8 ± 1.12 , average \pm SD, $n=10$) than in controls (65.04 ± 0.93 , average \pm SD, $n=7$, two-tailed t-test p -value < 0.0001). The increased percentage of progenitors after 48 hours favors an increased proliferative potential of the progenitors before they commit to neurogenesis.

Finally, staining against the apoptotic marker active caspase-3 confirmed the lack of apoptosis induction in 24 or 48-hours Casc15 overexpressing brain sections.

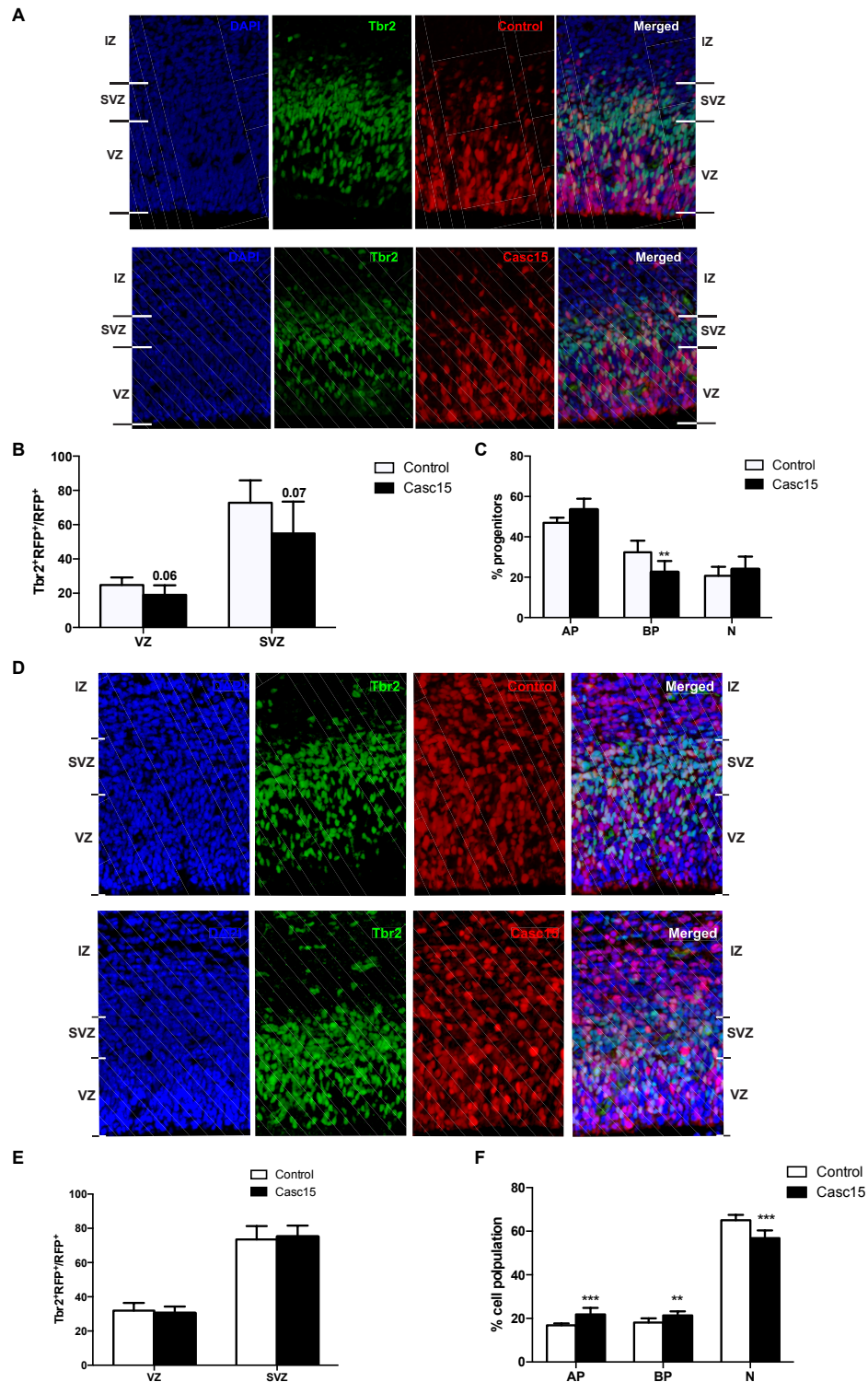


Figure 3.12: Casc15 induces proliferation in progenitors.

A: Immunofluorescent images of coronal sections of 24 hours control (up) and Casc15 (bottom) brains. B and E: Column graph representing the quantification of the percentages of RFP⁺Tbr2⁺ cells in the VZ or SVZ as a fraction of RFP⁺ cells in each cortical layer, respectively. C and F: Column graph representing the quantification of all RFP⁺Tbr2⁺ in VZ and SVZ as a fraction of total RFP⁺ cells. The fraction of AP, BP, and neurons was determined. D: Immunofluorescent images of coronal sections of 48 hours control (up) and Casc15 (bottom) brains. Cortical layers VZ, SVZ, IZ and CP are indicated. Error bars indicate SD, significance indicated with *, *** p-val < 0.001, * p-val < 0.05.

3.4 Molecular effects of Casc15

In order to resolve the phenotype described for Casc15, it was important to look at its effect on gene expression, if any. To this end, IUE with Casc15 or control plasmids was performed in E13.5 embryos of 3 mothers for each condition and mice were sacrificed after 24 hours. The lateral cortices were dissected and dissociated into single-cell suspension. RFP⁺ cells were sorted with Fluorescence-activated cell sorting (FACS, Figure 3.13A) and RNA was extracted. The poly (A) fraction was sequenced by massively parallelized short read sequencing (single-read), performed and bioinformatically analyzed at the Deep sequencing facility, Biotec. The sequencing was performed on Illumina Hiseq2000 platform and resulted in 30-40 million reads per sample. The sequencing reads were mapped to mus musculus mm10 genome (Ensembl 87). More than 99% of the mapped reads aligned to the reference with 86-88% of the fragments uniquely aligned to only one position on the reference (Figure 3.13B). The read counts per gene were normalized using DEseq (Anders and Huber, 2010). Sample to sample correlation of normalized gene expression resulted in a range between biological replicates that was highly reproducible ($r=0.98\pm 0.02$, Figure 3.13C).

3.4.1 Casc15 minimally changes gene expression in the developing cortex

The differential gene expression between Casc15 and control was tested according to a negative binomial distribution test with p-values adjusted (padj) for multiple-testing according to the Benjamini and Hochberg procedure (done by Mathias Lesche, sequencing facility). Differential expression analysis revealed that Casc15 minimally affects gene expression in the developing cortex of mouse. In total 105 genes changed their expression in Casc15 with a padj < 0.1, out of which 48 genes were upregulated and 57 were downregulated (Figure 3.14A and Table 4).

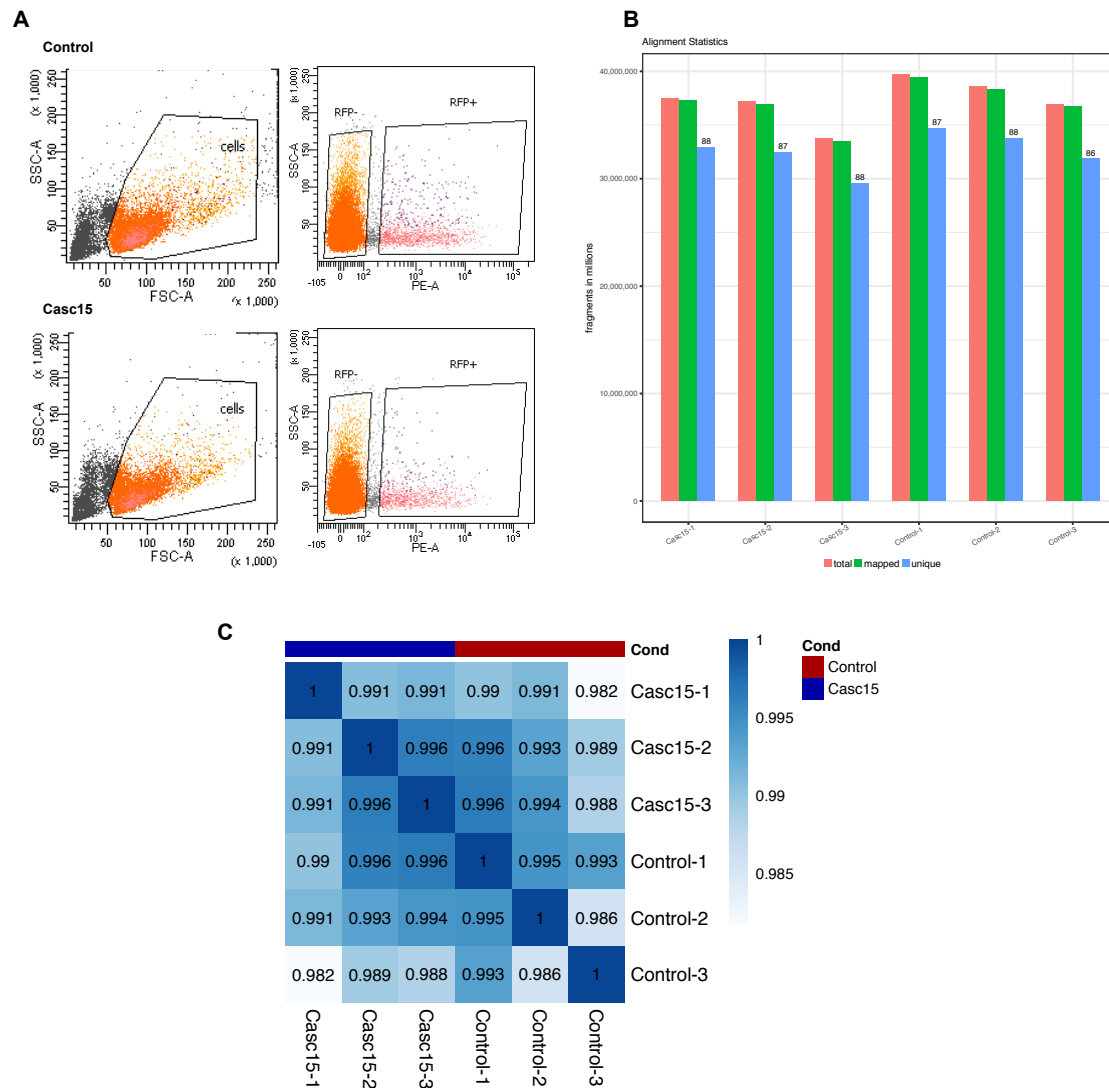


Figure 3.13: Transcriptome generation after Casc15 overexpression

A: FACs sorting plots representing the isolation of RFP+ cells from control (up) or Casc15 (bottom) overexpressing brains. Left: live cells sorting using the forward and side scatter. Right: gating around the RFP+ cells. B: Bar graph representing the alignment statistics with gsnap. Each sample is represented by a column which is divided into three bars. Red: Total number of fragment. Green: number of mapped fragments to the reference. Blue: number of uniquely aligned fragments to the reference. C: Sample to sample Pearson's correlation of DESeq-normalized gene expression between three biological replicates. Red: Casc15. Blue: control. Strong correlation is in dark blue, minimal correlation is in white as indicated.

The differentially expressed genes showed enrichment in GO terms for neurogenesis, axonogenesis and development of the nervous system (Figure 3.14B). The GO enrichment for the upregulated genes included pathways related to the innate immune response and virus induced immune response whereas for the downregulated genes mainly neurogenesis related pathways are enriched (Figure 3.14C and D).

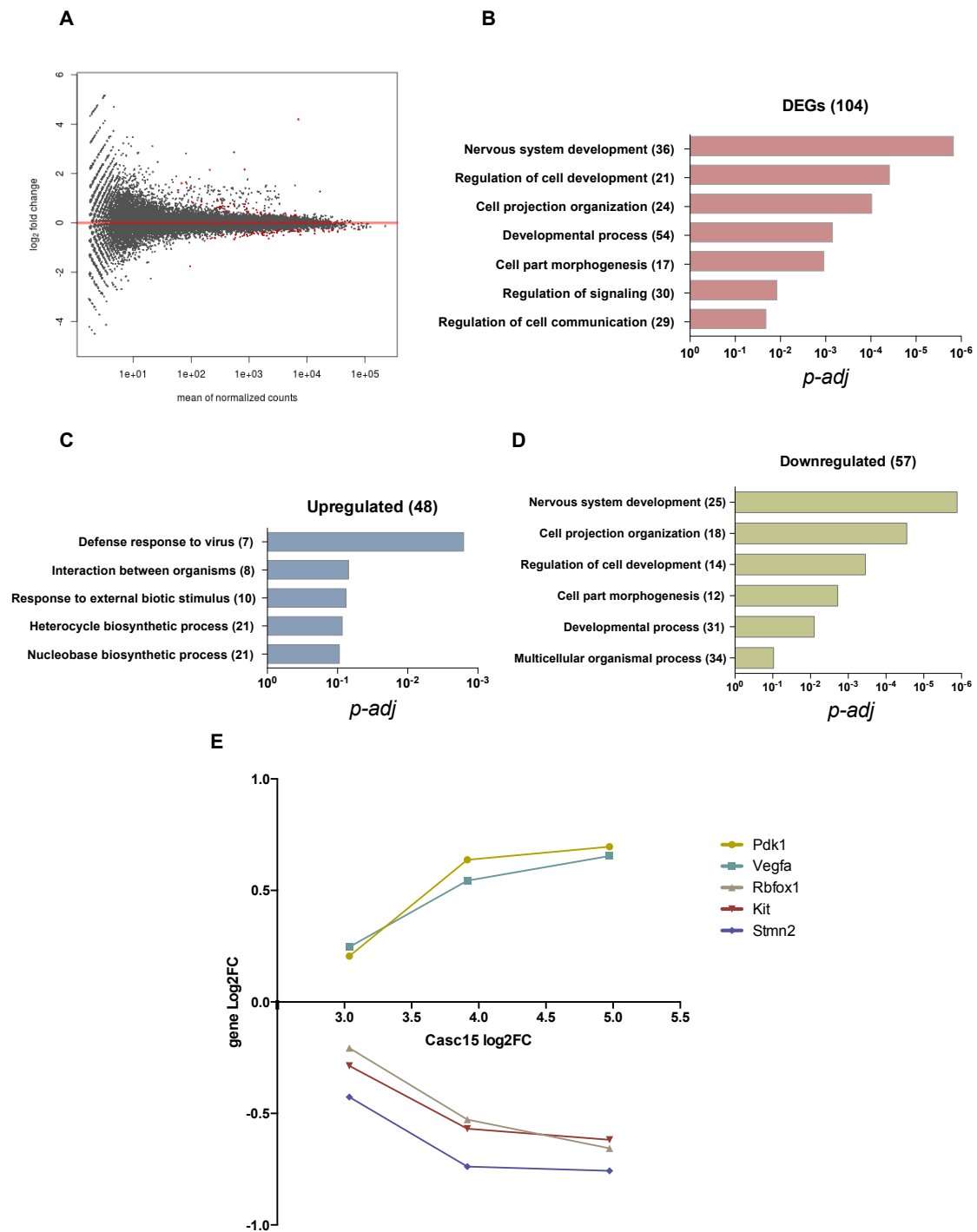


Figure 3.14: Differential expression analysis of RNA-seq.

A: Volcano plot representing the changes in gene expression upon Casc15 overexpression. Gene expression changes are represented in log₂ fold change. Each gene is represented by a single dot. Significantly changed genes are represented by red dots. B: Bar graph representing GO term enrichment for biological processes of differentially expressed genes. C: Bar graph representing GO term enrichment for biological processes of upregulated genes. D: Bar graph representing GO term enrichment for biological processes of down regulated genes. In brackets are number of genes contributing to each GO process. X-axis represents the *p*-adjusted value for the enrichment score. E: Correlation analysis between the log₂ fold change in Casc15 overexpression (x-axis) and the respective changes in gene expression (y-axis). Gene names and expression changes are indicated.

In attempt to better understand the changes induced upon *Casc15* overexpression, I examined the physiological expression of the deregulated genes upon *casc15* overexpression, i.e. examining their expression in the original transcriptome from PPs, DPs and N. Out of the 48 upregulated genes, 41 are physiologically enriched in downregulated in DPs and/or neurons compared to PPs. On the other hand, 54 out of the 57 downregulated genes were physiologically enriched in neurons. This is not surprising, given that *Casc15* increased the percentage of progenitors over neurons upon electroporation (Further discussed in the discussion section 4.2.1). Another interesting observation was that 42% of the deregulated genes (9 upregulated and 35 downregulated) showed a “dose response deregulation” to *Casc15* overexpression, where the efficiency of up or down regulation of target genes correlated with the magnitude of *Casc15* induction with a minimum of pearson correlation r squared = 0.75 (Further discussed in the discussion section 4.2.1). These genes will be selected for validation by RT-qPCR (Table 5). An example of which is shown in Figure 3.14E.

3.4.2 *Casc15* changes gene exon usage

Next, I wanted to assess if *Casc15* has any effect on alternative splicing. To this end, I analyzed the difference in the relative abundance of gene isoforms between *Casc15* and control RNA-seq samples.

Initially, Kallisto was used to align the sequencing fragments for each transcript and output the read counts in TPM for each isoform using *mus muclus mm10* (ensemble 87) as a reference. A cutoff was chosen for transcript expression where transcripts that have TPM < 1 were regarded as noise and only those with a minimum of 1 TPM in either *Casc15* or control were selected for further analysis. I, then, used SUPPA to calculate the relative abundance of each isoform of a gene relative to the total gene expression. SUPPA outputs the percentage spliced in (psi) for each isoform. SUPPA was also then used to calculate the difference in percentage spliced in (dpsi) for each isoform between *Casc15* and control (see section 2.2.9). In total 406 transcripts show a significant change in their abundance between *Casc15* and control (Figure 3.15A, p-value ≤ 0.05). The GO term analysis for those transcripts showed enrichment for pathways of primary metabolism, cellular metabolic processes and macromolecule metabolic processes (Figure 3.15B).

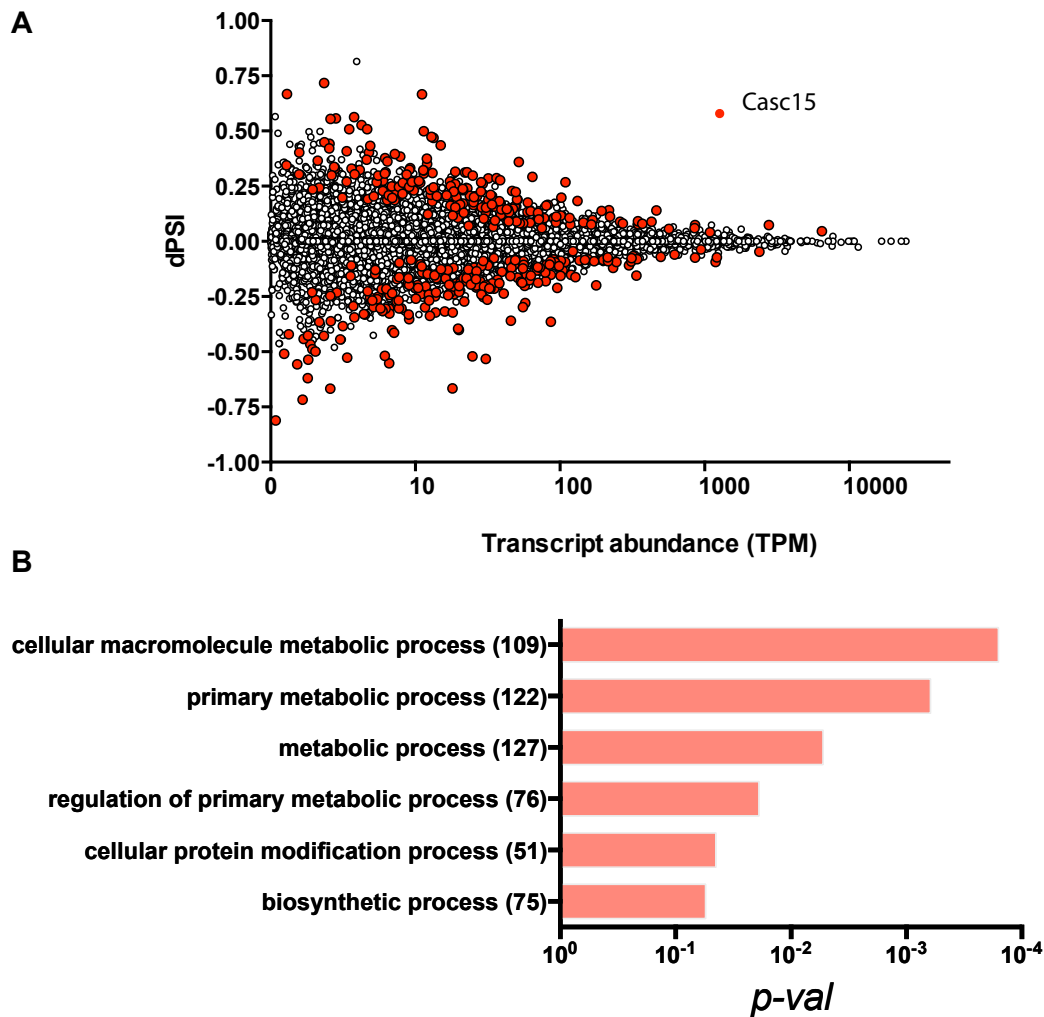


Figure 3.15: Effects of Casc15 on alternative splicing.

A: volcano plot representing differential exon usage. Each transcript is represented by a single dot. The changes in exon usage is denoted by dpsi (difference of percentage spliced in). Transcript abundance in is transcript per kilobase million (TPM). Significantly changing transcripts between control and Casc15 are denoted by red dots. B: Bar graph representing GO term enrichment of biological processes for genes with significant differential isoform usage between control and Casc15. Numbers in brackets represent the number of transcripts contributing to each GO term. X-axis is the p-adjusted value for the enrichment score.

These transcripts belong to 222 genes whose at least one isoform is differentially expressed with significance across the two conditions. Out of the 222 genes, 15 are for non-coding genes, including lincRNAs, antisense transcripts and TEC, while 207 are for protein coding genes. The alternative isoform usage in 114 out of the 207 coding genes (55%) leads to alteration in the coding sequence (cds). Changes in cds may result in inclusion/exclusion of known functional domains of a protein. For example, *ehd2* gene locus codes for a protein that is important for cortical actin cytoskeleton organization. Two isoforms for *ehd2* exist as per the mus muclus mm10, Ensembl 87, those isoforms are differentially spliced between Casc15 and control.

The longer isoform, Ehd2-201, is over represented in Casc15 overexpressing samples by 42% (dpsi = 0.42, p-value = 0.03) with a corresponding decrease in the relative abundance of the shorter isoform, Ehd2-202 (dpsi = -0.42, p-value = 0.03, Figure 3.16A). The protein encoded by the Ehd2-201 is 543aa that encodes for 3 main functional domains; Dynamin-type guanine nucleotide-binding (G) domain, EH domain and EF-hand domain. Ehd2-202, however, is 105aa retains only the Dynamin-type guanine nucleotide-binding (G) domain while the other two domains are lost (Figure 3.16A purple).

On the other hand, some alternative splicing changing CDS occurred in genes with no annotated function; i.e. fam102a, fam131a and A730017C20Rik. While in other cases, exon exclusion led to a loss of protein parts that have not been, so far, characterized. An example for this is the protein-coding gene is thap3, not much is known about the functional roles of this gene however it is known to act through DNA binding and regulate the transcriptional activity of RRM1, a cell cycle regulator. Three transcripts are transcribed from the gene locus as per the Ensemble 87, two of which are protein coding; Thap3-201 (218aa) and Thap3-202 (184aa), while the third is a processed transcript. The two coding transcripts differ in their 5' and 3' untranslated regions (UTR) but also Thap3-201 contains an extra 102 bps coding exon with unknown function (Figure 3.16B). The relative abundance of Thap3-201 in Casc15 is 19% lower than in control and vice versa (dpsi = 0.19, p-value = 0.037).

Figure 3.16 represents a sashimi plot that maps the reads of splice isoforms to the reference transcriptome. Sashimi plots are used to visualize the alternative splicing events of a gene through either the read counts of an exon (denoted in peaks) or the splice junction alterations (denoted by curves). In the presented figure, changes in Ehd2 gene splicing were elaborated by the disturbed proportion of the reads of the second and third exon (from the right) of the longer gene isoform. The increase in Ehd-201 in Casc15 is represented by the increase in the peak density of exon 2 in Casc15 overexpressing samples compared to controls.

In Thap3, however, the increase in Thap3-202 in Casc15 is represented by the increase in the splice junction reads that circumvent exon 3 (from the right) with a concomitant decrease in the splice junction reads that includes exon 3.

The validation of the differential splicing *in silico* predictions will be performed using RT-qPCR.

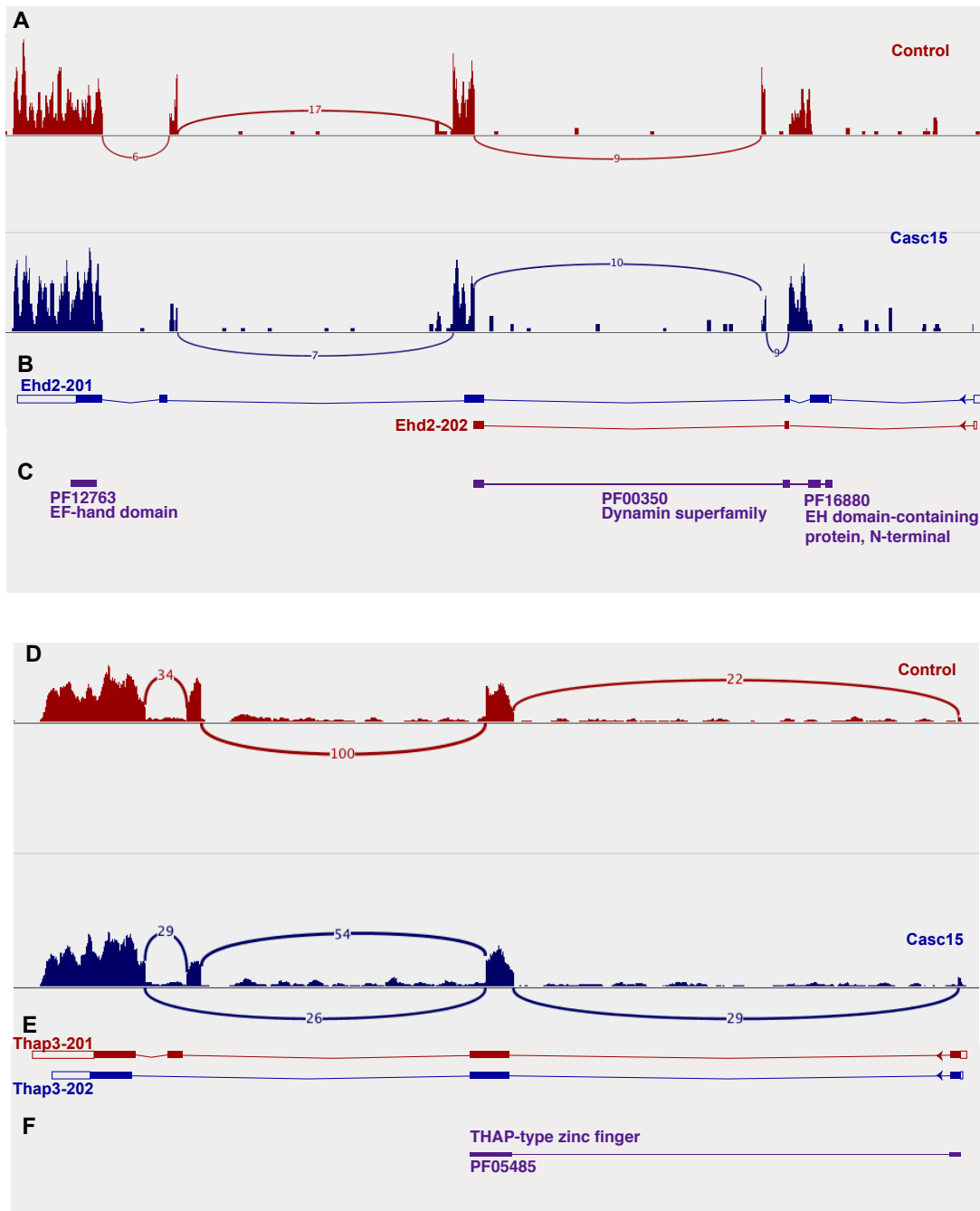


Figure 3.16: Alternative splicing changing the coding sequence of protein-coding genes.

A and D: an integrative genomic viewer snap of the raw reads aligned to the reference genome. Peaks represent the read fragments on each exon while curves represent splicing. Red and blue are for control and Casc15 merged samples, respectively. B and E: schematic drawing for isoforms that are alternatively expressed in control (red) or Casc15 (blue). Rectangles indicate exons, solid rectangles are protein-coding and lines indicate introns. C and F: Functional domains as predicted by the database Pfam (protein families). Each domain is represented by a Pfam code and the name of the respective domain.

Chapter 4

4 Discussion

The urge of massively parallel sequencing and development of RNAseq allowed the thorough assessment of the lncRNA component of several transcriptomes with thousands of novel lncRNAs identified. Though a few examples of lncRNAs have been known and studied for decades, lncRNAs remain, as a group, among the last classes of non-coding RNAs to have been described and least understood. Owing to their tissue and/or cell-specific expression, lncRNAs are considered to have regulatory functions in development and cell identity. The organ where lncRNA function seems to be relevant is the brain. First, lncRNAs expressed in the brain have a higher degree of evolutionary conservation. Evolutionary conservation was shown to be at the sequence level as well as at the RNA structure levels. Second, lncRNAs expressed in the brain display markedly specific patterns. Not only does the brain express that largest proportion of lncRNAs but also the highest proportion of the tissue-specific ones. Third, within the brain, lncRNAs present high temporal and spatial specificity. These observations highlight lncRNAs to act as novel regulators in the temporal and spatial control of the brain complex developmental programme, cell fates and function. In contrast to the homogenous cell cultures, the developing brain presents a complex organ in which the somatic stem cells are intermingled with more differentiated progenitors and terminally differentiated cells. This makes it difficult to isolate highly enriched pools of individual cell types, which is mandatory to study regulatory roles of lncRNAs. Our lab has addressed this problem by generating a double reporter mouse line in which the PPs, DPs and neurons could be discriminated. This allowed the isolation of the three cell populations and a transcriptome of the poly (A) fraction was generated. This transcriptome, in addition to the protein-coding genes, specified the expression of annotated lncRNAs in the three cell populations allowing further studies of their roles in cortex development. In this study, I focus on

2610307P16Rik, the mouse putative orthologue for the human CASC15, a lincRNA that is enriched in DPs.

4.1 **Casc15 is a potential regulator of neurogenesis**

2610307P16Rik is expressed in the neural epithelia of the developing cortex already at E8.5. At E14.5, our transcriptome shows that 2610307P16Rik is upregulated by more than two-folds from PP to DP, while it is again downregulated in neurons. This transient upregulation in DP, we call Onswitch, is remarkable for many protein-coding genes that play major roles in neurogenesis, including Ngn1, Ngn2, Tbr2, Insm1, Tis21 and NeuroD4. Moreover, the list of Onswitch lincRNAs included Miat and Rmst. Miat has been shown to be involved in cell fate commitment of retinal neural progenitors and in the developing cortex (Aprea et al., 2013; Rapicavoli et al., 2010). As well, Rmst has been shown to be a transcriptional coregulator of SOX2 in the regulation of proneural genes ((Ng et al., 2013)). This prompted the characterization of the cellular and molecular effects of 2610307P16Rik. 2610307P16Rik aligns to Cancer susceptibility 15 (CASC15) on chromosome 6 in the human genome. This suggests that CASC15 is the human orthologue of 2610307P16Rik. Although not yet given the name on the databases, I used the orthologue gene symbol *Casc15* to also represent the mouse gene 2610307P16Rik.

To identify the roles of *Casc15* in the developing cortex, I used IUE at mid neurogenesis. The expression plasmids are injected in the ventricles of the developing cortex and with small voltage, APs lining the ventricles take up the plasmids. The reporter protein allows tracing the targeted cells together with their progeny. By only determining the distribution of targeted cells across the cortical layers, many changes in progenitors and/or neurons can be deduced (3.1.2 **IUE as powerful tool for candidate genes screen**). By using 48 hours overexpression, I hoped to see the earliest changes encountered upon genetic interference.

Casc15 overexpression led to increased proportion of AP and BP with a consequent decrease in neuronal output. Moreover, it caused a delay in neuronal migration. This complex phenotype implies at least two different pathways being affected upon *Casc15* manipulation, each should be addressed independently.

4.1.1 Casc15 induces proliferation of progenitors in the developing cortex

After 48 hours of Casc15 overexpression, we observed an increase in the percentage of cells in the VZ, those cells were all SOX2⁺ indicating their stem cell identity (Figure 3.7 and Figure 3.10). Similarly, the percentage of cells in the SVZ was also increased compared to controls. Again those cells were positive for the SVZ marker Tbr2 (Figure 3.7 and Figure 3.12). Together this means that Casc15 overexpression increased the percentage of AP and BP after 48 hours. This increase might be due to an increased proliferative over differentiative potential of progenitors at an earlier time point. To question this possibility, overexpression was performed for only 24 hours and the percentage of progenitors was calculated. At 24 hours, there was a marked decrease in the BP population in Casc15 compared to controls, however, only minor non-significant changes were present in the AP (Figure 3.12F). The decrease in the proportion of BP could mean an enhanced premature production of neurons by AP, named direct neurogenesis, which we excluded because the data do not support it (Figure 3.10). Moreover, direct neurogenesis should cause an increase in the neuronal output as an immediate effect with a depletion of the AP progenitor pool rather than the opposite. An alternative explanation would be an acute increased proliferative potential of AP. If a greater percentage of AP switch to a proliferative division, this should decrease the number of differentiative progenitor, Btg2⁺, which should reflect on a decreased production of BPs at 24 hours. This proliferation will, then, lead to increased percentage of AP and BP seen after 48 hours. Another support of this hypothesis comes from the literature where overexpression of human CASC15 was shown to induce cell proliferation by increasing cell viability and cell cycle progression in gastric cancer (Wu et al., 2018), facilitated proliferation of melanoma cells (Yin et al., 2018), promoted colon cancer proliferation (Jing et al., 2018), induced cell proliferation in tongue squamous cell carcinoma (Zuo et al., 2018) and caused cardiac hypertrophy progression (Li et al., 2018) while its knockdown impaired cell proliferation in hepatocellular carcinoma models (He et al., 2017).

Beside the current evidence, an ultimate proof of increased proliferation in neural progenitors should be the determination of the reactivity to Btg2⁺, marker of differentiation, in APs. This is currently under progress.

4.1.2 Casc15 delays neuronal migration in the developing cortex

After 48 hours of electroporation, the percentage of neurons were similar in the IZ of Casc15 and controls, however, in Casc15 overexpressing brains more neurons resided in the early IZ closer to the SVZ, reflecting a defect in neuronal migration (Figure 3.8). Because the machinery involved in the neuronal migration, at least in part, intersects with that of INM, I assessed the effects of Casc15 on INM. As explained in section 1.2.1 INM is the process by which the nuclei of progenitors oscillate between the apical and basal membranes during the different phases of the cell cycle. INM allows reserving the limited apical space for mitosis by moving the interphase nuclei away from the apical surface thereby promoting the expansion of APs. A good method to detect perturbations in INM is by determining if mitosis took place anywhere in the VZ (abventricularly) rather than at the apical surface lining the ventricles. Using PH3, a marker of mitotic cells, I could not detect any changes in the percentages of apically dividing cells in Casc15 overexpressing brains compared to controls, thereby refuting an effect of Casc15 on INM (Figure 3.9). The evident effect of Casc15 on neuronal migration is again in alignment with our current knowledge of CASC15 being a regulator of migration in cancer cells. However this needs further elaboration.

Casc15 proliferative or differentiative, pro-migratory or anti-migratory lincRNA

The human CACS15 was first identified as part of the neuroblastoma susceptibility locus at chromosome 6p22 (Russell et al., 2015). In that study by Russell et al, CASC15 was reported as a tumor suppressing lincRNA whose upregulation is associated with better patient prognosis. Attenuating or stably depleting a short isoform of CASC15 (CASC15-004 on Ensembl 82, CASC15-204 on Ensembl 92) resulted in a highly reproducible increase in neuroblastoma proliferation and increased migratory capacity. Ever since, CASC15 has been characterized in many different cancers and as previously mentioned it was shown to induce proliferation in some studies or to inhibit proliferation in others. Similarly, those same studies showed a discrepancy in whether CASC15 is promoting or delaying the migratory potential of cancerous cells.

The increased migratory capacity of neuroblastoma cells upon CASC15 depletion as described by Russell et al, is in alignment with our data because our overexpression of Casc15 delayed migration of neurons. On the other hand, the controversy between the

proliferation phenotype they describe and ours is puzzling. In a follow up study, Mondal and coauthors also showed that CASC15 upregulation is associated with better overall survival (Mondal et al., 2018). The knockdown of CASC15-003 and CASC15-004 (Ensembl 82) in neuroblastoma cell lines again resulted in increased proliferation but lead to increased cell migration. Thus, both study agree on the induced proliferation upon CASC15 depletion, but have contradicting results concerning the effects of Casc15 on migration. Moreover, in the study by Mondal, CASC15 upregulation was shown to be important for retinoic acid mediated neuronal differentiation. However, in the same study, and in contrast to the retinoic acid-induced differentiation, CASC15 was downregulated in the sphere cultures of the same neuroblastoma cell line. As well, depletion of both CASC15 isoforms enhanced the sphere forming ability of that cell line. Together, these observations highlight that CASC15 behaves very differently moving from a monolayer culture to a more organized one. Then we could infer that the opposite phenotypes in either proliferation or migration comparing our data to any of those studies is not surprising given the following: first, our gene manipulation is performed *in vivo* rather in cell cultures. Second, the targeted cells in our system are the neural progenitors while the neuroblastoma cell lines are derived from neural crest cells. Third, cancerous cell lines do not well represent a physiological status of neuronal tissues. Fourth, we have previously shown that lncRNA overexpression or knockdown might result in similar phenotypes when applied by IUE (Aprea et al., 2013).

Hence, based on my current data and the publically available ones, we can only conclude that Casc15 is regulating proliferation of progenitors and neuronal migration and further experiments are needed to elaborate these functions.

4.2 Molecular aspects of Casc15 in neurogenesis

To gain further insight on the exact functions of Casc15 in neurogenesis, we sought to dissect the molecular changes encountered upon Casc15 overexpression. As reviewed in section 1.4.2 lncRNAs have been shown to regulate different biological processes with diverse tactics including the control of gene expression, mRNA processing and stability and protein translation or modifications. Each of these tactics can be achieved through different mechanisms. For example, positive or negative control of gene expression might be achieved through modulating the binding of chromatin modifiers on gene loci, recruiting the transcription machinery to the genomic loci or

forming a lncRNA-DNA triplex structures that can inhibit the assembly of the pre-initiation complex. Likewise, posttranscriptional modulation might be through increasing the mRNA stability by sequestering miRNAs or blocking miRNA binding sites on target mRNA, conversely lncRNAs may catalyze mRNA decay decreasing its stability. Moreover, lncRNAs have been shown to modulate mRNA alternative splicing by forming scaffolds for proteins of the spliceosome machinery (reviewed in (Geisler and Collier, 2013)). In order to address any of these possibilities, the most efficient approach was to look at the transcriptome upon *Casc15* overexpression *in vivo* which should reflect any of the changes happening at the mRNA level.

4.2.1 *Casc15* roles in neurogenesis cannot be explained in light of changes in gene expression

To this end, overexpression of *Casc15* was performed for 24 hours and RNA-seq was performed from RNA of the targeted cells. Although the cellular effects of *Casc15* overexpression at this time point are minimal, one can attribute that early changes in gene expression, if any, are responsible for the perturbed cellular distribution occurring later. Another important reason for choosing the 24-hour time point is that we were hoping to minimize the heterogeneity of the cell population in the developing cortex at this level. As shown in Figure 3.11 the majority of targeted cells after 24 hours belong to the AP and BP which do not have a very distinct gene expression profiles (Aprea et al., 2013). The high reproducibility between the biological replicates and between conditions indicated by a strong Pearson correlation coefficient > 0.982 (Figure 3.13), implied that *Casc15* did not cause major changes in the gene expression profile. In total only 105 genes were deregulated upon *Casc15* overexpression. The GO analysis showed that pathways involved in regulation of nervous system development are enriched. However, the RNA-seq results were, in general, astonishing for many reasons. Although *Casc15* was successfully overexpressed in the brain with at least 8 folds increase (\log_2 fold change > 3 , Figure 3.14E), the magnitude of changes in gene expression was minimum with the majority of genes having less than 2 fold change (\log_2 fold change < 1 or > -1 Table 4). Moreover, the genes that were upregulated with more than 2 folds (9 genes) and the only gene that was downregulated with more than 2 folds had minimal expression levels that were below the detection level of RT-qPCR (Table 4, data from PCR attempts not shown). This impeded the RNA-seq validation for the top deregulated

targets. Therefore, I chose other candidate genes with lower fold change upon *Casc15* overexpression for validation but, again, it was troublesome to detect minor changes in gene expression by RT-qPCR.

Interestingly, many genes that were deregulated upon *Casc15* overexpression showed a dose response to the magnitude of *Casc15* upregulation. In Figure 3.14E, I showed 5 genes whose expression was correlated to the magnitude of *Casc15* overexpression that are currently being validated (pearson correlation coefficient $r^2 \geq 0.75$). Those genes were selected based on their detectable expression levels in the developing cortex (Table 4) as well as their roles in different biological processes that is likely to explain the cellular phenotype encountered by *Casc15* overexpression (Table 1). Of note, other genes had a higher correlation coefficient to *Casc15* overexpression with $r^2 = 0.89$ to 1, however, those genes were excluded from further validation either because of their low expression levels, very low deregulation upon *Casc15* overexpression or because they are less likely to explain the cellular changes observed (Table 5).

Pdk1	Cell proliferation
Vegfa	Nervous system development Cell proliferation/differentiation Tube formation
Rbfox1	Regulation of alternative mRNA splicing (spliceosome) Nervous system development
Kit	Positive regulation of cell migration Stem cell differentiation
Stmn2	Neuron projection development Microtubule polymerization Regulation of cytoskeleton organization

Table 1: Protein-coding genes selected for validation by RT-qPCR.

Analysis of the physiological expression pattern of the deregulated genes revealed that the vast majority of the *Casc15*-upregulated genes (41/48) are physiologically downregulated in DPs and/or neurons. Conversely, 54/57 *Casc15*-downregulated genes are physiologically unregulated in neurons. This observation might reflect that the minor changes in gene expression upon *Casc15* overexpression are a consequence of the cellular phenotype rather than a cause. In other words, the increased proportion of AP over neurons upon *Casc15* overexpression (Figure 3.12F), led to the

appearance of AP specific genes as upregulated and neuron specific markers as downregulated. Although this assumption can not be ruled out based on the current data, we can also debate it because there is no statistical increase in AP or decrease in neurons in *Casc15* brains at 24 hours and those effects only appear at the 48-hour time point. On the other hand, one can argue that the high variability among the replicates observed at 24 hours (as shown in Figure 3.11 and explained in 3.3.4) does not allow us to fully exclude that RNA-seq data were generated from samples in which the neuronal count was less. With these downsides of the obtained data, a better approach for examining *Casc15* control of gene expression would be to perform overexpression in the double reporter mouse line that allows the isolation of targeted cells from each of the 3 populations independently and studying the changes that occur in each population. This approach was, however, proven very technically challenging owing to the double heterozygous nature of the mouse line and the difficulty in obtaining the RFP^+/GFP^+ embryos. Moreover, this approach necessitates the production of expression plasmids with a third reporter protein, e.g. BFP in order to sort the targeted cells in each population separately. The amount of material that is needed for RNA-seq, which is collected from a small number of targeted cells, makes this approach very time inefficient. Another approach would be to generate a transcriptome at an earlier time point of *Casc15* overexpression, e.g. 12 hours, in which mainly AP would be RFP^+ . This will allow us to look at the changes happening in a homogenous cell population; however, it will be impossible to explain the neuronal migration phenotype. Alternatively, the recently emerging single cell sequencing should allow tracing the expression changes in different populations of targeted cells and might lead to better understanding of the research question.

Last, another puzzling information from the RNA-seq data was the lack of change in *Tbr2* expression upon *Casc15* overexpression. The immunohistochemistry analysis showed a significant reduction in the $Tbr2^+$ cell population (Figure 3.12C), however that was not reflected on the mRNA level. This could have multiple explanations. First, *Casc15* had an acute effect on *Tbr2* gene expression that was fast compensated and therefore not seen on the mRNA level, however it caused a delay in *Tbr2* translation. The equal percentage of $Tbr2^+$ cells after 48 hours (Figure 3.12D and F) strengthens this assumption. Second, *Casc15* might affect *Tbr2* post-transcriptionally by causing protein degradation. A similar mechanism was shown for *CASC15* in neuroblastoma, where its overexpression led to reduction of the chromodomain

helicase DNA binding protein 7 (CHD7) protein, but not mRNA, presumably through increasing CHD7 ubiquitination (Mondal et al., 2018). Third, CASC15 might negatively regulate the translation of target genes. Collectively, further experiments, particularly western blots, are needed to overweight any of the presented assumptions. Because the RNA-seq data were not convincing of direct effects of Casc15 on gene expression, I used RNA-seq data to explore other possibilities. An effect of Casc15 over mRNA stability should be reflected in the gene expression analysis and is already excluded. As presented earlier lncRNAs can affect target genes at different levels, of which post-transcriptional regulations have been studied for many lncRNAs.

4.2.2 Casc15 changes the transcriptome at an isoform level

No *in vivo* data are currently available for the interaction of RNA-binding proteins and Casc15. However the *in silico* prediction tool, “The database of RNA-binding protein specificities (RBPDB)”, predicted many binding motifs for different members of the spliceosome machinery with a high score, these include Nono, Fus, Srsf9, Mbnl1 and Rbmx. As well, some proteins that play a role in protein translation were predicted to bind to Casc15; these include Aco1, Eif4b and Pum2. This suggests that Casc15 might affect mRNA splicing and/or translation. Moreover, Rbfox1, a member of the spliceosome machinery that was shown to affect alternative splicing of cytoskeleton proteins in the developing cortex, was downregulated upon Casc15 overexpression (Figure 3.14E). This downregulation, although was minimal, could have caused an alternative splicing of Rbfox1 downstream targets. Therefore, from the already available Casc15 transcriptome, I sought to assess if Casc15 causes alternative splicing of target mRNA. To this end, a series of bioinformatic tools was used consecutively to assess the changes in isoform abundance upon Casc15 overexpression (3.4.2). The differential isoform usage was represented as a difference in percent splice in (dpsi). Again, the results from the alternative splicing analysis were not conclusive for different reasons. First, the GO term analysis showed enrichment in pathways for biosynthesis and metabolism. Those enrichments cannot explain the cellular phenotype of Casc15. Second, in the majority of alternatively spliced genes, the isoform usage was only increased or decreased by less than 25% (Figure 3.15A). This might correspond to the minimal downregulation of Rbfox1 upon Casc15 overexpression. Third, the higher changes in isoform usage was associated

with lower transcript abundance (Figure 3.15A) as presented in the example of *Ehd2*, low transcript reads with higher $\text{dpsi} = 0.42$, and *Thap3*, higher transcript reads with minimal $\text{dpsi} = 0.18$ (Figure 3.16). Fourth, many changes occurred in the untranslated region of protein-coding genes for which the biological relevance is still very obscure, in protein coding genes with no annotated functions or in non-coding RNAs which are far less studied at the gene and isoform level. And finally, many of the predicted isoform changes were not easily visually detected when looking at the raw reads of the transcriptome on the integrative genome viewer, probably because of their small magnitude. Despite these negative impressions obtained at a first glance, looking at the biological processes for individual genes revealed that some of the alternatively spliced genes are involved in brain development, cell differentiation, SMAD signaling, positive regulation of cell cycle, actin cytoskeleton reorganization, Notch signaling and tissue regeneration among other processes. However none of those genes was, so far, studied at an isoform level. As well, whether the change in isoform usage is a direct effect of *Casc15* interaction with splicing factors or secondary to the downregulation of *Rbfox1* remains to be answered.

After validation of the RNA-seq data and alternative splicing predictions, knocking down of *Casc15* might be a helpful tool to further characterize *Casc15* roles in neurogenesis at cellular and molecular levels. However, the ultimate way to fully characterize lncRNA at a mechanistic level is by looking at their protein, chromatin or DNA interactions. This is currently achieved by one of the three stated protocols: ChIRP, CHART or RAP combined with either mass spectrometry or sequencing. Those protocols are similar to ChIP in which complementary oligonucleotides, rather than antibodies, are used to pull down the target lncRNA with all its binding partners. These experiments are technically very challenging, require a huge amount of cell material for the pull downs and a lot of control conditions and are highly costly in time and money. Moreover, the results are usually very difficult to filter and interpret as they produce a lot of false positive results. For compromise, biotinylated RNA pull downs are routinely used to identify protein interactions. An *in vitro* transcribed biotinylated lncRNA is adsorbed onto magnetic beads and introduced to a cell lysate. The protein partners that bind *in vitro* to the lncRNA, if any, are identified by mass spectrometry. This tool, although not perfectly recapitulating the *in vivo* status, is mostly complemented with RNA immunoprecipitation (RIP) to confirm the interaction of candidate proteins.

4.3 Concluding remarks

In this study we have identified *Casc15* as a novel regulator of neurogenesis, modulating at least two pathways in cortical development. The mechanistic insights of *Casc15* in the developing brain are not yet fully characterized. Other mechanisms through which lncRNAs can regulate biological processes include epigenetic modifications and protein translation and modifications. These aspects were not addressed given the time frame of the thesis work. Although the mechanisms are not yet clear, through positive or negative regulation of progenitors proliferation and neurons migration, *Casc15* might affect the final brain size and/or neuronal functionality. Future experiments should help to gain further insights on the effects of *Casc15* overexpression in the adult brains.

5 Appendix

Ensembl ID	Gene Symbol	log2FC(PPvsDP)	PP	DP	N	log2FC(DPvsN)
ENSMUSG00000091645	Gm17591	-0.822385	99.6765	56.3677	0.429961	-7.03452
ENSMUSG00000085587	Gm14493	-1.02888	52.497	25.7284	10.4247	-1.30335
ENSMUSG00000090534	Gm4675	-1.29963	36.0479	14.6438	0.362687	-5.33542
ENSMUSG00000063018	2010204K13Rik	-0.910832	30.2537	16.0913	1.42543	-3.49681
ENSMUSG00000075020	E530001K10Rik	-1.58481	29.4452	9.81609	1.93066	-2.34605
ENSMUSG00000090401	0610007N19Rik	-0.823449	21.195	11.9771	0.62477	-4.26081
ENSMUSG00000087579	1500017E21Rik	-1.11095	21.1683	9.80065	5.10458	-0.941085
ENSMUSG00000000031	H19	-1.1471	20.361	9.19365	1.45296	-2.66164
ENSMUSG00000086101	2610316D01Rik	-0.764429	18.0193	10.6077	3.8219	-1.47276
ENSMUSG00000087179	Gm14230	-1.034	17.1583	8.37931	1.9025	-2.13893
ENSMUSG00000064858	Snhg7	-0.830715	15.4163	8.66783	5.65393	-0.616416
ENSMUSG00000085069	Gm13111	-2.09638	15.4129	3.60422	0.378419	-3.25163
ENSMUSG00000075514	Gm13375	-0.605009	11.6699	7.6726	4.76774	-0.68641
ENSMUSG00000086308	G630016G05Rik	-1.43134	11.5559	4.28475	1.91062	-1.16517
ENSMUSG00000086888	A330033J07Rik	-1.26767	9.11094	3.78405	0.313813	-3.59195
ENSMUSG00000085848	Gm16790	-1.28948	7.6463	3.12809	0.373759	-3.0651
ENSMUSG00000091475	2810468N07Rik	-2.39954	7.05396	1.3369	0.091778	-3.8646
ENSMUSG00000086566	2810429I04Rik	-1.08359	6.45979	3.04808	0.497534	-2.61503
ENSMUSG00000085062	4933404O12Rik	-0.596942	6.35046	4.19863	1.78898	-1.23078
ENSMUSG00000085644	2310015A10Rik	-1.02754	4.67495	2.29329	0.535887	-2.09741
ENSMUSG00000087574	C030037D09Rik	-1.19897	4.2459	1.84945	0.762718	-1.27787
ENSMUSG00000073535	Gm5532	-2.01914	4.03235	0.994801	0.0763794	-3.70315
ENSMUSG00000091819	Gm17443	-1.21558	3.93878	1.69604	0.10735	-3.98178
ENSMUSG00000090771	Gm17501	-1.55283	3.62694	1.23621	0.0323023	-5.25814
ENSMUSG00000091138	E530011L22Rik	-1.0037	2.69275	1.34293	0.720814	-0.897681
ENSMUSG00000041674	BC006965	-0.743586	2.6361	1.57442	0.12993	-3.59901
ENSMUSG00000085259	Gm4890	-0.949044	2.5373	1.31426	0.0815961	-4.00961
ENSMUSG00000085582	3110099E03Rik	-1.40219	2.33549	0.883642	0.127024	-2.79836
ENSMUSG00000087541	Gm15830	-0.840112	1.90432	1.06376	0.0320252	-5.05382
ENSMUSG00000085013	4930556M19Rik	-1.38714	1.80092	0.688529	0.156648	-2.13599
ENSMUSG00000086342	Gm12932	-0.971648	1.74286	0.888726	0.325515	-1.44901
ENSMUSG00000072566	Pvt1	-0.995087	1.55853	0.781922	0.326694	-1.25908
ENSMUSG00000092274	Neat1	-0.935379	1.55255	0.811835	0.218983	-1.89037
ENSMUSG00000087480	Gm15910	-1.37436	1.35711	0.523471	0.145449	-1.8476
ENSMUSG00000086443	4933421A08Rik	-0.976534	0.677429	0.344269	0.0616059	-2.4824

Table 2: List of DownDown lincRNAs ordered by their expression level in PP.

lincRNAs are marked in red

Ensembl ID	Gene Symbol	log2FC(PPvsDP)	PP	DP	N	log2FC(DPvsN)
ENSMUSG00000086878	Miat	1.89618	94.4917	351.722	197.534	-0.832336
ENSMUSG00000085936	2610307P16Rik	1.25926	20.3544	48.7231	28.2796	-0.78484
ENSMUSG00000051295	9630028B13Rik	3.29136	1.86979	18.3059	5.45723	-1.74606
ENSMUSG00000089713	Gm16564	3.5213	1.1783	13.5292	1.25654	-3.42854
ENSMUSG00000085544	A930024N18Rik	1.08898	5.57674	11.8631	6.99943	-0.761165
ENSMUSG00000090454	Gm17341	2.38318	1.83947	9.59622	1.73946	-2.46382
ENSMUSG00000086180	Rmst	2.65663	1.07887	6.80289	1.22757	-2.47035
ENSMUSG00000086904	Gm13404	3.63839	0.245535	3.05758	1.37671	-1.15116
ENSMUSG00000085541	Gm16010	0.850076	1.5348	2.76662	0.799411	-1.79111
ENSMUSG00000073675	Gm10561	1.52901	0.898108	2.59182	0.40402	-2.68147
ENSMUSG00000086296	D030055H07Rik	1.14114	1.17425	2.58988	0.366899	-2.81943
ENSMUSG00000085410	2010110K18Rik	0.996926	1.28253	2.5596	0.124015	-4.36733
ENSMUSG00000087694	A530058N18Rik	4.63117	0.0406486	1.00732	0.411325	-1.29217
ENSMUSG00000092397	C130080G10Rik	4.63117	0.0406486	1.00732	0.411325	-1.29217
ENSMUSG00000085950	Gm13589	1.2644	0.331076	0.795334	0.41254	-0.947028

Table 3: List of Onswitch lincRNAs ordered by their expression level in DP.

lincRNAs are marked in red

Ensembl ID	Gene Symbol	log2FC	Control 1	Control 2	Control 3	Casc15 1	Casc15 2	Casc15 3
ENSMUSG00000085936	2610307P16Rik	4.19	840.5	437.1	946.6	23302.9	11186.8	6081.9
ENSMUSG00000069919	Hba-a1	2.16	205	441.1	274.4	1939.5	1427.2	742.3
ENSMUSG00000069917	Hba-a2	2.15	47.3	108.5	74	467.5	380.3	175
ENSMUSG00000032715	Trib3	1.66	42.7	42.4	31.6	85.3	206.8	76.1
ENSMUSG00000017830	Dhx58	1.6	39	29.6	32.6	38.2	130.1	139.1
ENSMUSG00000026628	Atf3	1.39	34.3	69.1	59.2	198.9	161.4	65.2
ENSMUSG00000024211	Grm8	1.32	43.6	39.5	18.8	84.3	74.6	96.7
ENSMUSG00000041827	Oasl1	1.16	231.9	163.8	185.6	255.8	466	580.4
ENSMUSG00000028977	Casz1	1.08	41.7	61.2	43.4	147	89.8	71.7
ENSMUSG00000027737	Slc7a11	1.04	51.9	108.5	41.5	149.9	155.3	109.8
ENSMUSG00000032265	Fam46a	0.96	198.5	174.7	191.5	279.3	374.2	449.9
ENSMUSG00000031297	Slc7a3	0.85	116	137.2	68.1	213.6	222.9	143.5
ENSMUSG00000026674	Ddr2	0.8	258.8	301	181.6	403.8	435.7	452.1
ENSMUSG00000069833	Ahnak	0.8	315.4	476.6	238.9	684.1	561.8	544.5
ENSMUSG00000054509	Parp4	0.8	99.3	62.2	74	140.1	124.1	146.7
ENSMUSG00000043279	Trim56	0.75	668.8	690.8	525.1	829.1	1259.8	1081.4
ENSMUSG00000097042	Gm17491	0.73	112.2	135.2	86.9	195	207.8	152.2
ENSMUSG00000001750	Tcirg1	0.69	208.7	169.7	150	289.1	290.5	276.1
ENSMUSG00000002227	Mov10	0.68	496.3	426.3	369.2	469.4	654.6	943.4
ENSMUSG00000053399	Adamts18	0.66	829.3	539.8	558.7	1125.1	894.7	1026
ENSMUSG00000072568	Fam84b	0.65	283.9	418.4	313.9	587	526.5	484.7
ENSMUSG00000018899	Irf1	0.65	282	183.5	262.6	370.4	389.3	384.7
ENSMUSG00000040613	Apobec1	0.64	306.1	208.2	262.6	392	429.7	393.4
ENSMUSG00000038872	Zfhx3	0.58	233.8	260.5	283.3	417.5	350	394.5
ENSMUSG00000040033	Stat2	0.58	994.5	764.8	1062.1	1085.9	1349.6	1791.1
ENSMUSG00000060924	Csmd1	0.58	248.6	218.1	175.7	324.4	288.5	350
ENSMUSG00000039384	Dusp10	0.57	690.2	667.1	834.1	1136.8	1221.5	903.1
ENSMUSG00000031523	Dlc1	0.55	356.2	283.2	281.3	466.5	434.7	449.9
ENSMUSG00000006494	Pdk1	0.53	999.1	1312.4	992	1783.6	1712.7	1269.4
ENSMUSG00000023951	Vegfa	0.49	2131.8	2665.3	2047.1	3590.8	3326.5	2706.2
ENSMUSG00000029313	Aff1	0.47	791.3	800.3	675.1	1039.8	995.5	1097.7
ENSMUSG00000018340	Anxa6	0.46	383.1	313.8	356.3	470.4	443.8	531.5
ENSMUSG00000032135	Mcam	0.43	1429.5	1454.5	1205.2	2141.3	1578.5	1801.9
ENSMUSG00000055322	Tns1	0.42	1390.6	1139.7	1058.1	1415.1	1623.9	1752
ENSMUSG00000078566	Bnip3	0.41	768.1	824	819.2	1105.5	1171	920.5
ENSMUSG00000030849	Fgfr2	0.39	3926.8	3711.3	3137.8	4907.9	4463.2	4709.2
ENSMUSG00000027217	Tspan18	0.39	2130.8	2019	1710.5	2590.2	2363.2	2725.7
ENSMUSG00000024457	Trim26	0.37	1454.6	1402.2	1385.8	1608.2	1953.7	1929.1
ENSMUSG00000027253	Lrp4	0.36	3814.6	3491.3	3030.2	4606.1	4346.2	4342.9
ENSMUSG00000025255	Zfhx4	0.35	1435.1	1600.6	1271.3	1856.2	1721.7	1925.8
ENSMUSG0000002688	Prkd1	0.34	1214.3	1091.4	1043.3	1425.9	1447.4	1356.4
ENSMUSG00000018593	Sparc	0.33	2145.7	1799.9	1803.3	2424.6	2309.8	2471.4
ENSMUSG00000052133	Sema5b	0.3	4710.7	4910.3	4443.7	6291.7	5260	5769.9
ENSMUSG00000053007	9430076C15Rik	0.3	1975	1831.5	1914.9	2499	2214	2307.3

ENSMUSG00000022708	Zbtb20	0.29	5531.7	5561.6	5195.8	6570	6576.3	6718.7
ENSMUSG00000022687	Boc	0.28	5953.8	5753	5625.2	7059.1	6950.5	7068.7
ENSMUSG00000043668	Tox3	0.27	4149.5	3806.1	3834.7	4788.4	4648.8	4772.2
ENSMUSG00000005973	Rcn1	0.26	3181.9	3194.2	3189.1	3707.4	3948.8	3806
ENSMUSG00000022129	Dct	-1.76	68.6	128.3	243.8	34.3	32.3	64.1
ENSMUSG00000044912	Syt16	-0.73	193.9	249.7	190.5	110.7	106.9	166.3
ENSMUSG00000056812	St8sia3	-0.66	666.1	707.5	650.5	337.1	465	477.1
ENSMUSG00000054976	Nyap2	-0.64	252.3	264.5	280.3	143.1	172.5	197.8
ENSMUSG00000027500	Stmn2	-0.63	2086.3	2644.6	3220.7	1568	1588.6	1972.6
ENSMUSG00000028039	Efna3	-0.61	270.9	333.5	330.7	183.3	199.7	228.2
ENSMUSG00000063646	Jakmip1	-0.58	936	717.4	866.6	433.2	620.3	634.7
ENSMUSG00000002908	Kcnn1	-0.54	1010.2	1126.9	1234.8	686	661.7	971.6
ENSMUSG00000037664	Cdkn1c	-0.52	1982.4	2523.2	2598.9	1793.4	1524	1634.6
ENSMUSG00000040907	Atp1a3	-0.51	4370.2	5005	4457.5	2797	3140.9	3775.6
ENSMUSG00000001552	Jup	-0.51	394.3	414.5	409.6	268.5	268.3	317.4
ENSMUSG00000036913	Trim67	-0.49	898	1091.4	886.4	667.4	670.7	711.9
ENSMUSG00000026817	Ak1	-0.49	599.3	749	709.7	497.8	462	506.5
ENSMUSG00000034993	Vat1	-0.48	7966.8	9658.7	9199.3	5980.1	6043.7	7146.9
ENSMUSG00000005672	Kit	-0.48	2004.7	2167	1857.6	1309.3	1355.6	1647.6
ENSMUSG00000018865	Sult4a1	-0.47	874.8	1179.2	1106.5	710.5	778.7	787.9
ENSMUSG00000021194	Chga	-0.45	2780.2	2308.1	2804.2	1930.6	1893.2	1973.7
ENSMUSG00000008658	Rbfox1	-0.45	1658.7	1432.8	1899.1	1055.5	1153.9	1441.1
ENSMUSG00000040136	Abcc8	-0.45	1347.9	1172.3	1279.2	756.6	930	1104.2
ENSMUSG00000048899	Rimk1a	-0.44	705	768.7	602.1	456.7	517.4	552.1
ENSMUSG00000001313	Rnd2	-0.43	13108.9	16383.7	17040.3	10481.3	11185.8	12818
ENSMUSG00000023017	Asic1	-0.43	1742.2	2014	1999.8	1387.7	1238.6	1644.4
ENSMUSG00000042078	Svop	-0.43	1168.9	1531.5	1474.6	955.5	971.3	1165.1
ENSMUSG00000031028	Tub	-0.42	1756.1	2094	1870.4	1231.9	1473.6	1574.8
ENSMUSG00000063446	Plpp1	-0.41	2070.6	1914.4	2132	1489.6	1547.2	1556.3
ENSMUSG00000040258	Nxph4	-0.41	1349.8	1421	1264.4	984.9	978.4	1074.9
ENSMUSG00000027581	Stmn3	-0.41	2975	3395.5	3947.2	2622.5	2733.4	2401.9
ENSMUSG00000032064	Dixdc1	-0.41	1173.5	1405.2	1245.6	906.5	908.8	1061.8
ENSMUSG00000025854	Fam20c	-0.4	1238.4	1049	1159.8	763.4	897.7	948.8
ENSMUSG00000025582	Nptx1	-0.4	907.3	753.9	778.8	574.3	610.2	665.1
ENSMUSG00000021700	Rab3c	-0.4	2429.6	2190.7	2349.2	1427.9	1752	2092.1
ENSMUSG00000031840	Rab3a	-0.39	2877.6	2887.4	2908.8	1979.6	2260.4	2369.3
ENSMUSG00000027950	Chrn2	-0.39	2881.3	3035.4	3329.3	2147.2	2184.7	2702.9
ENSMUSG00000021087	Rtn1	-0.38	7061.4	8722.2	8567.5	6182.9	5668.5	6847
ENSMUSG00000027612	Mmp24	-0.38	1165.1	1109.2	1307.8	836	887.6	1027
ENSMUSG00000064339	mt-Rnr2	-0.37	34229	35006.4	46350.6	28456.8	32066.5	28708.4
ENSMUSG00000042834	Nrep	-0.35	20705.5	22010.4	23311	16661.3	16522.4	18554.2
ENSMUSG00000024501	Dpysl3	-0.35	26024.8	29269.2	25732.2	19384.8	20799.1	23198.2
ENSMUSG00000046598	Bdh1	-0.35	3330.3	3496.2	3681.7	2559.8	2665.8	3038.8
ENSMUSG00000031530	Dusp4	-0.35	5590.1	6977.6	5909.4	4828.5	4660.9	5022.2
ENSMUSG00000048385	Scrt1	-0.35	3283	3447.8	3359.9	2406.9	2453	3074.6
ENSMUSG00000048895	Cdk5r1	-0.34	8913.9	8679.8	8706.7	6542.6	6797.2	7401.3

ENSMUSG00000053192	Mllt11	-0.34	5526.1	5781.6	5981.5	4273.9	4658.9	4758.1
ENSMUSG00000029126	Nsg1	-0.34	6198.7	7074.3	7165.9	5298	5134	5761.2
ENSMUSG00000032024	Clmp	-0.34	3624.4	3247.5	3447.7	2478.5	2617.4	3064.8
ENSMUSG00000062444	Ap3b2	-0.33	2015.8	2125.5	1844.8	1503.3	1588.6	1682.4
ENSMUSG00000026796	Fam129b	-0.33	1435.1	1495	1424.3	1227	1067.1	1174.9
ENSMUSG00000022658	Tagln3	-0.32	6897.2	7649.6	8240.8	5949.7	5732.1	6544.8
ENSMUSG00000047139	Cd24a	-0.31	20716.6	20341.7	22208.5	16510.4	16589	17964.1
ENSMUSG00000062380	Tubb3	-0.31	27899.6	30895.4	32184.5	23887	23865.3	25672.9
ENSMUSG00000096847	Tmem151b	-0.3	4608.6	4444.5	4473.3	3449.7	3522.2	4009.3
ENSMUSG00000020547	Bzw2	-0.29	7545.6	8129.2	8440.2	6175.1	6770	6802.4
ENSMUSG00000032181	Scg3	-0.29	3469.5	3529.8	3668.8	2809.7	2842.3	3097.4
ENSMUSG00000056895	Hist3h2ba	-0.29	2377.6	2630.8	2652.2	2069.8	2068.7	2146.5
ENSMUSG00000008575	Nfib	-0.28	45326.7	50180.3	51843.5	37766	41309.6	42587.1
ENSMUSG00000029121	Crmp1	-0.26	13855.6	15455.1	14835.3	12257.1	12218.6	12385.4
ENSMUSG00000072235	Tuba1a	-0.26	79555.7	82543.1	89680.9	69859.6	68780.8	71642.2

Table 4: List of genes that are up or down regulated upon Casc15 overexpression.

Gene Symbol	Average Control	Casc15 1	log FC Casc15-1	Casc15 2	Log FC Casc15-2	Casc15 3	Log FC Casc15-3
Casc15	741.4	23302.9	4.974	11186.8	3.915	6081.9	3.036
Hba-a1	306.8	1939.5	2.660	1427.2	2.218	742.3	1.275
Hba-a2	76.6	467.5	2.610	380.3	2.312	175	1.192
Atf3	54.2	198.9	1.876	161.4	1.574	65.2	0.267
Casz1	48.8	147	1.591	89.8	0.880	71.7	0.555
Ahnak	343.6	684.1	0.993	561.8	0.709	544.5	0.664
Fam84b	338.7	587	0.793	526.5	0.636	484.7	0.517
Pdk1	1101.2	1783.6	0.696	1712.7	0.637	1269.4	0.205
Vegfa	2281.4	3590.8	0.654	3326.5	0.544	2706.2	0.246
Nfib	49116.8	37766	-0.379	41309.6	-0.250	42587.1	-0.206
Bzw2	8038.3	6175.1	-0.380	6770	-0.248	6802.4	-0.241
Scg3	3556	2809.7	-0.340	2842.3	-0.323	3097.4	-0.199
Tmem151b	4508.8	3449.7	-0.386	3522.2	-0.356	4009.3	-0.169
Cd24a	21088.9	16510.4	-0.353	16589	-0.346	17964.1	-0.231
Ap3b2	1995.4	1503.3	-0.409	1588.6	-0.329	1682.4	-0.246
Cdk5r1	8766.8	6542.6	-0.422	6797.2	-0.367	7401.3	-0.244
Mllt11	5763.1	4273.9	-0.431	4658.9	-0.307	4758.1	-0.276
Clmp	3439.9	2478.5	-0.473	2617.4	-0.394	3064.8	-0.167
Dpysl3	27008.7	19384.8	-0.478	20799.1	-0.377	23198.2	-0.219
Bdh1	3502.7	2559.8	-0.452	2665.8	-0.394	3038.8	-0.205
Scrt1	3363.6	2406.9	-0.483	2453	-0.455	3074.6	-0.130
Mmp24	1194	836	-0.514	887.6	-0.428	1027	-0.217
Rab3a	2891.3	1979.6	-0.547	2260.4	-0.355	2369.3	-0.287
Chrn2	3082	2147.2	-0.521	2184.7	-0.496	2702.9	-0.189
Fam20c	1149.1	763.4	-0.590	897.7	-0.356	948.8	-0.276
Nptx1	813.3	574.3	-0.502	610.2	-0.415	665.1	-0.290
Rab3c	2323.1	1427.9	-0.702	1752	-0.407	2092.1	-0.151
Plppr1	2039	1489.6	-0.453	1547.2	-0.398	1556.3	-0.390
Tub	1906.8	1231.9	-0.630	1473.6	-0.372	1574.8	-0.276
Rnd2	15511	10481.3	-0.565	11185.8	-0.472	12818	-0.275
Svop	1391.7	955.5	-0.543	971.3	-0.519	1165.1	-0.256
Rimk1a	691.9	456.7	-0.599	517.4	-0.419	552.1	-0.326
Rbfox1	1663.5	1055.5	-0.656	1153.9	-0.528	1441.1	-0.207
Abcc8	1266.5	756.6	-0.743	930	-0.446	1104.2	-0.198
Sult4a1	1053.5	710.5	-0.568	778.7	-0.436	787.9	-0.419
Vat1	8941.6	5980.1	-0.580	6043.7	-0.565	7146.9	-0.323
Kit	2009.8	1309.3	-0.618	1355.6	-0.568	1647.6	-0.287
Trim67	958.6	667.4	-0.522	670.7	-0.515	711.9	-0.429
Atp1a3	4610.9	2797	-0.721	3140.9	-0.554	3775.6	-0.288
Jakmip1	840	433.2	-0.955	620.3	-0.437	634.7	-0.404
Efna3	311.7	183.3	-0.766	199.7	-0.642	228.2	-0.450
Stmn2	2650.5	1568	-0.757	1588.6	-0.739	1972.6	-0.426
Nyap2	265.7	143.1	-0.893	172.5	-0.623	197.8	-0.426
St8sia3	674.7	337.1	-1.001	465	-0.537	477.1	-0.500

Table 5: List of Deregulated genes that show a dose response correlation to Casc15 overexpression.

Genes selected for validation by RT-qPCR are highlighted in red.

6 Bibliography

- Angevine, J.B., Sidman, R.L., 1961. Autoradiographic study of cell migration during histogenesis of cerebral cortex in the mouse. *Nature* 192, 766–768.
- Apra, J., Calegari, F., 2015. Long non-coding RNAs in corticogenesis: deciphering the non-coding code of the brain. *The EMBO Journal* 34, 2865–2884. <https://doi.org/10.15252/emj.201592655>
- Apra, J., Lesche, M., Massalini, S., Prenninger, S., Alexopoulou, D., Dahl, A., Hiller, M., Calegari, F., 2015. Identification and expression patterns of novel long non-coding RNAs in neural progenitors of the developing mammalian cortex. *Neurogenesis (Austin)* 2, e995524. <https://doi.org/10.1080/23262133.2014.995524>
- Apra, J., Prenninger, S., Dori, M., Ghosh, T., Monasor, L.S., Wessendorf, E., Zocher, S., Massalini, S., Alexopoulou, D., Lesche, M., Dahl, A., Groszer, M., Hiller, M., Calegari, F., 2013. Transcriptome sequencing during mouse brain development identifies long non-coding RNAs functionally involved in neurogenic commitment. *EMBO J.* 32, 3145–3160. <https://doi.org/10.1038/emboj.2013.245>
- Arai, Y., Pulvers, J.N., Haffner, C., Schilling, B., Nüsslein, I., Calegari, F., Huttner, W.B., 2011. Neural stem and progenitor cells shorten S-phase on commitment to neuron production. *Nat Commun* 2, 154. <https://doi.org/10.1038/ncomms1155>
- Artavanis-Tsakonas, S., Rand, M.D., Lake, R.J., 1999. Notch signaling: cell fate control and signal integration in development. *Science* 284, 770–776.
- Artegiani, B., de Jesus Domingues, A.M., Bragado Alonso, S., Brandl, E., Massalini, S., Dahl, A., Calegari, F., 2015. Tox: a multifunctional transcription factor and novel regulator of mammalian corticogenesis. *EMBO J.* 34, 896–910. <https://doi.org/10.15252/emj.201490061>
- Attardo, A., Calegari, F., Haubensak, W., Wilsch-Bräuninger, M., Huttner, W.B., 2008. Live imaging at the onset of cortical neurogenesis reveals differential appearance of the neuronal phenotype in apical versus basal progenitor progeny. *PLoS ONE* 3, e2388. <https://doi.org/10.1371/journal.pone.0002388>
- Barry, G., Briggs, J.A., Vanichkina, D.P., Poth, E.M., Beveridge, N.J., Ratnu, V.S., Nayler, S.P., Nones, K., Hu, J., Bredy, T.W., Nakagawa, S., Rigo, F., Taft, R.J., Cairns, M.J., Blackshaw, S., Wolvetang, E.J., Mattick, J.S., 2014. The long non-

coding RNA Gomafu is acutely regulated in response to neuronal activation and involved in schizophrenia-associated alternative splicing. *Mol. Psychiatry* 19, 486–494. <https://doi.org/10.1038/mp.2013.45>

Baye, L.M., Link, B.A., 2008. Nuclear migration during retinal development. *Brain Res.* 1192, 29–36. <https://doi.org/10.1016/j.brainres.2007.05.021>

Bellion, A., Baudoin, J.-P., Alvarez, C., Bornens, M., Métin, C., 2005. Nucleokinesis in tangentially migrating neurons comprises two alternating phases: forward migration of the Golgi/centrosome associated with centrosome splitting and myosin contraction at the rear. *J. Neurosci.* 25, 5691–5699. <https://doi.org/10.1523/JNEUROSCI.1030-05.2005>

Bertrand, N., Castro, D.S., Guillemot, F., 2002. Proneural genes and the specification of neural cell types. *Nat. Rev. Neurosci.* 3, 517–530. <https://doi.org/10.1038/nrn874>

Bond, A.M., Vangompel, M.J.W., Sametsky, E.A., Clark, M.F., Savage, J.C., Disterhoft, J.F., Kohtz, J.D., 2009. Balanced gene regulation by an embryonic brain ncRNA is critical for adult hippocampal GABA circuitry. *Nat. Neurosci.* 12, 1020–1027. <https://doi.org/10.1038/nn.2371>

Bray, N.L., Pimentel, H., Melsted, P., Pachter, L., 2016. Near-optimal probabilistic RNA-seq quantification. *Nature Biotechnology* 34, 525–527. <https://doi.org/10.1038/nbt.3519>

Brockdorff, N., 2002. X-chromosome inactivation: closing in on proteins that bind Xist RNA. *Trends Genet.* 18, 352–358.

Bylund, M., Andersson, E., Novitch, B.G., Muhr, J., 2003. Vertebrate neurogenesis is counteracted by Sox1-3 activity. *Nat. Neurosci.* 6, 1162–1168. <https://doi.org/10.1038/nn1131>

Calegari, F., Haubensak, W., Haffner, C., Huttner, W.B., 2005. Selective lengthening of the cell cycle in the neurogenic subpopulation of neural progenitor cells during mouse brain development. *J. Neurosci.* 25, 6533–6538. <https://doi.org/10.1523/JNEUROSCI.0778-05.2005>

Clark, M.B., Johnston, R.L., Inostroza-Ponta, M., Fox, A.H., Fortini, E., Moscato, P., Dinger, M.E., Mattick, J.S., 2012. Genome-wide analysis of long noncoding RNA stability. *Genome Res.* 22, 885–898. <https://doi.org/10.1101/gr.131037.111>

Davis, R.L., Turner, D.L., 2001. Vertebrate hairy and Enhancer of split related proteins: transcriptional repressors regulating cellular differentiation and embryonic patterning. *Oncogene* 20, 8342–8357. <https://doi.org/10.1038/sj.onc.1205094>

- Del Bene, F., Wehman, A.M., Link, B.A., Baier, H., 2008. Regulation of neurogenesis by interkinetic nuclear migration through an apical-basal notch gradient. *Cell* 134, 1055–1065. <https://doi.org/10.1016/j.cell.2008.07.017>
- Derrien, T., Johnson, R., Bussotti, G., Tanzer, A., Djebali, S., Tilgner, H., Guernec, G., Martin, D., Merkel, A., Knowles, D.G., Lagarde, J., Veeravalli, L., Ruan, X., Ruan, Y., Lassmann, T., Carninci, P., Brown, J.B., Lipovich, L., Gonzalez, J.M., Thomas, M., Davis, C.A., Shiekhattar, R., Gingeras, T.R., Hubbard, T.J., Notredame, C., Harrow, J., Guigó, R., 2012. The GENCODE v7 catalog of human long noncoding RNAs: analysis of their gene structure, evolution, and expression. *Genome Res.* 22, 1775–1789. <https://doi.org/10.1101/gr.132159.111>
- Dinger, M.E., Pang, K.C., Mercer, T.R., Mattick, J.S., 2008. Differentiating protein-coding and noncoding RNA: challenges and ambiguities. *PLoS Comput. Biol.* 4, e1000176. <https://doi.org/10.1371/journal.pcbi.1000176>
- Djebali, S., Davis, C.A., Merkel, A., Dobin, A., Lassmann, T., Mortazavi, A., Tanzer, A., Lagarde, J., Lin, W., Schlesinger, F., Xue, C., Marinov, G.K., Khatun, J., Williams, B.A., Zaleski, C., Rozowsky, J., Röder, M., Kokocinski, F., Abdelhamid, R.F., Alioto, T., Antoshechkin, I., Baer, M.T., Bar, N.S., Batut, P., Bell, K., Bell, I., Chakraborty, S., Chen, X., Chrast, J., Curado, J., Derrien, T., Drenkow, J., Dumais, E., Dumais, J., Duttagupta, R., Falconnet, E., Fastuca, M., Fejes-Toth, K., Ferreira, P., Foissac, S., Fullwood, M.J., Gao, H., Gonzalez, D., Gordon, A., Gunawardena, H., Howald, C., Jha, S., Johnson, R., Kapranov, P., King, B., Kingswood, C., Luo, O.J., Park, E., Persaud, K., Preall, J.B., Ribeca, P., Risk, B., Robyr, D., Sammeth, M., Schaffer, L., See, L.-H., Shahab, A., Skancke, J., Suzuki, A.M., Takahashi, H., Tilgner, H., Trout, D., Walters, N., Wang, H., Wrobel, J., Yu, Y., Ruan, X., Hayashizaki, Y., Harrow, J., Gerstein, M., Hubbard, T., Reymond, A., Antonarakis, S.E., Hannon, G., Giddings, M.C., Ruan, Y., Wold, B., Carninci, P., Guigó, R., Gingeras, T.R., 2012. Landscape of transcription in human cells. *Nature* 489, 101–108. <https://doi.org/10.1038/nature11233>
- Dubreuil, V., Marzesco, A.-M., Corbeil, D., Huttner, W.B., Wilsch-Bräuninger, M., 2007. Midbody and primary cilium of neural progenitors release extracellular membrane particles enriched in the stem cell marker prominin-1. *J. Cell Biol.* 176, 483–495. <https://doi.org/10.1083/jcb.200608137>
- Englund, C., Fink, A., Lau, C., Pham, D., Daza, R.A.M., Bulfone, A., Kowalczyk, T., Hevner, R.F., 2005. Pax6, Tbr2, and Tbr1 are expressed sequentially by radial glia,

- intermediate progenitor cells, and postmitotic neurons in developing neocortex. *J. Neurosci.* 25, 247–251. <https://doi.org/10.1523/JNEUROSCI.2899-04.2005>
- Fan, G., Martinowich, K., Chin, M.H., He, F., Fouse, S.D., Hutnick, L., Hattori, D., Ge, W., Shen, Y., Wu, H., ten Hoeve, J., Shuai, K., Sun, Y.E., 2005. DNA methylation controls the timing of astrogliogenesis through regulation of JAK-STAT signaling. *Development* 132, 3345–3356. <https://doi.org/10.1242/dev.01912>
- Gambello, M.J., Darling, D.L., Yingling, J., Tanaka, T., Gleeson, J.G., Wynshaw-Boris, A., 2003. Multiple dose-dependent effects of *Lis1* on cerebral cortical development. *J. Neurosci.* 23, 1719–1729.
- Geisler, S., Coller, J., 2013. RNA in unexpected places: long non-coding RNA functions in diverse cellular contexts. *Nat. Rev. Mol. Cell Biol.* 14, 699–712. <https://doi.org/10.1038/nrm3679>
- Gilbert, S.F., 2014. *Developmental Biology*. Sinauer Associates, Incorporated Publishers.
- Götz, M., Huttner, W.B., 2005. The cell biology of neurogenesis. *Nat. Rev. Mol. Cell Biol.* 6, 777–788. <https://doi.org/10.1038/nrm1739>
- Greig, L.C., Woodworth, M.B., Galazo, M.J., Padmanabhan, H., Macklis, J.D., 2013. Molecular logic of neocortical projection neuron specification, development and diversity. *Nat. Rev. Neurosci.* 14, 755–769. <https://doi.org/10.1038/nrn3586>
- Gross, R.E., Mehler, M.F., Mabie, P.C., Zang, Z., Santschi, L., Kessler, J.A., 1996. Bone morphogenetic proteins promote astroglial lineage commitment by mammalian subventricular zone progenitor cells. *Neuron* 17, 595–606.
- Guillemot, F., 2007. Cell fate specification in the mammalian telencephalon. *Prog. Neurobiol.* 83, 37–52. <https://doi.org/10.1016/j.pneurobio.2007.02.009>
- Guttman, M., Amit, I., Garber, M., French, C., Lin, M.F., Feldser, D., Huarte, M., Zuk, O., Carey, B.W., Cassady, J.P., Cabili, M.N., Jaenisch, R., Mikkelsen, T.S., Jacks, T., Hacohen, N., Bernstein, B.E., Kellis, M., Regev, A., Rinn, J.L., Lander, E.S., 2009. Chromatin signature reveals over a thousand highly conserved large non-coding RNAs in mammals. *Nature* 458, 223–227. <https://doi.org/10.1038/nature07672>
- Hatakeyama, J., Bessho, Y., Katoh, K., Ookawara, S., Fujioka, M., Guillemot, F., Kageyama, R., 2004. *Hes* genes regulate size, shape and histogenesis of the nervous system by control of the timing of neural stem cell differentiation. *Development* 131, 5539–5550. <https://doi.org/10.1242/dev.01436>

- Haubensak, W., Attardo, A., Denk, W., Huttner, W.B., 2004. Neurons arise in the basal neuroepithelium of the early mammalian telencephalon: a major site of neurogenesis. *Proc. Natl. Acad. Sci. U.S.A.* 101, 3196–3201. <https://doi.org/10.1073/pnas.0308600100>
- He, T., Zhang, Lufei, Kong, Y., Huang, Y., Zhang, Y., Zhou, D., Zhou, X., Yan, Y., Zhang, Linshi, Lu, S., Zhou, J., Wang, W., 2017. Long non-coding RNA CASC15 is upregulated in hepatocellular carcinoma and facilitates hepatocarcinogenesis. *Int. J. Oncol.* 51, 1722–1730. <https://doi.org/10.3892/ijo.2017.4175>
- Heins, N., Malatesta, P., Cecconi, F., Nakafuku, M., Tucker, K.L., Hack, M.A., Chapouton, P., Barde, Y.-A., Götz, M., 2002. Glial cells generate neurons: the role of the transcription factor Pax6. *Nat. Neurosci.* 5, 308–315. <https://doi.org/10.1038/nn828>
- Hevner, R.F., Hodge, R.D., Daza, R.A.M., Englund, C., 2006. Transcription factors in glutamatergic neurogenesis: conserved programs in neocortex, cerebellum, and adult hippocampus. *Neurosci. Res.* 55, 223–233. <https://doi.org/10.1016/j.neures.2006.03.004>
- Hirabayashi, Y., Itoh, Y., Tabata, H., Nakajima, K., Akiyama, T., Masuyama, N., Gotoh, Y., 2004. The Wnt/beta-catenin pathway directs neuronal differentiation of cortical neural precursor cells. *Development* 131, 2791–2801. <https://doi.org/10.1242/dev.01165>
- Hrdlickova, B., de Almeida, R.C., Borek, Z., Withoff, S., 2014. Genetic variation in the non-coding genome: Involvement of micro-RNAs and long non-coding RNAs in disease. *Biochimica et Biophysica Acta (BBA) - Molecular Basis of Disease, From genome to function* 1842, 1910–1922. <https://doi.org/10.1016/j.bbadis.2014.03.011>
- Huttner, W.B., Brand, M., 1997. Asymmetric division and polarity of neuroepithelial cells. *Curr. Opin. Neurobiol.* 7, 29–39.
- Iacopetti, P., Michelini, M., Stuckmann, I., Oback, B., Aaku-Saraste, E., Huttner, W.B., 1999. Expression of the antiproliferative gene TIS21 at the onset of neurogenesis identifies single neuroepithelial cells that switch from proliferative to neuron-generating division. *Proc. Natl. Acad. Sci. U.S.A.* 96, 4639–4644.
- Jepsen, K., Solum, D., Zhou, T., McEvelly, R.J., Kim, H.-J., Glass, C.K., Hermanson, O., Rosenfeld, M.G., 2007. SMRT-mediated repression of an H3K27 demethylase in progression from neural stem cell to neuron. *Nature* 450, 415–419. <https://doi.org/10.1038/nature06270>

- Jing, N., Huang, T., Guo, H., Yang, J., Li, M., Chen, Z., Zhang, Y., 2018. LncRNA CASC15 promotes colon cancer cell proliferation and metastasis by regulating the miR-4310/LGR5/Wnt/ β -catenin signaling pathway. *Mol Med Rep* 18, 2269–2276. <https://doi.org/10.3892/mmr.2018.9191>
- Kandel, E.R., 2012. Principles of Neural Science, Fifth Edition [WWW Document]. McGraw-Hill Education. URL <https://www.mhprofessional.com/9780071390118-usa-principles-of-neural-science-fifth-edition-group> (accessed 10.5.18).
- Kapusta, A., Feschotte, C., 2014. Volatile evolution of long noncoding RNA repertoires: mechanisms and biological implications. *Trends Genet.* 30, 439–452. <https://doi.org/10.1016/j.tig.2014.08.004>
- Khaitovich, P., Kelso, J., Franz, H., Visagie, J., Giger, T., Joerchel, S., Petzold, E., Green, R.E., Lachmann, M., Pääbo, S., 2006. Functionality of intergenic transcription: an evolutionary comparison. *PLoS Genet.* 2, e171. <https://doi.org/10.1371/journal.pgen.0020171>
- Koch, F., Fenouil, R., Gut, M., Cauchy, P., Albert, T.K., Zacarias-Cabeza, J., Spicuglia, S., de la Chapelle, A.L., Heidemann, M., Hintermair, C., Eick, D., Gut, I., Ferrier, P., Andrau, J.-C., 2011. Transcription initiation platforms and GTF recruitment at tissue-specific enhancers and promoters. *Nat. Struct. Mol. Biol.* 18, 956–963. <https://doi.org/10.1038/nsmb.2085>
- Kohtz, J.D., 2014. Long non-coding RNAs learn the importance of being in vivo. *Front Genet* 5, 45. <https://doi.org/10.3389/fgene.2014.00045>
- Kotake, Y., Nakagawa, T., Kitagawa, K., Suzuki, S., Liu, N., Kitagawa, M., Xiong, Y., 2011. Long non-coding RNA ANRIL is required for the PRC2 recruitment to and silencing of p15(INK4B) tumor suppressor gene. *Oncogene* 30, 1956–1962. <https://doi.org/10.1038/onc.2010.568>
- Kriegstein, A.R., Götz, M., 2003. Radial glia diversity: a matter of cell fate. *Glia* 43, 37–43. <https://doi.org/10.1002/glia.10250>
- Krystal, G.W., Armstrong, B.C., Battey, J.F., 1990. N-myc mRNA forms an RNA-RNA duplex with endogenous antisense transcripts. *Mol. Cell. Biol.* 10, 4180–4191.
- Kwon, G.S., Hadjantonakis, A.-K., 2007. Eomes::GFP—a tool for live imaging cells of the trophoblast, primitive streak, and telencephalon in the mouse embryo. *Genesis* 45, 208–217. <https://doi.org/10.1002/dvg.20293>
- Lange, C., Huttner, W.B., Calegari, F., 2009. Cdk4/cyclinD1 overexpression in neural stem cells shortens G1, delays neurogenesis, and promotes the generation and

- expansion of basal progenitors. *Cell Stem Cell* 5, 320–331. <https://doi.org/10.1016/j.stem.2009.05.026>
- Li, A.W., Murphy, P.R., 2000. Expression of alternatively spliced FGF-2 antisense RNA transcripts in the central nervous system: regulation of FGF-2 mRNA translation. *Mol. Cell. Endocrinol.* 170, 233–242.
- Li, C., Zhou, G., Feng, J., Zhang, J., Hou, L., Cheng, Z., 2018. Upregulation of lncRNA VDR/CASC15 induced by facilitates cardiac hypertrophy through modulating miR-432-5p/TLR4 axis. *Biochem. Biophys. Res. Commun.* 503, 2407–2414. <https://doi.org/10.1016/j.bbrc.2018.06.169>
- Li, W., Cogswell, C.A., LoTurco, J.J., 1998. Neuronal differentiation of precursors in the neocortical ventricular zone is triggered by BMP. *J. Neurosci.* 18, 8853–8862.
- Lin, N., Chang, K.-Y., Li, Z., Gates, K., Rana, Z.A., Dang, J., Zhang, D., Han, T., Yang, C.-S., Cunningham, T.J., Head, S.R., Duester, G., Dong, P.D.S., Rana, T.M., 2014. An evolutionarily conserved long noncoding RNA TUNA controls pluripotency and neural lineage commitment. *Mol. Cell* 53, 1005–1019. <https://doi.org/10.1016/j.molcel.2014.01.021>
- Livak, K.J., Schmittgen, T.D., 2001. Analysis of relative gene expression data using real-time quantitative PCR and the 2^{(-Delta Delta C(T))} Method. *Methods* 25, 402–408. <https://doi.org/10.1006/meth.2001.1262>
- Lukaszewicz, A., Savatier, P., Cortay, V., Giroud, P., Huissoud, C., Berland, M., Kennedy, H., Dehay, C., 2005. G1 phase regulation, area-specific cell cycle control, and cytoarchitectonics in the primate cortex. *Neuron* 47, 353–364. <https://doi.org/10.1016/j.neuron.2005.06.032>
- Lukaszewicz, A., Savatier, P., Cortay, V., Kennedy, H., Dehay, C., 2002. Contrasting effects of basic fibroblast growth factor and neurotrophin 3 on cell cycle kinetics of mouse cortical stem cells. *J. Neurosci.* 22, 6610–6622. <https://doi.org/20026666>
- MacFarlane, L.-A., Gu, Y., Casson, A.G., Murphy, P.R., 2010. Regulation of fibroblast growth factor-2 by an endogenous antisense RNA and by argonaute-2. *Mol. Endocrinol.* 24, 800–812. <https://doi.org/10.1210/me.2009-0367>
- Manzini, M.C., Walsh, C.A., 2011. What disorders of cortical development tell us about the cortex: one plus one does not always make two. *Curr. Opin. Genet. Dev.* 21, 333–339. <https://doi.org/10.1016/j.gde.2011.01.006>
- Mariner, P.D., Walters, R.D., Espinoza, C.A., Drullinger, L.F., Wagner, S.D., Kugel, J.F., Goodrich, J.A., 2008. Human Alu RNA is a modular transacting repressor of

- mRNA transcription during heat shock. *Mol. Cell* 29, 499–509. <https://doi.org/10.1016/j.molcel.2007.12.013>
- Martynoga, B., Drechsel, D., Guillemot, F., 2012. Molecular control of neurogenesis: a view from the mammalian cerebral cortex. *Cold Spring Harb Perspect Biol* 4. <https://doi.org/10.1101/cshperspect.a008359>
- McKenney, R.J., Vershinin, M., Kunwar, A., Vallee, R.B., Gross, S.P., 2010. LIS1 and NudE Induce a Persistent Dynein Force-Producing State. *Cell* 141, 304–314. <https://doi.org/10.1016/j.cell.2010.02.035>
- Mercer, T.R., Dinger, M.E., Sunken, S.M., Mehler, M.F., Mattick, J.S., 2008. Specific expression of long noncoding RNAs in the mouse brain. *Proc. Natl. Acad. Sci. U.S.A.* 105, 716–721. <https://doi.org/10.1073/pnas.0706729105>
- Miyata, T., Kawaguchi, A., Saito, K., Kawano, M., Muto, T., Ogawa, M., 2004. Asymmetric production of surface-dividing and non-surface-dividing cortical progenitor cells. *Development* 131, 3133–3145. <https://doi.org/10.1242/dev.01173>
- Mondal, T., Juvvuna, P.K., Kirkeby, A., Mitra, S., Kosalai, S.T., Traxler, L., Hertwig, F., Wernig-Zorc, S., Miranda, C., Deland, L., Volland, R., Bartenhagen, C., Bartsch, D., Bandaru, S., Engesser, A., Subhash, S., Martinsson, T., Carén, H., Akyürek, L.M., Kurian, L., Kanduri, M., Huarte, M., Kogner, P., Fischer, M., Kanduri, C., 2018. Sense-Antisense lncRNA Pair Encoded by Locus 6p22.3 Determines Neuroblastoma Susceptibility via the USP36-CHD7-SOX9 Regulatory Axis. *Cancer Cell* 33, 417–434.e7. <https://doi.org/10.1016/j.ccell.2018.01.020>
- Munroe, S.H., Lazar, M.A., 1991. Inhibition of c-erbA mRNA splicing by a naturally occurring antisense RNA. *J. Biol. Chem.* 266, 22083–22086.
- Necsulea, A., Soumillon, M., Warnefors, M., Liechti, A., Daish, T., Zeller, U., Baker, J.C., Grützner, F., Kaessmann, H., 2014. The evolution of lncRNA repertoires and expression patterns in tetrapods. *Nature* 505, 635–640. <https://doi.org/10.1038/nature12943>
- Ng, S.-Y., Bogu, G.K., Soh, B.S., Stanton, L.W., 2013. The long noncoding RNA RMST interacts with SOX2 to regulate neurogenesis. *Mol. Cell* 51, 349–359. <https://doi.org/10.1016/j.molcel.2013.07.017>
- Nieto, M., Monuki, E.S., Tang, H., Imitola, J., Haubst, N., Khoury, S.J., Cunningham, J., Gotz, M., Walsh, C.A., 2004. Expression of Cux-1 and Cux-2 in the subventricular zone and upper layers II-IV of the cerebral cortex. *J. Comp. Neurol.* 479, 168–180. <https://doi.org/10.1002/cne.20322>

- Norton, J.D., 2000. ID helix-loop-helix proteins in cell growth, differentiation and tumorigenesis. *J. Cell. Sci.* 113 (Pt 22), 3897–3905.
- O’Leary, D.D.M., Chou, S.-J., Sahara, S., 2007. Area patterning of the mammalian cortex. *Neuron* 56, 252–269. <https://doi.org/10.1016/j.neuron.2007.10.010>
- Onoguchi, M., Hirabayashi, Y., Koseki, H., Gotoh, Y., 2012. A noncoding RNA regulates the neurogenin1 gene locus during mouse neocortical development. *Proc. Natl. Acad. Sci. U.S.A.* 109, 16939–16944. <https://doi.org/10.1073/pnas.1202956109>
- Pauli, A., Rinn, J.L., Schier, A.F., 2011. Non-coding RNAs as regulators of embryogenesis. *Nat. Rev. Genet.* 12, 136–149. <https://doi.org/10.1038/nrg2904>
- Ponjavic, J., Oliver, P.L., Lunter, G., Ponting, C.P., 2009. Genomic and transcriptional co-localization of protein-coding and long non-coding RNA pairs in the developing brain. *PLoS Genet.* 5, e1000617. <https://doi.org/10.1371/journal.pgen.1000617>
- Ponjavic, J., Ponting, C.P., Lunter, G., 2007. Functionality or transcriptional noise? Evidence for selection within long noncoding RNAs. *Genome Res.* 17, 556–565. <https://doi.org/10.1101/gr.6036807>
- Raballo, R., Rhee, J., Lyn-Cook, R., Leckman, J.F., Schwartz, M.L., Vaccarino, F.M., 2000. Basic fibroblast growth factor (Fgf2) is necessary for cell proliferation and neurogenesis in the developing cerebral cortex. *J. Neurosci.* 20, 5012–5023.
- Rakic, P., 1995. A small step for the cell, a giant leap for mankind: a hypothesis of neocortical expansion during evolution. *Trends Neurosci.* 18, 383–388.
- Rakic, P., Knyihar-Csillik, E., Csillik, B., 1996. Polarity of microtubule assemblies during neuronal cell migration. *Proc. Natl. Acad. Sci. U.S.A.* 93, 9218–9222.
- Ramos, A.D., Diaz, A., Nellore, A., Delgado, R.N., Park, K.-Y., Gonzales-Roybal, G., Oldham, M.C., Song, J.S., Lim, D.A., 2013. Integration of genome-wide approaches identifies lncRNAs of adult neural stem cells and their progeny in vivo. *Cell Stem Cell* 12, 616–628. <https://doi.org/10.1016/j.stem.2013.03.003>
- Rapicavoli, N.A., Poth, E.M., Blackshaw, S., 2010. The long noncoding RNA RNCR2 directs mouse retinal cell specification. *BMC Dev. Biol.* 10, 49. <https://doi.org/10.1186/1471-213X-10-49>
- Rinn, J.L., Chang, H.Y., 2012. Genome regulation by long noncoding RNAs. *Annu. Rev. Biochem.* 81, 145–166. <https://doi.org/10.1146/annurev-biochem-051410-092902>

- Rinn, J.L., Kertesz, M., Wang, J.K., Squazzo, S.L., Xu, X., Bruggmann, S.A., Goodnough, L.H., Helms, J.A., Farnham, P.J., Segal, E., Chang, H.Y., 2007. Functional demarcation of active and silent chromatin domains in human HOX loci by noncoding RNAs. *Cell* 129, 1311–1323. <https://doi.org/10.1016/j.cell.2007.05.022>
- Ross, S.E., Greenberg, M.E., Stiles, C.D., 2003. Basic helix-loop-helix factors in cortical development. *Neuron* 39, 13–25.
- Rossant, J., Tam, P.P.L., 2009. Blastocyst lineage formation, early embryonic asymmetries and axis patterning in the mouse. *Development* 136, 701–713. <https://doi.org/10.1242/dev.017178>
- Roth, S.Y., Denu, J.M., Allis, C.D., 2001. Histone acetyltransferases. *Annu. Rev. Biochem.* 70, 81–120. <https://doi.org/10.1146/annurev.biochem.70.1.81>
- Rubenstein, J.L.R., 2011. Annual Research Review: Development of the cerebral cortex: implications for neurodevelopmental disorders. *J Child Psychol Psychiatry* 52, 339–355. <https://doi.org/10.1111/j.1469-7610.2010.02307.x>
- Russell, M.R., Penikis, A., Oldridge, D.A., Alvarez-Dominguez, J.R., McDaniel, L., Diamond, M., Padovan, O., Raman, P., Li, Y., Wei, J.S., Zhang, S., Gnanchandran, J., Seeger, R., Asgharzadeh, S., Khan, J., Diskin, S.J., Maris, J.M., Cole, K.A., 2015. CASC15-S Is a Tumor Suppressor lncRNA at the 6p22 Neuroblastoma Susceptibility Locus. *Cancer Res.* 75, 3155–3166. <https://doi.org/10.1158/0008-5472.CAN-14-3613>
- Salzman, J., Gawad, C., Wang, P.L., Lacayo, N., Brown, P.O., 2012. Circular RNAs are the predominant transcript isoform from hundreds of human genes in diverse cell types. *PLoS ONE* 7, e30733. <https://doi.org/10.1371/journal.pone.0030733>
- Sandberg, M., Källström, M., Muhr, J., 2005. Sox21 promotes the progression of vertebrate neurogenesis. *Nat. Neurosci.* 8, 995–1001. <https://doi.org/10.1038/nn1493>
- Sasai, Y., Kageyama, R., Tagawa, Y., Shigemoto, R., Nakanishi, S., 1992. Two mammalian helix-loop-helix factors structurally related to *Drosophila* hairy and Enhancer of split. *Genes Dev.* 6, 2620–2634.
- Sauer, F.C., 1935. Mitosis in the neural tube. *Journal of Comparative Neurology* 62, 377–405. <https://doi.org/10.1002/cne.900620207>
- Scardigli, R., Bäumer, N., Gruss, P., Guillemot, F., Le Roux, I., 2003. Direct and concentration-dependent regulation of the proneural gene Neurogenin2 by Pax6. *Development* 130, 3269–3281.

- Schaar, B.T., McConnell, S.K., 2005. Cytoskeletal coordination during neuronal migration. *Proc. Natl. Acad. Sci. U.S.A.* 102, 13652–13657. <https://doi.org/10.1073/pnas.0506008102>
- Schenk, J., Wilsch-Bräuninger, M., Calegari, F., Huttner, W.B., 2009. Myosin II is required for interkinetic nuclear migration of neural progenitors. *Proc. Natl. Acad. Sci. U.S.A.* 106, 16487–16492. <https://doi.org/10.1073/pnas.0908928106>
- Schmid, R.S., McGrath, B., Berechid, B.E., Boyles, B., Marchionni, M., Sestan, N., Anton, E.S., 2003. Neuregulin 1-erbB2 signaling is required for the establishment of radial glia and their transformation into astrocytes in cerebral cortex. *Proc. Natl. Acad. Sci. U.S.A.* 100, 4251–4256. <https://doi.org/10.1073/pnas.0630496100>
- Schwamborn, J.C., Berezikov, E., Knoblich, J.A., 2009. The TRIM-NHL protein TRIM32 activates microRNAs and prevents self-renewal in mouse neural progenitors. *Cell* 136, 913–925. <https://doi.org/10.1016/j.cell.2008.12.024>
- Sessa, A., Mao, C.-A., Hadjantonakis, A.-K., Klein, W.H., Broccoli, V., 2008. Tbr2 directs conversion of radial glia into basal precursors and guides neuronal amplification by indirect neurogenesis in the developing neocortex. *Neuron* 60, 56–69. <https://doi.org/10.1016/j.neuron.2008.09.028>
- Siegenthaler, J.A., Tremper-Wells, B.A., Miller, M.W., 2008. Foxg1 haploinsufficiency reduces the population of cortical intermediate progenitor cells: effect of increased p21 expression. *Cereb. Cortex* 18, 1865–1875. <https://doi.org/10.1093/cercor/bhm209>
- Solecki, D.J., Model, L., Gaetz, J., Kapoor, T.M., Hatten, M.E., 2004. Par6alpha signaling controls glial-guided neuronal migration. *Nat. Neurosci.* 7, 1195–1203. <https://doi.org/10.1038/nn1332>
- Spigoni, G., Gedressi, C., Mallamaci, A., 2010. Regulation of Emx2 expression by antisense transcripts in murine cortico-cerebral precursors. *PLoS ONE* 5, e8658. <https://doi.org/10.1371/journal.pone.0008658>
- Takahashi, T., Nowakowski, R.S., Caviness, V.S., 1993. Cell cycle parameters and patterns of nuclear movement in the neocortical proliferative zone of the fetal mouse. *J. Neurosci.* 13, 820–833.
- Tarabykin, V., Stoykova, A., Usman, N., Gruss, P., 2001. Cortical upper layer neurons derive from the subventricular zone as indicated by Svet1 gene expression. *Development* 128, 1983–1993.

- Taverna, E., Huttner, W.B., 2010. Neural progenitor nuclei IN motion. *Neuron* 67, 906–914. <https://doi.org/10.1016/j.neuron.2010.08.027>
- Tiberi, L., Vanderhaeghen, P., van den Aemele, J., 2012. Cortical neurogenesis and morphogens: diversity of cues, sources and functions. *Curr. Opin. Cell Biol.* 24, 269–276. <https://doi.org/10.1016/j.ceb.2012.01.010>
- Trincado, J.L., Entizne, J.C., Hysenaj, G., Singh, B., Skalic, M., Elliott, D.J., Eyra, E., 2018. SUPPA2: fast, accurate, and uncertainty-aware differential splicing analysis across multiple conditions. *Genome Biol.* 19, 40. <https://doi.org/10.1186/s13059-018-1417-1>
- Tripathi, V., Ellis, J.D., Shen, Z., Song, D.Y., Pan, Q., Watt, A.T., Freier, S.M., Bennett, C.F., Sharma, A., Bubulya, P.A., Blencowe, B.J., Prasanth, S.G., Prasanth, K.V., 2010. The nuclear-retained noncoding RNA MALAT1 regulates alternative splicing by modulating SR splicing factor phosphorylation. *Mol. Cell* 39, 925–938. <https://doi.org/10.1016/j.molcel.2010.08.011>
- Tsai, J.-W., Bremner, K.H., Vallee, R.B., 2007. Dual subcellular roles for LIS1 and dynein in radial neuronal migration in live brain tissue. *Nat. Neurosci.* 10, 970–979. <https://doi.org/10.1038/nn1934>
- Tsai, L.-H., Gleeson, J.G., 2005. Nucleokinesis in neuronal migration. *Neuron* 46, 383–388. <https://doi.org/10.1016/j.neuron.2005.04.013>
- Tsai, M.-C., Manor, O., Wan, Y., Mosammaparast, N., Wang, J.K., Lan, F., Shi, Y., Segal, E., Chang, H.Y., 2010. Long noncoding RNA as modular scaffold of histone modification complexes. *Science* 329, 689–693. <https://doi.org/10.1126/science.1192002>
- Tsuiji, H., Yoshimoto, R., Hasegawa, Y., Furuno, M., Yoshida, M., Nakagawa, S., 2011. Competition between a noncoding exon and introns: Gomafu contains tandem UACUAAC repeats and associates with splicing factor-1. *Genes Cells* 16, 479–490. <https://doi.org/10.1111/j.1365-2443.2011.01502.x>
- Tuoc, T.C., Stoykova, A., 2008. Trim11 modulates the function of neurogenic transcription factor Pax6 through ubiquitin-proteasome system. *Genes Dev.* 22, 1972–1986. <https://doi.org/10.1101/gad.471708>
- Ulitsky, I., Bartel, D.P., 2013. lincRNAs: genomics, evolution, and mechanisms. *Cell* 154, 26–46. <https://doi.org/10.1016/j.cell.2013.06.020>

- Ulitsky, I., Shkumatava, A., Jan, C.H., Sive, H., Bartel, D.P., 2011. Conserved function of lincRNAs in vertebrate embryonic development despite rapid sequence evolution. *Cell* 147, 1537–1550. <https://doi.org/10.1016/j.cell.2011.11.055>
- Vallee, R.B., Seale, G.E., Tsai, J.-W., 2009. Emerging roles for myosin II and cytoplasmic dynein in migrating neurons and growth cones. *Trends Cell Biol.* 19, 347–355. <https://doi.org/10.1016/j.tcb.2009.03.009>
- Vance, K.W., Sansom, S.N., Lee, S., Chalei, V., Kong, L., Cooper, S.E., Oliver, P.L., Ponting, C.P., 2014. The long non-coding RNA Paupar regulates the expression of both local and distal genes. *EMBO J.* 33, 296–311. <https://doi.org/10.1002/emboj.201386225>
- Walcher, T., Xie, Q., Sun, J., Irmeler, M., Beckers, J., Öztürk, T., Niessing, D., Stoykova, A., Cvekl, A., Ninkovic, J., Götz, M., 2013. Functional dissection of the paired domain of Pax6 reveals molecular mechanisms of coordinating neurogenesis and proliferation. *Development* 140, 1123–1136. <https://doi.org/10.1242/dev.082875>
- Wang, K.C., Yang, Y.W., Liu, B., Sanyal, A., Corces-Zimmerman, R., Chen, Y., Lajoie, B.R., Protacio, A., Flynn, R.A., Gupta, R.A., Wysocka, J., Lei, M., Dekker, J., Helms, J.A., Chang, H.Y., 2011. A long noncoding RNA maintains active chromatin to coordinate homeotic gene expression. *Nature* 472, 120–124. <https://doi.org/10.1038/nature09819>
- Wilusz, J.E., JnBaptiste, C.K., Lu, L.Y., Kuhn, C.-D., Joshua-Tor, L., Sharp, P.A., 2012. A triple helix stabilizes the 3' ends of long noncoding RNAs that lack poly(A) tails. *Genes Dev.* 26, 2392–2407. <https://doi.org/10.1101/gad.204438.112>
- Wodarz, A., Huttner, W.B., 2003. Asymmetric cell division during neurogenesis in *Drosophila* and vertebrates. *Mech. Dev.* 120, 1297–1309.
- Wu, Q., Xiang, S., Ma, J., Hui, P., Wang, T., Meng, W., Shi, M., Wang, Y., 2018. Long non-coding RNA CASC15 regulates gastric cancer cell proliferation, migration and epithelial mesenchymal transition by targeting CDKN1A and ZEB1. *Mol Oncol* 12, 799–813. <https://doi.org/10.1002/1878-0261.12187>
- Wutz, A., Rasmussen, T.P., Jaenisch, R., 2002. Chromosomal silencing and localization are mediated by different domains of Xist RNA. *Nat. Genet.* 30, 167–174. <https://doi.org/10.1038/ng820>
- Yap, K.L., Li, S., Muñoz-Cabello, A.M., Raguz, S., Zeng, L., Mujtaba, S., Gil, J., Walsh, M.J., Zhou, M.-M., 2010. Molecular interplay of the noncoding RNA ANRIL

and methylated histone H3 lysine 27 by polycomb CBX7 in transcriptional silencing of INK4a. *Mol. Cell* 38, 662–674. <https://doi.org/10.1016/j.molcel.2010.03.021>

Yin, Q.-F., Yang, L., Zhang, Y., Xiang, J.-F., Wu, Y.-W., Carmichael, G.G., Chen, L.-L., 2012. Long noncoding RNAs with snoRNA ends. *Mol. Cell* 48, 219–230. <https://doi.org/10.1016/j.molcel.2012.07.033>

Yin, Y., Zhao, B., Li, D., Yin, G., 2018. Long non-coding RNA CASC15 promotes melanoma progression by epigenetically regulating PDCD4. *Cell Biosci* 8, 42. <https://doi.org/10.1186/s13578-018-0240-4>

Yoon, K., Nery, S., Rutlin, M.L., Radtke, F., Fishell, G., Gaiano, N., 2004. Fibroblast growth factor receptor signaling promotes radial glial identity and interacts with Notch1 signaling in telencephalic progenitors. *J. Neurosci.* 24, 9497–9506. <https://doi.org/10.1523/JNEUROSCI.0993-04.2004>

Zhang, X., Lei, K., Yuan, X., Wu, X., Zhuang, Y., Xu, T., Xu, R., Han, M., 2009. SUN1/2 and Syne/Nesprin-1/2 complexes connect centrosome to the nucleus during neurogenesis and neuronal migration in mice. *Neuron* 64, 173–187. <https://doi.org/10.1016/j.neuron.2009.08.018>

Zhao, J., Sun, B.K., Erwin, J.A., Song, J.-J., Lee, J.T., 2008. Polycomb proteins targeted by a short repeat RNA to the mouse X chromosome. *Science* 322, 750–756. <https://doi.org/10.1126/science.1163045>

Zhao, X., D' Arca, D., Lim, W.K., Brahmachary, M., Carro, M.S., Ludwig, T., Cardo, C.C., Guillemot, F., Aldape, K., Califano, A., Iavarone, A., Lasorella, A., 2009. The N-Myc-DLL3 cascade is suppressed by the ubiquitin ligase Huwe1 to inhibit proliferation and promote neurogenesis in the developing brain. *Dev. Cell* 17, 210–221. <https://doi.org/10.1016/j.devcel.2009.07.009>

Zuo, Z., Ma, L., Gong, Z., Xue, L., Wang, Q., 2018. Long non-coding RNA CASC15 promotes tongue squamous carcinoma progression through targeting miR-33a-5p. *Environ Sci Pollut Res Int* 25, 22205–22212. <https://doi.org/10.1007/s11356-018-2300-z>

Acknowledgments

I would like to thank everyone who provided support during my Doctorate work.

Special thanks should go to Federico Calegari for allowing me to work under his supervision. Thank you for all the support and advice you provided in the thesis work and for the extracurricular support.

I would like to thank Julieta Aprea who started the project on which I focused in this thesis.

I would like to thank Andreas Dahl and Mathias Lesche for all the bioinformatics analysis.

I would like to thank my Thesis Advisory Committee, Jochen Rink and Nadine Vastenhouw, who guided the project and made all the valuable comments and critiques.

Special thanks to Stanislava Popova and Müge Akpinar for proof reading my thesis and for helping with translation.

Thanks to all the facilities in the CRTD and MPI-CBG that made all the work smoother and provided technical and conceptual support.

Special thanks to all the members of Calegari lab, thank you for being nice and friendly and setting an enjoyable working environment.

Thanks to all the friends in Dresden, you made it much easier for me to live in Dresden and endure the stress that comes with the PhD period.

Special thanks to my Parents; Baba and Matoos and my sisters Salma and Samar for your ever-lasting support and love. Also to my dearest brother Mohammad whom I miss so much. May Allah rest your soul in peace.

Thanks to the Almighty Allah for giving me the strength and intelligence to fulfill this work and to have endured the difficulties that came along the road.

Technische Universität Dresden
Medizinische Fakultät Carl Gustav Carus
Promotionsordnung vom 24. Juli 2011

Erklärungen zur Eröffnung des Promotionsverfahrens

1. Hiermit versichere ich, dass ich die vorliegende Arbeit ohne unzulässige Hilfe Dritter und ohne Benutzung anderer als der angegebenen Hilfsmittel angefertigt habe; die aus fremden Quellen direkt oder indirekt übernommenen Gedanken sind als solche kenntlich gemacht.
2. Bei der Auswahl und Auswertung des Materials sowie bei der Herstellung des Manuskripts habe ich Unterstützungsleistungen von folgenden Personen erhalten: nicht zutreffend.
3. Weitere Personen waren an der geistigen Herstellung der vorliegenden Arbeit nicht beteiligt. Insbesondere habe ich nicht die Hilfe eines kommerziellen Promotionsberaters in Anspruch genommen. Dritte haben von mir weder unmittelbar noch mittelbar geldwerte Leistungen für Arbeiten erhalten, die im Zusammenhang mit dem Inhalt der vorgelegten Dissertation stehen.
4. Die Arbeit wurde bisher weder im Inland noch im Ausland in gleicher oder ähnlicher Form einer anderen Prüfungsbehörde vorgelegt.
5. Die Inhalte dieser Dissertation wurden in folgender Form veröffentlicht: nicht zutreffend
6. Ich bestätige, dass es keine zurückliegenden erfolglosen Promotionsverfahren gab.
7. Ich bestätige, dass ich die Promotionsordnung der Medizinischen Fakultät der Technischen Universität Dresden anerkenne.
8. Ich habe die Zitierrichtlinien für Dissertationen an der Medizinischen Fakultät der Technischen Universität Dresden zur Kenntnis genommen und befolgt.

Dresden, den 29.11.2018

Sara S. Tayel

Hiermit bestätige ich die Einhaltung der folgenden aktuellen gesetzlichen Vorgaben im Rahmen meiner Dissertation

- das zustimmende Votum der Ethikkommission bei Klinischen Studien, epidemiologischen Untersuchungen mit Personenbezug oder Sachverhalten, die das Medizinproduktegesetz betreffen

Aktenzeichen der zuständigen Ethikkommission DD 24-9168.11-1/2011-11, HD 35-9185.81/G-61/15

- die Einhaltung der Bestimmungen des Tierschutzgesetzes Aktenzeichen der Genehmigungsbehörde zum Vorhaben/zur Mitwirkung

LDS Aktenzeichen: 11-1-2011-41, TVV 16-2018

- die Einhaltung des Gentechnikgesetzes

Projektnummer: LDS Aktenzeichen: 55-8811.71/210

- die Einhaltung von Datenschutzbestimmungen der Medizinischen Fakultät und des Universitätsklinikums Carl Gustav Carus.

Dresden, den 29.11.2018

Sara S. Tayel